AALBORG UNIVERSITY
STUDENTS STUDYREPORT

Department of Energy Technology - Pontoppidanstræde 101
Aalborg University, Denmark

Control of a Multilevel Converter for Power Quality Improvement in Wind Power Plants

Conducted by group PED4/WPS4 - 1045
-Autumn and Spring Semester, 2011/2012-

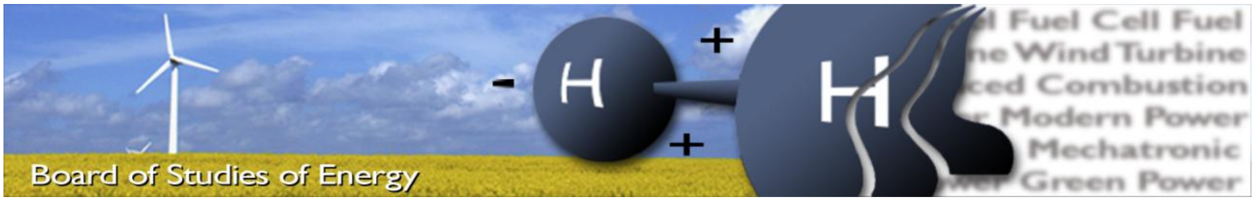

Title:	Control of a Multilevel Converter for Power Quality Improvement in WPPs
Semester:	9th and 10th
Semester theme:	Master Thesis
Project period:	1st September 2011 – 31st May 2012
ECTS:	60
Supervisor:	Remus Teodorescu, Pedro Rodriguez
Project group:	PED4/WPS4 – 1045

____

Nicolae – Cristian Sintamarean

____

Antoni Mir Cantarellas

Copies:	3
Pages, total:	113
Appendix:	20
Supplements:	3CDs

SYNOPSIS:

High penetration of wind energy into the grid may introduce stability and power quality problems due to the fluctuating nature of the wind and the increasing complexity of the power system. By implementing advanced functionalities in power converters, it is possible to improve the performance of the wind farm and also to provide grid support, as it is required by the grid codes. One of the main compliance difficulties that can be found in such power plants are related to reactive power compensation and to keep the harmonics content within the allowed limits, even if the power of the WPP converters is increasing. This paper deals with an advanced control strategy design of a three-level converter performing STATCOM and Active Filter functionalities. A novel control strategy called Smart-STATCOM is introduced, since it has the capability of self-controlling reactive power and harmonic voltages at the same time. Therefore, deciding the amount of non-active currents (fundamental, 5th and 7th harmonics) to be injected depending on the PCC voltage quality. Experimental results of the proposed control strategy are analyzed in order to validate the performance of the entire system.

By signing this document, each member of the group confirms that all group members have participated in the project work, and thereby all members are collectively liable for the contents of the report. Furthermore, all group members confirm that the report does not include plagiarism.

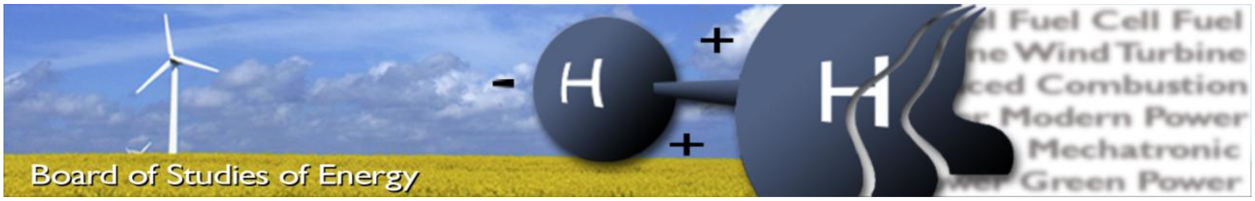

Preface

The present report is written by Nicolae – Cristian Sintamarean and Antoni Mir Cantarellas, master students throughout the 9th and 10th semester of PED and WPS MSc degree. This Thesis is entitled Control of a Multilevel Converter for Power Quality Improvement in Wind Power Plants , and the main purpose of the project is to contribute to the power quality improvement of WPPs by implemented an advanced control strategy which combines STATCOM and Active Filter functionalities.

The project is documented in a main report and appendixes. The main report can be read as an independent piece, from which they derive the appendices including mathematical calculations, simulations and more details in order to make the main report more understandable. In this project, the chapters are arranged numerically whereas appendixes are sorted alphabetically.

Figures, equations and tables are numbered in succession within the chapters. For example, Fig. 2-3 is the third figure of the chapter 2.

Bibliography is referred in brackets, using IEEE style, for example [1];

The proposed control structure is applied in simulation by mainly using S-function builder blocks from MATLAB – Simulink, while the laboratory implementation has been directly programmed with C-language in a dSpace system.

A CD-ROM containing the main report and appendixes, list of references, simulation and laboratory implementation models is attached to the project.

We would like to thank our supervisors, Remus Teodorescu and Pedro Rodriguez, for all their support, as well as to the PhD student Henan Miranda, who considerably helped us in several aspects. Furthermore, we also would like to thank Vestas for providing us such a great opportunity in improving our specific skills towards outstanding professors and research experts in the field of integration of Wind Power in power systems. Finally special thanks are given to our families and to Iulia who supported us along all this large period.

Summary

Nowadays, an increasing awareness regarding power quality and stability problems has been experienced mainly due to the high penetration levels of wind energy into the power systems. It is worth to mention that some of the most important grid code compliance difficulties that can be found in WPPs are related to reactive power compensation and to keep the harmonics content within the allowed limits. Therefore, in order to improve the power quality of the WPPs, this project is focused on the control design implementation of a 3L-DNPC power conditioner based on a STATCOM which is able to perform as an Active Filter for 5^{th} and 7^{th} harmonics. The project is structured in five chapters.

The first chapter presents a brief overview of the wind power technology historical background and an introduction of the main power quality problems which arise when high penetration of wind energy is present into the grid. Additionally the problem statement, objectives and limitations of the project are introduced in order to provide a clear image about the purpose of this work.

The second chapter presents an overview of the proposed grid connected converter topology in charge of providing power quality improvement for WPPs applications. Furthermore, in order to achieve the desired converter functionalities, the current status of the applied control techniques are presented. Additionally the used grid synchronization and harmonic detection techniques are introduced. In order to provide or absorb a desired quantity of active or reactive power into the grid by using a power converter, special attention has been paid to the implementation of Instantaneous Power Theory. Finally, the proposed non-active power refer strategies (STATCOM and Active Filter) are introduced as a solution for improving the power quality of the PCC.

Chapter three introduces the overall control design of the proposed power conditioner in order to achieve the desired functionalities (STATCOM, Active Filter and Smart STATCOM). Firstly, an accurate model of the system (based on a 3L-DNPC and LCL-filter) is required, as a more realistic approach to the laboratory setup behavior will be obtained. Afterwards, the design of the current controllers for each of the desired compensation frequencies (50Hz, 250Hz and 350Hz) is introduced. Furthermore, the voltage controller design is performed in order to keep the DC link voltage constant at the desired value. Additionally, the proposed non-active power reference strategies are presented, which main purpose is to operate under STATCOM and Active Filter operation mode. A novel control strategy is proposed, which simultaneously combines the implementation of STATCOM and Active Filter functionalities in order to provide maximum power quality at the PCC. Finally the simulation results are discussed in order to validate the performance of the control design. In simulation, the control has been implemented in C-code by using S-Function Builder blocks from Matlab/Simulink.

This laboratory implementation of the proposed control strategies is presented in the fourth chapter. It is worth to mention that identical system conditions and controller parameters have been considered as the ones specified in chapter 3.

Therefore the achievement of similar laboratory results as in the simulations is expected. Furthermore, the main laboratory setup components are introduced in order to achieve a better understanding of the system behavior.

Finally, the obtained laboratory results have been used to validate the system performance in STATCOM, Active Filter and Smart-STATCOM operation modes.

The last chapter introduces the conclusions and future work of the present project. In this case, it can be stated that the proposed novel control strategy, which simultaneously combines STATCOM and Active Filter functionalities (Smart-STATCOM operation mode), was validated in the laboratory setup. Therefore, the overall objectives of this project were accomplished, since the designed control strategy provides voltage control and harmonic voltage mitigation at the PCC. Thus, the power quality of the WPP can be improved by implementing the proposed control structure in a shunt-connected three level power converter.

Table of Contents

Nomenclature

2LC, 3LC, 4LC, 5LC – 2 Level Converter, 3 Level Converter, 4 Level Converter, 5 Level Converter

AC – Alternative Current

AF – Active Filter

ANPC – Active Neutral Point Clamped

CSC – Current Source Converters

DC – Direct Current

DFIG – Doubly Fed Induction Generator

DNPC – Diode Neutral Point Clamped

DSP – Digital Signal Processor

DWO – Digital Waveform Output

FACTS – Flexible AC Transmission Systems

FPGA – Field Programmable Gate Array

F_{SW} – Switching Frequency

GTO Thyristors – Gate Turn Off Thryristors

IGBT – Insulated Gate Bipolar Transistor

IGCT – Integrated Gate Commutated Thyristor

I/O Board – Input/Output Board

IARC – Instantaneous Active and Reactive Control

M-SOGI – Multiple Second Order Generalized Integrator

NREAP – National Renewable Action Plan

PC – Personal Computer

PCC – Point of Common Coupling

Pu – per unit

PR, PI – Proportional Resonant, Proportional Integrator Controllers

PF – Passive Filter

PV – Photovoltaic

RMS – Root Mean Square

SOGI-QSG FLL – Second Order Generalized Integrator-Quadrature Signal Generator Frequency Locked Loop

SG – Sharing Gain

SVC – Static Var Compensator

STATCOM – STATic synchronous COMpensator

SVM – Space Vector Modulation

THD – Total Harmonic Distortion

T_S – Sampling Period

TSC – Thyristor Switched Capacitor

TCR – Thyristor Controlled Reactor

TSR – Thyristor Switched Reactor

TSO – Transmission System Operator

VSI – Voltage Source Converter

VSC – Voltage Source Converter

V_{PCC} – Point of Common Coupling Voltage

V_{ref} – Voltage Reference

WPP – Wind Power Plant

WT – Wind Turbine

1. Introduction

In this chapter a brief overview of the wind power technology historical background and an introduction of the main power quality problems which arise when high penetration of wind energy is present into the grid. Additionally the problem statement, objectives and limitations of the project are introduced in order to provide a clear image regarding the purpose of this work.

1.1 Background of Wind Energy Technology and Introduction of Power Quality Problems

The employment of wind power dates at least since 3000 years ago, where its first usage was based on obtaining mechanical energy for agriculture related purposes, such as irrigating and grinding systems. Later on, once with the industrialization period, the wind systems were replaced by the electrical grid or combustion engines, as these energy sources were able to provide more constant power than the wind. The use of wind resources as electrical power generation units became popular in the 1970s due to the first oil crisis. Moreover it is worth to point that the first wind turbine generation unit was built by the Dane Poul LaCour in 1891. After its first appearance, a progressively improvement on this technology was experienced and by the end of the twentieth century, wind power became one of the most important technologies among the renewable energies [1]

From Fig. 1-1, it can be observed that Europe has played a key role in contributing to the global cumulative installed wind power, and even nowadays, it is an important actor providing more than 40% of the global wind power capacity. It is worth to mention that a noticeable growth was experienced, as in the last 5 years the global wind power capacity increased approximately by a 62% from 74.1GW to 197GW . [2]

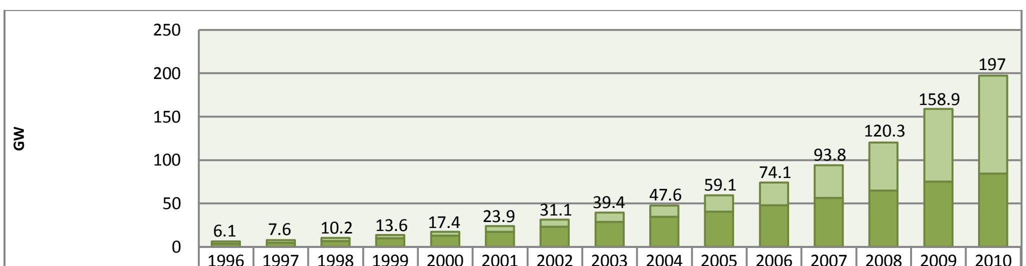

	1996	1997	1998	1999	2000	2001	2002	2003	2004	2005	2006	2007	2008	2009	2010
Rest of the World	2,6	2,8	3,7	3,9	4,5	6,6	8	10,9	13,2	18,6	26,1	37,3	55,6	83,8	112,7
EU	3,5	4,8	6,5	9,7	12,9	17,3	23,1	28,5	34,4	40,5	48	56,5	64,7	75,1	84,3

Fig. 1-1 Global cumulative installed wind power capacity from 1996 to 2010 [2]

Nowadays, the introduction of sustainable and clean energy generation into the power system has become popular, mainly motivated by the increasing concern regarding the harmful effect of the global warming and climate change. Due to this increasing demand of renewable energy generation, a considerable development of technologies such as wind power or photovoltaic systems has been experienced [1, 2].

As it can be observed in Fig. 1-2(b), wind energy was one of the leading renewable energy source in 2010 and its installed capacity experienced the second biggest growth, increasing a 9.13% from 1995 to 2010. The evolution through these 15 years period (depicted in Fig. 1-2(c)) shows that from one hand, energy sources such as gas, wind and photovoltaics(PV) increased considerably their power capacity installation and on the other hand traditional generation units based on fossil fuels and nuclear became less representative in the overall power capacity mix [2].

(a)

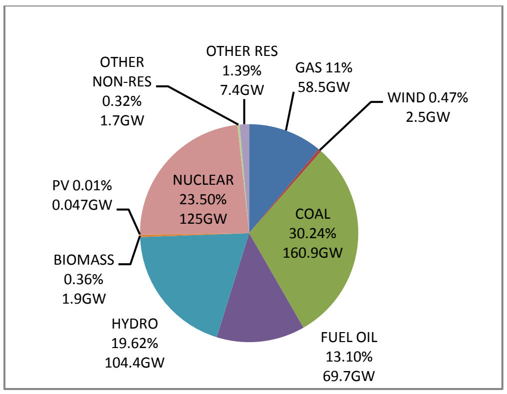

(b)

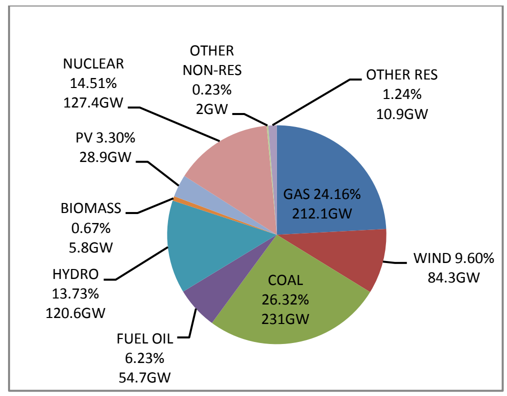

(c)

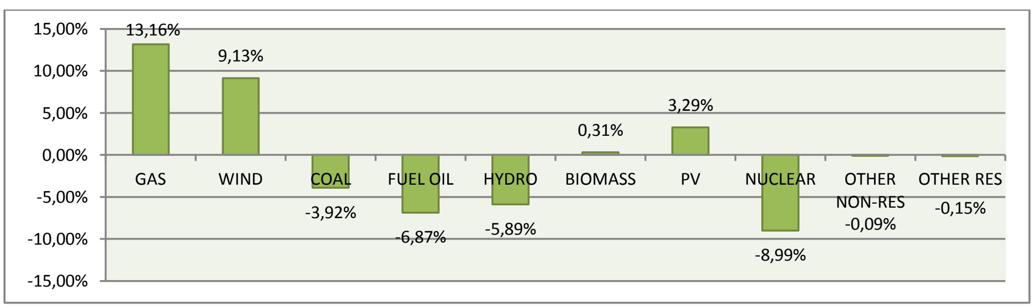

Fig. 1-2 (a)EU power capacity mix in 1995 considering a total of 532.213GW installed, (b) EU power capacity mix in 2010 considering a total of 877.9GW installed, (c)Increase/decrease of power capacity from 1995 to 2010 in percentage[2]

The future trends predict that the installed wind power capacity will keep increasing during the following years in order to obtain a higher wind energy penetration of the total electricity demand. In order to achieve this goal, political agreements play an important role in setting new directives and legislative actions. The 2009 Energy Directive of the European Commission fixed the 2020 goals in renewable energy sharing. It can be stated that it is the strongest directive ever established in the world encouraging renewable energy integration with the grid. The directive pointed out an increase of 11.4% in the total share of renewable energy from 2005(8.6%) to 2020(20%). Moreover, the European Commission settled the share for renewable energies in electricity consumption to be 34% as a 2020 target. Furthermore, according to wind energy penetration, it is expected that EU will be supplying 12% of its total electrical consumption by the end of 2020. Besides that, each Member State defined a National Renewable Action Plan (NREAP) with the purpose of determining the 2020 targets for each EU country. According to the NREAP, the 2020 predicted objectives regarding the wind energy share of electricity consumption per each EU Member State were introduced, as appears in Fig. 1-3. [2]

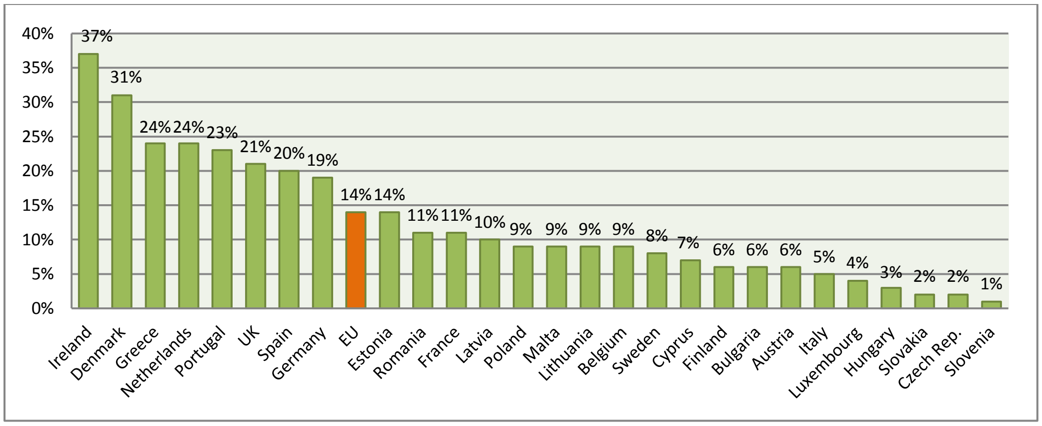

Fig. 1-3 Wind power share of electricity consumption per member state in 2020 according to NREAPs [2]

Therefore each country will be providing a percentage of the total power consumption. In Fig. 1-3 it can be observed that there are some countries such as for example Ireland (37%), Denmark (31%), Greece (24%), etc. which has extremely promising targets in wind power share of electricity consumption.

According to the integration levels achieved and considering the future goals fixed by the EU countries, it is expected to develop a high penetration of wind power, allocating large wind power plants of hundreds of MWs of capacity far away from the load centres, mainly where there is a high availability of wind resources. Furthermore, as it is mentioned in [2] offshore technology is a valuable candidate for the introduction of new large wind power plants. The wind farms of this size will usually be connected to the transmission network.

Due to the intermittence and fluctuating nature of the wind, the power quality and stability of the grid can be affected when high wind power integration is present. Therefore, high penetration level of wind energy (>30%) in to the power systems, which were build based on large synchronous generators, may lead to a convenient redesign of the power system [1]. As WPPs will tend to increase considerably its capacity, the impact of the disturbances introduced by such power plants into the network cannot longer be avoided and need to be limited. As a consequence, the transmission system operators (TSO) reinforced their grid connection demands. According to these rules, the WPPs are required to behave as conventional power plants, performing voltage and frequency control, regulating the generated active and reactive power during steady state and dynamic operation, and providing grid support in case it is needed [3].

In order to achieve these power plant characteristics and to overcome some of these grid code requirements, power electronic converters play an important role in WPPs, providing active control capabilities and improving their impact in power systems stability. Power electronic converters are able to provide several functionalities, which increase the electrical performance of the WPPs, such as control of active and reactive power generation, local reactive power supply (in case of weak grids), and improvement of wind parks power quality. However, as a main drawback, the use of power electronic converters generates harmonic currents injected to the grid [1].

Considering the above TSO restrictions, the main challenges introduced by high penetration of wind energy into the power system are related to the steady state and dynamic control capabilities of reactive power and voltage at the PCC, as well as keeping the power quality within the desired limits [4-6].

Nowadays, it has been experienced an increased awareness regarding the power quality of the grid mainly due to the high use of electronically controlled, energy-efficient equipment by many industrial power customers. This equipment is usually very sensitive to power quality disturbances, then, the apparition of voltage interferences may lead to miss operation and failure of the equipment, which is translated in quantitative economical losses [7]. Regarding wind energy production, the power quality concept defines the electrical behaviour of the wind power plant during its interaction with the grid. It determines the generation of grid disturbances introduced by the wind park and its impact in the power and voltage quality of the grid. Some of the main power quality problems that can be found in wind power plants are related to voltage variations and fluctuations and harmonic distortion in the case when wind turbines are connected to the grid through power electronic converters. The main causes of voltage variations and fluctuations arise due to the power changes introduced by the variable nature of the wind, and other wind turbine behaviour characteristics, such as tower shadow effect and switching operations of wind turbines (start-up or shutdown). [1][8].

It is worth to mention that power generation units can only control the voltage quality at their PCC, as the current quality will be determined by its particular loads. Therefore, it can be stated that any significant disturbance of the grid voltage will lead to potential power quality problems [7].

Finally, in order to determine if the power quality of the wind power plant stays between the allowed limits, the standard IEC 61400-21 ”Measurement and assessment of power quality characteristics of grid connected wind turbines” is widely used[9].

1.2 Problem Description

1.2.1 Impact of wind power plants in power systems voltage control

Traditionally, grid voltage was kept constant and close to the rated value, along all the nodes in power system by means of controlling the output voltage of large conventional power plants, which were usually based on fossil or nuclear energy sources.

In transmission systems, the power plants and compensation equipment control the node voltages by injecting or absorbing reactive power. The main aim of controlling the voltage is to avoid voltage variations, even when disturbances are present into the power system, limiting in this way the appearance of overvoltages and undervoltages.

Moreover, in the actuality, this traditional way of controlling the node voltages is being challenged mainly due to high penetration of wind generation systems, as large wind power plants connected to the transmission system are prone to introduce voltage variations at the PCC. Furthermore, the transmission system voltage control capabilities can be decreased even more in the case where conventional power plants, which were highly contributing to voltage regulation, are replaced by large scale wind parks. Therefore when the voltage control cannot be guaranteed any more between the allowed limits, (since existent voltage control capabilities are not sufficient to compensate the impact of wind power plants in the transmission system), additional measures will have to be taken [1].

In addition the voltage control capabilities of conventional power plants are decreasing mainly due to some recent developments of the transmission systems, such as unbundling and decentralisation. As a result, power plants are not any more performing voltage control as a natural part of their planning and dispatch. Therefore, in order to ensure this voltage control capability, grid companies required that power plants must have reactive power generation equipment enough for satisfying voltage control need (grid supporting) independently of the type of power plant or the applied technology. As a consequence, wind power plants, will have to contribute actively in performing voltage control, as any other type of generation units [10-12].

Furthermore, it can be stated that asynchronous generators are the most used wind turbine generator technology, as it provides robustness and cost – effective performance. Moreover, induction generators are potential consumers of reactive power, fact that introduce a considerable drawback in keeping a proper voltage quality and stability when such generator types are not connected to stiff grids. As a result, doubly – fed induction generators (DFIG) were introduced in order to overcome this reactive power balance. However, during transient operation mode, the DFIG may give rise to some voltage control capability problems, even forcing in some case to crowbar the rotor for protecting the converter from overload. Therefore, in this case, dynamic reactive power support may be needed by FACTS devices in order to improve the situation, as the behaviour of this generator type will be the same as a squirrel-cage induction generator [5].

Finally, another recent transmission system development specific to wind power is the trend to allocate wind power plants in remote areas or offshore, due to the high availability of wind resources and the reduced impact on the visual landscape. In this specific case where the wind power plant is grid connected through long AC cables, the need for controlling the voltage at the PCC is required. The global amount of reactive power needed will have to cover the wind power plant and the AC cable demands. Due to the fact that the voltage is a local quantity and the appearance of a voltage drop through the AC cable, the wind farm will have difficulties in providing dynamic voltage control capabilities, even if wind turbine technology has the ability of generating reactive power (DFIG and Full – Scale topologies). Therefore external reactive power compensation units such as FACTS devices may be needed at the PCC in order to actively contribute in dynamic voltage control [5].

1.2.2 Impact of wind power plants in power systems harmonic injection

The problems caused in power system by harmonics are not something new, as this topic has been discussed since the early 1920s. Nowadays the main harmonic sources are caused by an extensive use of nonlinear loads like: rotating machines, transformers, arcing devices (arc furnaces) and power electronic converters. As it can be observed in Fig. 1-4, during the last decades, a high increase in the use of electronic equipment has changed the composition of electrical loads. Due to power electronics evolution, every year the price of electronic components has a downward trend favouring their use in all branches.

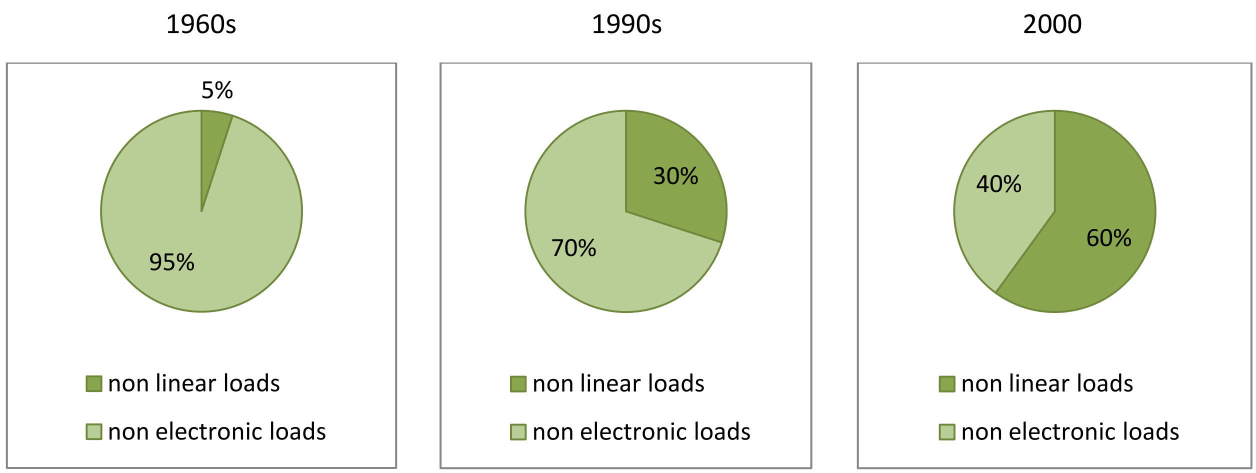

Fig. 1-4 Evolution of non-linear loads usage [16]

In the last couple of years it has been observed an increased dependence of the producers and consumers on equipment with nonlinear components (Fig. 1-4). This trend has a negative influence into the power system, as the amount of harmonics introduced into the grid is increasing [13].

In order to achieve a high productivity, power quality issues are of greatly importance under consumer point of view. However, from power producers side, the quality of the delivered power is the most important factor which is ensuring customer loyalty. Any producers do not want to face the responsibility of the customer equipment malfunctioning consequences. Therefore, in order not to disturb power system quality, harmonic voltages generated by the WPP must stay within the allowed standard levels described in EN 50160 [14]. The purpose of applying the previous guidelines is to keep controlling the harmonic voltages by comparing the total harmonic distortion THD provided by the WPP with the one specified in the standards [15].

Harmonics may have a harmful effect in power systems, causing a variety of undesired problems having a chain effect, reflected from economical point of view. The main problems generated by harmonics are summarized as follows [16]:

- Power system losses (heating) – results in a reduction in the efficiency of the generation, transmission and utilization of the electrical energy.
- Excessive heating in transformers and capacitors – life expectancy decreases causing the failure of the component.
- Under the electrical machines point of view, stator and rotor losses increase due to the flow of harmonic currents – pulsating torque and less efficiency. In case of a permanent magnet synchronous machine, excessive motor heating is accelerating the demagnetization of the magnets.
- Harmonics are accelerating the components aging which results in an increase of the maintenance costs.

- In resonant conditions (when the harmonic frequencies are close to the resonant frequency) harmonics magnitudes are amplified. Therefore, even a reduced amount of harmonics can have disastrous consequences to the system, causing equipment damage.

Finally, two main methods are available in order to mitigate the problems introduced by harmonics:

- PF – Passive Filtering
- AF – Active Filtering

In WPPs a large number of high power converters are usually used, therefore the generated output power contains a high level of harmonics. By applying one of the above mentioned methods (AF or PF), output harmonics can be alleviated in order to accomplish with the required power quality of the standards.

1.3 Objectives of the Project

In present, the high penetration of wind power into the power systems, which were traditionally build around large synchronous generators, may give rise to power quality and stability problems mainly caused by the fluctuating nature of the wind and the increasing complexity of the system. It is worth to point out that by implementing advanced functionalities in power converters, it is possible to improve the performance of the wind farms. Taking into consideration the fact that the main wind power plant compliance difficulties are related to reactive power compensation and keeping the harmonics content within the allowed limits, a control design of a three-level DNPC converter for high power applications will be implemented based on a STATCOM with Active Filter capabilities. Fig. 1-5 emphasizes with red dotted line the area of interest of this project.

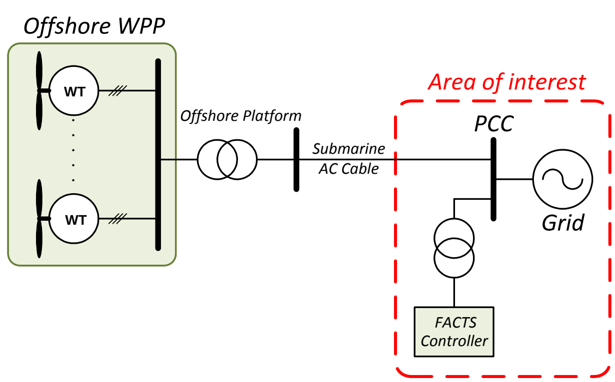

Fig. 1-5 General Schematic of the proposed system

In the proposed system, the quality of the PCC voltage will be improved by the injection or absorption of non-active currents for fundamental, 5th and 7th harmonic frequencies. The STATCOM operation mode, which is the main functionality, is responsible of the reactive power compensation and control of the PCC voltage by injecting or absorbing reactive fundamental frequency currents. Besides that the voltage quality at the PCC can be improved when the system is operating in the Active filter mode. In this way, the harmonic voltages can be mitigated by the control of 5th and 7th harmonic non-active currents. Finally, an advanced control strategy will be implemented, which combines both STATCOM and Active filter functionalities at the same time. In this case, the concept of Smart-STATCOM will be introduced, as depending on the grid voltage conditions the system is self-controlled, deciding at any instant the amount of compensation currents in order to provide maximum PCC voltage quality considering the limitations of the system.

Due to the fact that the system is considered for high power applications, the minimum switching frequency has to be properly selected in order to achieve high controllability for fundamental, 5th and 7th harmonic currents. According to the desired switching frequency and with the system specifications, a LCL filter will be designed.

The proposed system, depicted in Fig. 1-6, will be implemented in a laboratory setup based on a three-level DNPC converter connected to a grid simulator through an LCL filter. The grid simulator will be used to create the desired voltage quality disturbances at the PCC. The control algorithm will be implemented in a dSPACE DS1006 + DS5101 FPGA board by directly programming in C-code language.

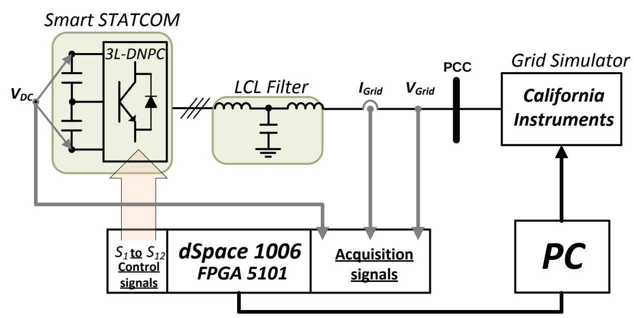

Fig. 1-6 Laboratory setup schematic of the proposed power conditioner system (STATCOM + AF)

1.4 Limitations of the project

During the development of the project, several limitations were considered. The most important limitations are presented as follows:

- The injection of rated harmonic reactive currents was limited due to the restriction of the dc-link voltage and filter parameters.
- Due to time limitations, the proposed control strategy could not be tested under unbalances and grid fault conditions.

1.5 List of Publications

1. A. Cantarellas, C. Sintamarean, Hector Beltran, “Control of a Three-Level Converter for Power Quality Improvement in Wind Power Plants”, *21st IEEE International Symposium on Industrial Electronics (ISIE), 2012.*

2. C. Sintamarean, A. Cantarellas, R. Teodorescu, P. Rodriguez, H. Miranda, “Smart-STATCOM Control Strategy Implementation in Wind Power Plants”, *3rd IEEE International Symposium on Power Electronics for Distributed Generation Systems (PEDG), 2012,* paper accepted.

2. State of the Art of VSI-based power conditioner for WPP applications

Firstly, this chapter presents an overview of the proposed grid connected converter topology in charge of providing power quality improvement for WPPs applications. Furthermore, in order to achieve the desired converter functionalities, the actual status of the applied control techniques are presented. Additionally the used grid synchronization and harmonic detection techniques are introduced. In order to provide or absorb a desired quantity of active or reactive power into the grid by using a power converter, special attention has been paid to the implementation of Instantaneous Power Theory. Finally, the proposed non-active power refer strategies, STATCOM and Active Filter, are introduced as a solution for improving the power quality of the PCC.

2.1 Overview of grid connected converters

Power electronics converters are divided in two main categories: voltage source converters (VSC) and current source converters (CSC). This project will deal with voltage source inverter (VSI) technology, as nowadays the use of this converter type is one of the most favourable solutions in terms of cost, physical size and efficiency [17]. Its main purpose (VSI) is to convert the DC input voltage into AC voltage with desired magnitude and frequency. Therefore the output parameters can be achieved by providing a suitable control and modulation strategy for the inverter switches. The VSI which allows the interaction with the grid is called "grid connected converter".

The number of inverter levels is given by the steps number in the output voltage with respect to any internal reference point. Three phase two level voltage source inverter (2L-VSI) is one of the most frequently used converter topologies. As it can be seen in Fig. 2-1 , a standard 2L-VSI is composed of two switches per phase. In order to avoid the dc bus short-circuit, the switches from the same leg are not allowed to be ON simultaneously [18] [19].

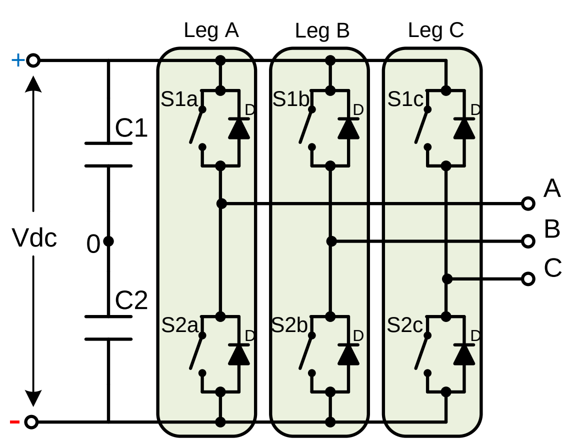

Fig. 2-1 Three-phase 2L-VSC topology schematic

By using this topology, the obtained output phase to neutral voltage, swings between –Vdc/2 and +Vdc/2, hence the name of 2L converter. Moreover, it is worth to mention that the main disadvantages are that each switch has to withstand full DC link voltage, high harmonic distortion and high dV/dt.

Nevertheless, these main drawbacks can be overcome by increasing the number of converter levels. Generally the multilevel converters can be found as 3LC, 4LC and 5LC topology. However, the 3LC is the most often applied in high-power medium-voltage applications.

Nowadays an increasing trend on developing 3LC has been experienced in order to improve the performance and reliability of the converter for high power applications. However this technology is not a novelty in power electronics. The concept of 3L-VSC can be carried out by the following three topologies: staked cells, flaying capacitor and neutral point clamped (NPC).

By using 3L-NPC a better solution can be applied in order to extend the voltage and power ranges and to achieve a superior output power quality compared with existing 2L-VSC technology. The main features of the 3L-NPC in comparison with 2L inverter are summarized in the Table 2-1 [18].

Two-level inverter	**Three-level NPC inverter**
The inverter terminal voltages swings between Vdc/2 and –Vdc/2, which implies higher dv/dt in comparison with 3L converter. ☒	The inverter terminal voltages swings between Vdc/2,0 and –Vdc/2, obtaining a lower dv/dt in comparison with 2L converter. ☑
Higher total harmonic distortion (THD) than 3L converter which implies a larger filter in the output of the converter. ☒	Lower total harmonic distortion (THD) than 2L converter which implies a smaller filter in the output of the converter. ☑
Each of the switches withstands full dc voltage during commutation. This issue implies higher voltage stress for switches comparing with 3LC. ☒	Each of the switches withstands only half of the total dc voltage during commutation. This implies lower voltage stress for switches comparing with 2LC. ☑
Lower number of components which implies a simple structure comparing with 3LC. ☑	Higher number of components than 2LC which implies a more complex structure. ☒
2LC cannot perform in high power range like 3LC. ☒	3LC can perform in higher power range than 2LC. ☑
Lower efficiency than 3L converter. ☒	Higher efficiency than 2L converter. ☑
Lower production cost than 3L converter. ☑	Higher production cost than 2L converter. ☒

Table 2-1 Comparison between 2LC and 3LC

Taking into consideration the advantages and disadvantages presented in the above table (Table 2-1), it can be stated that the use of the 3L-NPC is more suitable than 2LC regarding power quality issues. Therefore an improvement in the output power quality can be achieved by using 3LC instead the classical 2LC [15].

Among the 3L-NPC converters, two topologies can be distinguished: diode neutral point clamped (DNPC) and active neutral point clamped (ANPC). A generalized structure of a 3phase 3L-DNPC inverter is presented in Fig. 2-2. As it can be observed the inverter is composed of four active switches S1,S2,S3,S4 (with four antiparallel diodes - for the reverse current protection) and two clamping diodes D1,D2 per phase.

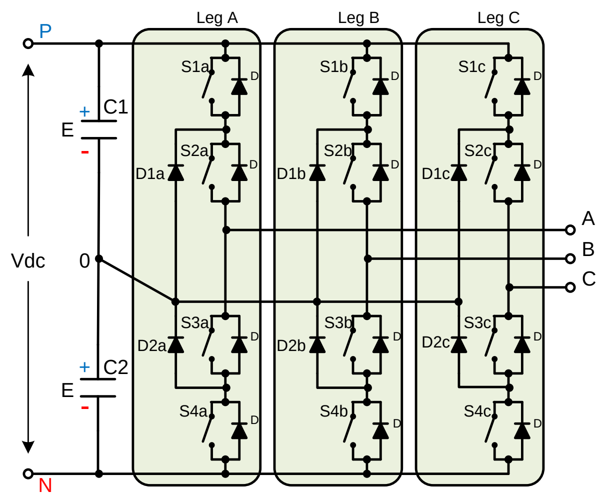

Fig. 2-2 Three-phase 3L-VSC topology schematic

The clamping diodes D1 and D2 are connected to the neutral point 0 obtained by splitting the DC bus capacitor into two series connected ones. Thus, the voltage across each capacitor (E) will be half of the main supply voltage Vdc. Further on the voltages at terminals A,B or C with respect to the neutral point 0 are called the inverter terminal voltages Va0,Vb0 and Vc0. If the inverter DC link is supplied with 700Vdc, in Fig. 2-3 it can be seen that the obtained inverter terminal voltages swings between +Vdc/2(+350V), 0 and –Vdc/2(-350V), hence the name of 3LC is given [18].

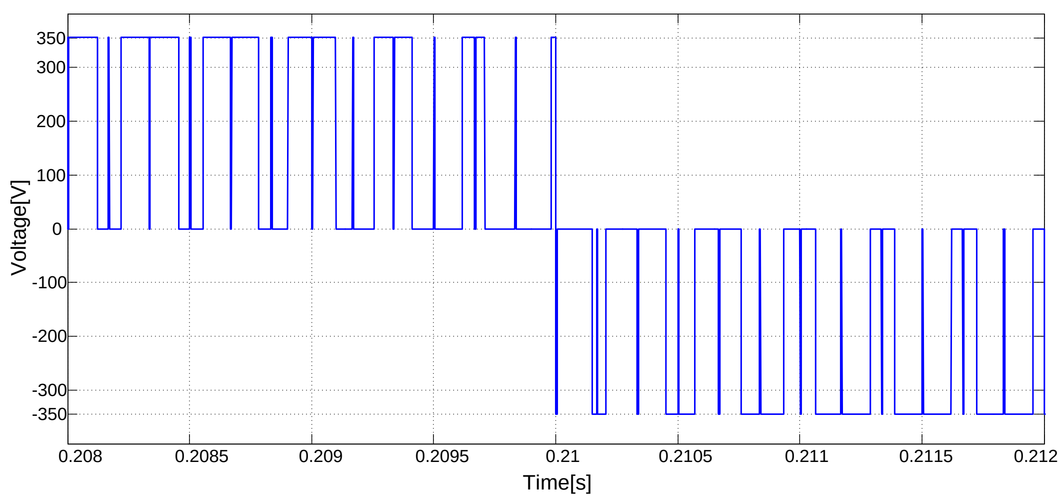

Fig. 2-3 Inverter terminal voltage in a 3L-VSC

In order to achieve the inverter terminal voltages presented above, the switching states must follow the table bellow (Table 2-2).

Switching state	Device Switching Status (phase A)				Inverter terminal voltage
	S1	S2	S3	S4	
P	*ON*	*ON*	OFF	OFF	+E
0	OFF	*ON*	*ON*	OFF	0
N	OFF	OFF	*ON*	*ON*	-E

Table 2-2 3L-VSC switching states

According to Table 2-2, the switching states for each leg are shown in Fig. 2-4 in order to achieve PON vector in the output:

- Positive (P)-If the two upper switches (S1 and S2) from leg A(B or C) are ON then the phase A inverter terminal is connected to the positive (P) bus of the dc link. Therefore, the inverter terminal voltage is Va0 = +E.
- Zero (0)- If the middle switches (S2 and S3) from leg B(A or C) are ON then the phase B inverter terminal is connected to the neutral point (0). So the inverter terminal voltage is Vb0 = 0.
- Negative (N)- When the lower two switches (S3 and S4) from leg C(A or B) are ON then the phase C inverter terminal is connected to the negative (N) bus of the dc-link. The inverter terminal voltage in this case is Vc0 = -E.

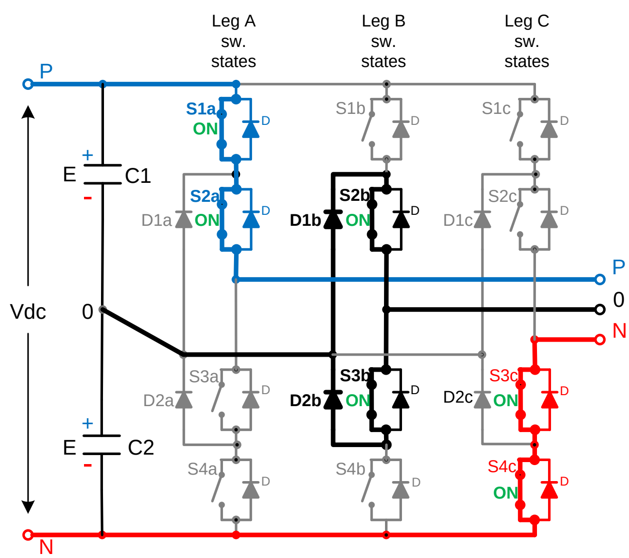

Fig. 2-4 PON vector paths in 3L-VSC

Taking into consideration that 3L-NPC inverter has three switching states (P,0 and N) per phase, it can be stated that there are 27 combinations of the possible switching states. In Fig. 2-4, one switching state is presented in order to achieve P0N vector.

The desired output waveform can be obtained by applying the appropriate switching sequence to the inverter switches. The modulation strategy methods applied for 3L-NPC inverter topology can be classified in two main categories:

- Carrier based methods
- Space vector modulation methods (SVM)

One of the main advantages of using a modulation method based on SVM, is that a higher output converter voltage can be obtained compared with the carrier based modulation methods.

It is worth to note that SVM is a widely used modulation method, as it provides a suitable set of duty-cycles with the purpose of accurately controlling a three-phase converter [18].

2.2 Overview of Control of Grid Connected Converters

This section presents an overview of the used control techniques dealing with grid connected converters for power quality improvement in WPPs. Taking into consideration that the proposed system deals with STATCOM and Active Filter functionalities, a special attention has to be carried out to the control structure implementation. Fig. 2-5 introduces the main control blocks which are used in achieving the desired converter functionalities. This section introduces a review of the current status for each of the control blocks which appear in Fig. 2-5, emphasizing in each specific case which are the most suitable techniques for achieving a high performance in the most cost effective way [19].

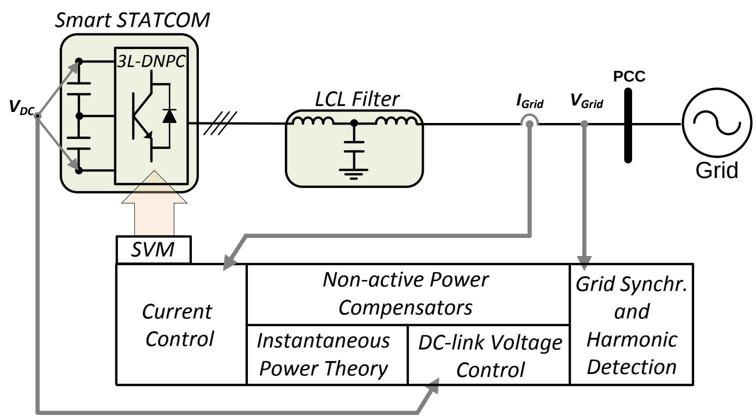

Fig. 2-5 Overview of grid connected converter control structure [19]

2.2.1 Grid Synchronization and Harmonic Detection Techniques

The synchronization with the PCC voltage waveforms is one of the main important issues when dealing with grid connected converters. By having a proper synchronization with the grid it is possible to stay actively connected in order to control the active and reactive power flow, supporting the grid services (voltage and frequency).

One of the main demands according with grid connected requirements is to stay actively connected and ride through any grid disturbances. Therefore, it is crucial to have an accurate and fast grid voltage synchronization technique, in order to perform under unbalanced and distorted conditions.

Nowadays, the main wide used methods for synchronization of the converters with the grid are based on PLL and FLL. In spite of its good performance under ideal voltage conditions, as the name is suggesting the PLL is phase variation sensitive, therefore the response is less accurate than in the case of FLL technique (frequency dependent), as the frequency is one of the strongest parameter of the grid.

Due to the above explanations, it has been decided to use a synchronization based on FLL technique. In this project a quadrature signal generator (QSG) based on a second order generalized integrator (SOGI) will be used when implementing the FLL grid synchronization method. The SOGI-QSG FLL diagram can be depicted in Fig. 2-6.

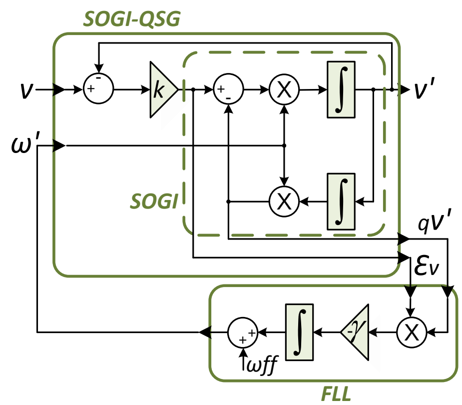

Fig. 2-6 The SOGI-QSG FLL control diagram [21]

In order to calculate the transfer function of the SOGI-QSG block, first of all the SOGI's transfer function has to be deducted. Therefore the SOGI's transfer function is obtained (2.1) by defining the input as $(v - v')k$ and v' as the output.

$$S(s) = \frac{v'}{(v - v')k}(s) = \frac{s\omega'}{s^2 + \omega'^2} \tag{2.1}$$

Finally the SOGI-QSG transfer function can be calculated in (2.2) when considering v as the input and the direct signal v' as the output.

$$D(s) = \frac{v'}{v}(s) = \frac{k\omega' s}{s^2 + k\omega' s + \omega'^2} \tag{2.2}$$

Applying the previous case, but considering now the quadrature signal qv' as the output, the SOGI-QSG transfer function has the following form (2.3):

$$Q(s) = \frac{qv'}{v}(s) = \frac{k\omega'^2}{s^2 + k\omega' s + \omega'^2} \tag{2.3}$$

In equation (2.3) k and ω' set the damping factor and resonant frequency respectively.

Once presented the SOGI-QSG, and showing that is possible to track the input signal, the only problem which has to be solved is to make it frequency adaptive. This goal is achieved by using the FLL structure. The diagram of the proposed FLL is depicted in Fig. 2-6, where the grid frequency is estimated by using an integrator controller which has the product of –qv' and the error εv as the input [19-21].

In these applications in which harmonics components should be selectively controlled a more precise characterization of the power signal is necessary. The proposed system relies on a STATCOM which is able to perform also as an Active Filter for 5th and 7th harmonics. Then the synchronization method used in this control strategy is based on a SOGI-FLL algorithm. Additionally, this grid synchronization method is able to detect the grid voltages if an individual SOGI for each of the harmonic frequencies is used. Therefore this synchronization and harmonics detection method is named MSOGI-FLL since it is based on multiple SOGIs, for fundamental, 5th and 7th harmonics, working together inside of a decoupling detection network which is frequency adapted due to FLL use.

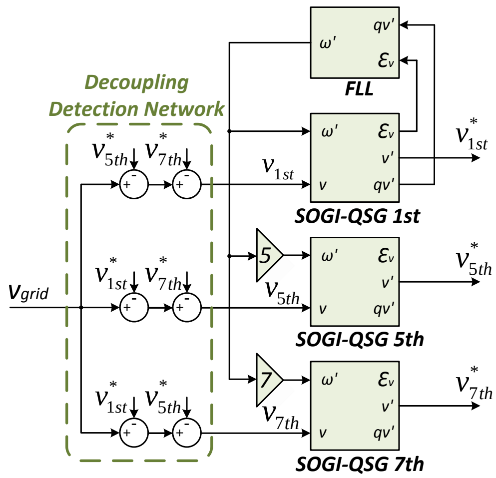

Fig. 2-7 The MSOGI FLL control diagram [22]

The FLL inputs are provided by the SOGI-QSG 1st block, which is tuned at the fundamental frequency. Multiplying the fundamental frequency detected by the FLL with constants (5 and 7) which emphasize the harmonic order, the tuning frequency of each SOGI-QSG is defined. In order to maintain a constant relationship between the centre frequency and the bandwidth, the gain of each SOGI-QSG 5th and 7th have to be calculated. Therefore by dividing the SOGI-QSG 1st gain by the harmonic order 5 and 7 respectively, the desired gains are obtained. As it can be seen in Fig. 2-7, the input voltage of each SOGI-QSG is determined by using a Decoupling Detection Network. Subtracting in this way the output (V^*) of all the other SOGI-QSGs from the original input signal (voltage measured at the PCC). Using this method, the input signal of each SOGI-QSG is cleaned up. Therefore a less distorted signal will be obtained in the output [22].

2.2.2 Current Control

The importance of implementing the current control structure relies on the necessity of controlling the injected currents into the grid within the desired dynamic conditions. Therefore an accurate injection of active and reactive power will be obtained by implementing a suitable current control strategy. This section introduces the main used current control techniques dealing with linear controllers.

Synchronous reference frame control strategy

The synchronous reference frame control strategy is based on the reference frame transformation of the control variables from natural (abc) to rotating reference (dq) frame, which uses the grid frequency as a rotational speed. Therefore, as the reference frame is rotating synchronously with the grid voltage vector, the control signals are transformed from AC to DC control variables. Furthermore, if the d axis is aligned with the grid voltage vector, the current injection on the d-axis (I_d), will generate active power, meanwhile the current injection in the q axis (I_q) will produce reactive power. In this control structure PI controllers are usually used, as it provides zero steady state error when controlling DC magnitudes. The PI controller transfer function is introduced in (2.4).

$$G_{PI}{}^{(dq)}(s) = \begin{bmatrix} K_P + \dfrac{K_i}{s} & 0 \\ 0 & K_P + \dfrac{K_i}{s} \end{bmatrix} \tag{2.4}$$

The general structure implemented when using synchronous reference frame current control is introduced in Fig. 2-8.

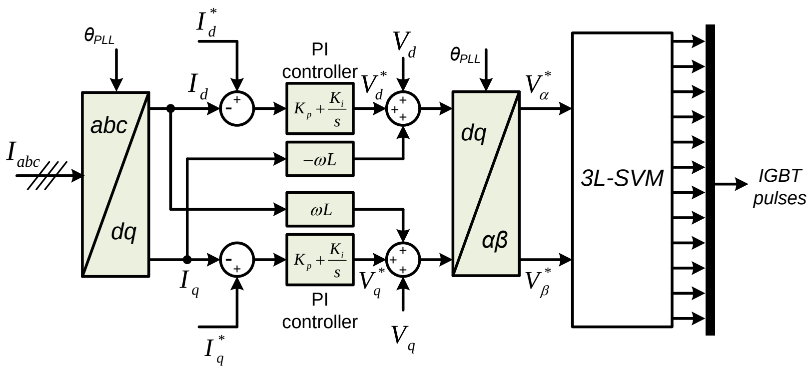

Fig. 2-8 d-q synchronous reference frame current control structure [23]

As it can be observed in Fig. 2-8, in order to obtain an accurate controller dynamics, the use of grid voltage feedforward and crosscoupling terms between the dq axes is needed. Furthermore, the phase angle estimation of the grid is required, as it is essential in obtaining DC signals from the synchronous frame transformation. Then a PLL structure is used in order to synchronize the current controller with the grid voltage. It is worth to mention that this control technique is phase voltage dependent, as in the case the phase detection is not accurately obtained, a poor current control performance will be achieved.

Another considerable drawback arise in the case when harmonic compensation is additionally required, as a control structure like the one in Fig. 2-8 would be needed for each of the desired harmonic frequencies. Furthermore, it is worth to mention that in case of unbalanced situations, both positive and negative sequence harmonic compensators are required, since the control structure appearing in Fig. 2-8 is able to control only one sequence for a desired frequency. Therefore, 4 current controller structures are needed in order to compensate 5th and 7th harmonics properly [23][19].

As a conclusion it can be stated that the main advantage of this current control strategy is the facility encountered in controlling DC signals by using PI controllers. Besides that, several reference frame transformations, feedforward voltages, crosscoupling terms, and the system complexity in compensating harmonics can be considered significant drawbacks due to the complexity of the system and its difficulty in implementing the control in low-cost DSPs [24].

In order to overcome some of the previously mentioned drawbacks, Proportional Resonant (PR) controllers are introduced for obtaining an accurate control in stationary reference frame.

Stationary reference frame control strategy

Another possibility that can be found in controlling the injection of grid currents is to implement the current controllers in the stationary reference frame ($\alpha - \beta$). Due to the incapacity of obtaining zero steady-state error when PI controllers are used in controlling AC signals, PR controllers are introduced in (2.5). In this case, zero steady-state error is achieved by providing infinite gain to a selected resonance frequency of the controller. In this case, the three phase control signals are transformed to the stationary reference frame by using the Clarke Transformation, which is introduced Appendix A.

$$G_{PR}{}^{(\alpha\beta)}(s) = \begin{bmatrix} K_P + \dfrac{K_i s}{s^2 + \omega^2} & 0 \\ 0 & K_P + \dfrac{K_i s}{s^2 + \omega^2} \end{bmatrix} \tag{2.5}$$

As it can be observed in Fig. 2-9, the complexity of the stationary reference frame current control implementation becomes lower than in the dq control structure, as dq transformations, crosscoupling terms and feedforward voltages are not needed any more.

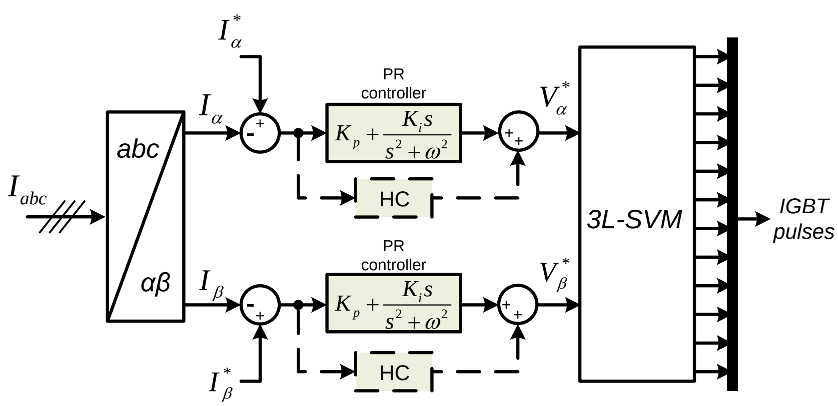

Fig. 2-9 α-β Stationary reference frame current control [23]

In this case, more robust control behaviour is obtained than in the dq-frame, as the accuracy of the controllers depends on the voltage frequency, which is one of the most stable parameters of the grid. Therefore it can be stated that this control structure is frequency dependent.

Another interesting feature of this current control technique is the ability of compensating harmonics by parallel implementation of resonant controllers, which are tuned to resonate at the desired harmonic frequencies. The Harmonic Compensators (HC bloc in Fig. 2-9) has the following transfer function:

$$G_{HC}(s) = \sum_{h=2}^{\infty} K_{ih} \frac{s}{s^2 + (\omega \cdot h)^2} \tag{2.6}$$

Where h is the harmonic order, K_{ih} is the integral gain of the controller and ω is the fundamental frequency of the grid. It can be stated that no interaction will be present between the parallel HC and the fundamental PR controller, by selectively tuning each of the resonant controllers to the specified harmonic frequencies. Furthermore, due to the fact that the resonant controller is providing infinite gain for ±ωh frequencies, both positive and negative sequence harmonic compensation is obtained. Therefore one HC bloc is needed to compensate the positive and negative sequences for each of the harmonic frequency currents [23][24].

As a conclusion it can be stated that the use of proportional resonant controllers becomes a successful solution in achieving current control capabilities, as it offers a simple control structure where high dynamics and harmonic compensation can be easily obtained by using a low computational effort. Therefore, PR controllers will be used in this project since a high current control performance can be achieved.

2.2.3 Instantaneous Power Theory

In order to provide or absorb a desired quantity of active or reactive power into the grid by using a power converter, special attention has to be given to the injected current.

The traditional theories regarding active, reactive and apparent power concepts were widely used since 1930s, as the three-phase system was mainly consisting of sinusoidal and balanced voltages and currents. Nevertheless, a discussion about the review of power calculation parameters appeared, as during the last century the power system experienced several considerable changes. Some of these changes came due to the large integration of power electronics and the consequent appearance of non-sinusoidal voltages and currents. Furthermore neutral current flow appeared as a consequence of voltage and current unbalances. Finally, new grid codes were introduced, mainly focus on the active and reactive power supplied in order to provide voltage and frequency grid support.

The aim of this section is to briefly introduce the main instantaneous power theories in order to obtain the needed reference currents which will determine the amount of active and reactive power injected to the grid [19].

The original p-q theory

The first definition of instantaneous power theory (p-q) which was well accepted in three-phase three-wire systems, was made by Akagi in 1983 [2papers from Akagi]. In this theory, the three-phase voltages and currents are considered as space vectors. Therefore, the three instantaneous voltage and current components in a-b-c reference frame (v_a, v_b, v_c and i_a, i_b, i_c) can be transformed into $\alpha - \beta$ coordinates (v_α, v_β and i_α, i_β) by using the Clarke transformation introduced in Appendix A [19] .

Fig. 2-10 shows the instantaneous space vectors proposed by Akagi, and it can be observed that the instantaneous imaginary power is perpendicular to the plane created by the alpha-beta axes, which is producing real power. It is worth to note that the instantaneous active power expressed in (2.7) is obtained by the multiplication between voltages and currents belonging to the same axis and its magnitude is measured in Watts unit [W].

$$p = v_\alpha \cdot i_\alpha + v_\beta \cdot i_\beta \tag{2.7}$$

On the other hand, the instantaneous reactive power (2.8), which was defined by Akagi as imaginary power, is the space vector resulting by the multiplication of the instantaneous voltage of one phase and the instantaneous current from another phase. In this case, Akagi proposed the “Imaginary Watts” as a measurement unit, but over the time volt-ampere reactive [Var] was adopted as a reactive power unit [25].

$$q = v_\alpha \times i_\beta + v_\beta \times i_\alpha \tag{2.8}$$

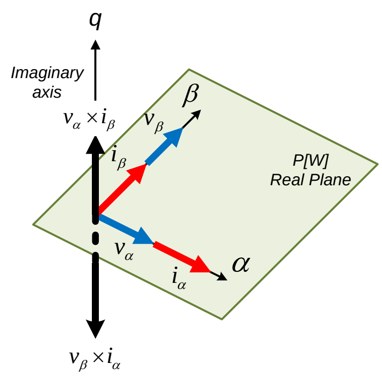

Fig. 2-10 Instantaneous space vectors [25]

In case a three-phase four-wire system is considered, zero-sequence voltage and current components are introduced to the previous expressions. Furthermore, the Clarke transformation from natural (abc) reference frame to stationary ($\alpha\beta0$) reference frame is given in Appendix A. Therefore, as it is shown in (2.9), four-wire systems introduce the additional instantaneous real power p_0 from the zero-sequence circuit together with the previously mentioned instantaneous active and reactive powers for the αβ axes ($p_{\alpha\beta}$ and $q_{\alpha\beta}$).

$$\begin{bmatrix} p_{\alpha\beta} \\ q_{\alpha\beta} \\ p_0 \end{bmatrix} = \begin{bmatrix} v_\alpha & v_\beta & 0 \\ -v_\beta & v_\alpha & 0 \\ 0 & 0 & v_0 \end{bmatrix} \begin{bmatrix} i_\alpha \\ i_\beta \\ i_0 \end{bmatrix} \tag{2.9}$$

Furthermore by adding both $p_{\alpha\beta}$ and p_0 the total instantaneous active power flowing in the three-phase system is given in (2.10).

$$p_{3phase} = p_{\alpha\beta} + p_0 = v_\alpha i_\alpha + v_\beta i_\beta + v_0 i_0 = v_a i_a + v_b i_b + v_c i_c \tag{2.10}$$

Afterwards, equation (2.11) can be deducted from equation (2.9) in order to obtain the instantaneous currents required to inject a determined amount of active and reactive power in to the grid.

$$\begin{bmatrix} i_\alpha \\ i_\beta \\ i_0 \end{bmatrix} = \frac{1}{|v|^2_{\alpha\beta} v_0} \begin{bmatrix} v_0 v_\alpha & -v_0 v_\beta & 0 \\ v_0 v_\beta & v_0 v_\alpha & 0 \\ 0 & 0 & |v|^2_{\alpha\beta} \end{bmatrix} \begin{bmatrix} p_{\alpha\beta} \\ q_{\alpha\beta} \\ p_0 \end{bmatrix} \tag{2.11}$$

$$i_\alpha = \frac{1}{|v|^2_{\alpha\beta}} v_\alpha p_{\alpha\beta} + \frac{1}{|v|^2_{\alpha\beta}} \left(-v_\beta q_{\alpha\beta}\right) \equiv i_{\alpha p} + i_{\alpha q} \tag{2.12}$$

$$i_\beta = \frac{1}{|v|_{\alpha\beta}^2} v_\beta p_{\alpha\beta} + \frac{1}{|v|_{\alpha\beta}^2}(v_\alpha q_{\alpha\beta}) \equiv i_{\beta p} + i_{\beta q} \tag{2.13}$$

$$i_0 = \frac{1}{v_0} p_0 \left(= \frac{1}{v_0} v_0 i_0 = i_0\right) \tag{2.14}$$

Where $|v|_{\alpha\beta}^2$ is $v_\alpha^2 + v_\beta^2$, $i_{\alpha p}$ is the alpha-phase instantaneous active current, $i_{\beta p}$ is the beta-phase instantaneous active current, $i_{\alpha q}$ is the alpha-phase instantaneous reactive current, $i_{\beta q}$ is the beta-phase instantaneous reactive current and i_0 is the zero-sequence instantaneous current. From the right side expression of equations (2.12), (2.13) and (2.14) it can be observed that the instantaneous currents are composed by a combination of active power and reactive power producing components. Then the following expressions can be derived [26]:

$$\begin{aligned} & v_\alpha i_{\alpha p} + v_\beta i_{\beta p} + v_0 i_0 \\ &= v_\alpha \left(\frac{1}{|v|_{\alpha\beta}^2} v_\alpha p_{\alpha\beta}\right) + v_\beta \left(\frac{1}{|v|_{\alpha\beta}^2} v_\beta p_{\alpha\beta}\right) + v_0 i_0 \\ &= p_{\alpha p} + p_{\beta p} + p_0 = p \end{aligned} \tag{2.15}$$

$$\begin{aligned} & v_\alpha i_{\alpha q} + v_\beta i_{\beta q} \\ &= v_\alpha \left\{\frac{1}{|v|_{\alpha\beta}^2}(-v_\beta q_{\alpha\beta})\right\} + v_\beta \left\{\frac{1}{|v|_{\alpha\beta}^2}(v_\alpha q_{\alpha\beta})\right\} \\ &= p_{\alpha q} + p_{\beta q} = 0 \end{aligned} \tag{2.16}$$

Where

- $p_{\alpha p}(v_\alpha i_{\alpha p})$ is the instantaneous active power in α-phase.
- $p_{\beta p}(v_\beta i_{\beta p})$ is the instantaneous active power in β-phase.
- $p_{\alpha q}(v_\alpha i_{\alpha q})$ is the instantaneous reactive power in α-phase.
- $p_{\beta q}(v_\beta i_{\beta q})$ is the instantaneous reactive power in β-phase.
- $p_0(v_0 i_0)$ is the instantaneous power in zero sequence-phase.

Moreover it is worth to point out that the previous equations ((2.12), (2.13) and (2.14)) were obtained under the assumption that $v_0 \neq 0$, otherwise in the case when $v_0 = 0$, the instantaneous currents cannot be obtained from the equation (2.11)[the theory of instantaneous power in three-phase four-wire systems: A comprehensive approach]. From the same equation, the zero-sequence instantaneous current can be set to zero by simply removing the last raw and column of the voltage matrix. As a result, the instantaneous αβ current references required to inject a determined amount of active and reactive power to the grid can be derived from the equation introduced in (2.17).

$$\begin{bmatrix} i_\alpha^* \\ i_\beta^* \end{bmatrix} = \frac{1}{|v|_{\alpha\beta}^2} \begin{bmatrix} v_\alpha & -v_\beta \\ v_\beta & v_\alpha \end{bmatrix} \begin{bmatrix} p_{\alpha\beta}^* \\ q_{\alpha\beta}^* \end{bmatrix} \tag{2.17}$$

In this case, the instantaneous power conservation principle can be achieved from equation (2.17) and assuming that $v_0 = 0$:

$$\left(v_\alpha{}^2 + v_\beta{}^2\right)\left(i_\alpha{}^2 + i_\beta{}^2\right) = |v|_{\alpha\beta}^2 |i|_{\alpha\beta}^2 = s^2 = p_{\alpha\beta}^2 + q_{\alpha\beta}^2 \tag{2.18}$$

However, according to equation (2.19) the instantaneous power conservation principle is not fulfilled in the case when $v_0 \neq 0$:

$$\left(v_\alpha{}^2 + v_\beta{}^2 + v_0{}^2\right)\left(i_\alpha{}^2 + i_\beta{}^2\right) = |v|_{\alpha\beta}^2 |i|_{\alpha\beta}^2 = s^2 \neq p_{\alpha\beta}^2 + q_{\alpha\beta}^2 \tag{2.19}$$

Several modifications of the p-q theory were appearing over the years, due to the existing mismatch in the power conservation principle where general conditions are applied [Appendix-B]. However, only the modified p-q theory is introduced here, as it is considered a suitable solution in overcoming the mentioned drawback [19].

The Modified p-q Theory

The modified p-q theory was first time introduced by Nabae in 1995 and it appeared as an improvement of the original p-q theory for three-phase four-wire systems. The modified theory is also dealing with instantaneous space vectors. Then, the three phase voltages and currents can also be transformed in $\alpha\beta0$ components by using the Clarke transformation (Appendix A). Considering the instantaneous currents and voltages the following instantaneous powers can be defined as:

$$\begin{bmatrix} p_{\alpha\beta0} \\ q_\alpha \\ q_\beta \\ q_0 \end{bmatrix} = \begin{bmatrix} v_\alpha & v_\beta & v_0 \\ 0 & -v_0 & v_\beta \\ v_0 & 0 & -v_\alpha \\ -v_\beta & v_\alpha & 0 \end{bmatrix} \begin{bmatrix} i_\alpha \\ i_\beta \\ i_0 \end{bmatrix} \tag{2.20}$$

Therefore if equation (2.20) is inverted, the instantaneous reference currents are obtained according to a desired active and reactive power injection set point. Additionally, as it can be observed in (2.21), each of the calculated currents will be dependent only on three independent power variables instead of four ones:

$$\begin{bmatrix} i_\alpha \\ i_\beta \\ i_0 \end{bmatrix} = \frac{1}{|v|_{\alpha\beta0}^2} \begin{bmatrix} v_\alpha & 0 & v_0 & -v_\beta \\ v_\beta & -v_0 & 0 & v_\alpha \\ v_0 & v_\beta & -v_\alpha & 0 \end{bmatrix} \begin{bmatrix} p_{\alpha\beta0} \\ q_\alpha \\ q_\beta \\ q_0 \end{bmatrix} \tag{2.21}$$

Where $|v|_{\alpha\beta0}^2 = v_\alpha^2 + v_\beta^2 + v_0^2$ and the $\alpha\beta0$ currents are introduced as follows:

$$i_\alpha = \frac{1}{|v|_{\alpha\beta0}^2} v_\alpha p_{\alpha\beta0} + \frac{1}{|v|_{\alpha\beta0}^2}\left(v_0 q_\beta - v_\beta q_0\right) \equiv i_{\alpha p} + i_{\alpha q} \tag{2.22}$$

$$i_\beta = \frac{1}{|v|_{\alpha\beta0}^2} v_\beta p_{\alpha\beta0} + \frac{1}{|v|_{\alpha\beta0}^2}\left(v_\alpha q_0 - v_0 q_\alpha\right) \equiv i_{\beta p} + i_{\beta q} \tag{2.23}$$

$$i_0 = \frac{1}{|v|_{\alpha\beta0}^2} v_0 p_{\alpha\beta0} + \frac{1}{|v|_{\alpha\beta0}^2} \left(v_\beta q_\alpha - v_\alpha q_\beta \right) \equiv i_{0p} + i_{0q} \tag{2.24}$$

Afterwards, as a result of the instantaneous currents calculation (equations (2.22), (2.23) and (2.24)), it can be observed that each of the currents is based on a combination of active and reactive current components. Consequently, the following expressions are valid [26]:

$$\begin{aligned} & v_\alpha i_{\alpha p} + v_\beta i_{\beta p} + v_0 i_{0p} \\ & = v_\alpha \left(\frac{1}{|v|_{\alpha\beta0}^2} v_\alpha p_{\alpha\beta0} \right) + v_\beta \left(\frac{1}{|v|_{\alpha\beta0}^2} v_\beta p_{\alpha\beta0} \right) + v_0 \left(\frac{1}{|v|_{\alpha\beta0}^2} v_0 p_{\alpha\beta0} \right) \\ & = p_{\alpha p} + p_{\beta p} + p_{0p} = p \end{aligned} \tag{2.25}$$

$$\begin{aligned} & v_\alpha i_{\alpha q} + v_\beta i_{\beta q} + v_0 i_{0q} \\ & = v_\alpha \left\{ \frac{1}{|v|_{\alpha\beta0}^2} \left(v_0 q_\beta - v_\beta q_0 \right) \right\} + v_\beta \left\{ \frac{1}{|v|_{\alpha\beta0}^2} \left(v_\alpha q_0 - v_0 q_\alpha \right) \right\} \\ & + v_0 \left\{ \frac{1}{|v|_{\alpha\beta0}^2} \left(v_\beta q_\alpha - v_\alpha q_\beta \right) \right\} = p_{\alpha q} + p_{\beta q} + p_{0q} = 0 \end{aligned} \tag{2.26}$$

Finally, by fulfilling the instantaneous power conservation principle, it can be stated that this modified theory is successfully dealing with three-phase four-wire systems independently on the zero-sequence current and voltage, as shown in (2.27) [19].

$$s^2 = |v|_{\alpha\beta0}^2 |i|_{\alpha\beta0}^2 = p_{\alpha\beta0}^2 + q_\alpha^2 + q_\beta^2 + q_0^2 \tag{2.27}$$

As a conclusion it can be stated that the original p-q theory and the modified theory are equivalent if a three-phase three-wires system is considered, i.e. when $i_0 = 0$ and $v_0 = 0$. As in can be observed in Fig. 2-11, the main difference between both aproaches is that the original instantaneous power theory is considering the zero-sequence as an independent single phase circuit. In this case only zero-sequence active power can appear in the circuit, as no instantaneous reactive power exists, since there is no energy exchange between the zero sequence and the other phases of the system.

In the case of the modified p-q theory, the zero-sequence circuit is treated in the same way as the α and β circuits. Therefore, the zero sequence is able to contribute in the instantaneous active and reactive power generation. As a consequence, the zero sequence current will be divided, as well as it occurs to the other phase circuits, in instantaneous active and reactive currents [26].

(a) (b)

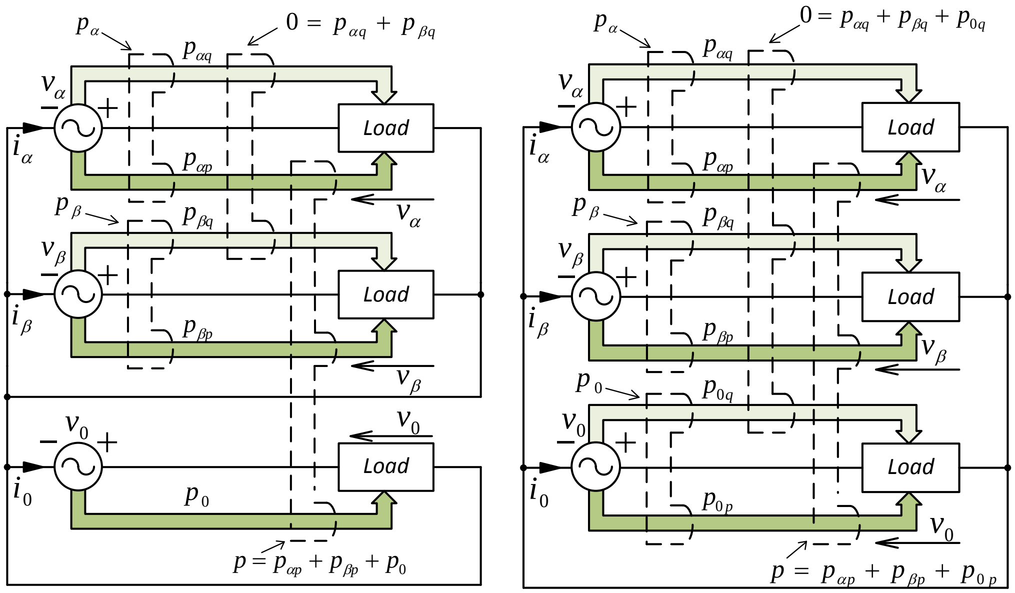

Fig. 2-11 (a) Original p-q instantaneous power theory circuit diagram, (b) Modified p-q instantaneous power theory circuit diagram [26]

The real and imaginary nature of the active and reactive powers can be observed from equations (2.15)-(2.16)-(2.25)-(2.26) and from Fig. 2-11 where the instantaneous active power is able of transferring energy from the source to the load, while the instantaneous reactive power represents the energy interaction between the phases of the three-phase system.

Finally, in 1996, a generalization of the Akagi's instantaneous p-q theory under distorted grid conditions was introduced by Aredes. In this case, the voltage and currents were defined as a sum of positive and negative sequences for each of the harmonic frequencies and the multiplication between these terms introduced a new concept of instantaneous active and reactive powers:

$$\begin{aligned} p &= \bar{p} + \tilde{p} \\ q &= \bar{q} + \tilde{q} \end{aligned} \tag{2.28}$$

In equation (2.28) it can be observed that the instantaneous active and reactive powers are composed by a constant and oscillatory terms. The first one ($\bar{p}$ and $\bar{q}$) is appearing as a result of the interaction between currents and voltages belonging to the same harmonic order and sequence while the second term ($\tilde{p}$ and $\tilde{q}$) appears from the combination of currents and voltages from different harmonic frequencies and sequences [19].

2.2.4 Voltage Control

Since the converter is performing without an external DC voltage source, the voltage control of the DC link is needed in order to achieve the required non-active currents controllability. Therefore, according with Fig. 2-12, the desired DC voltage can be obtained by regulating the active power exchange between the DC and AC sides of the converter [19].

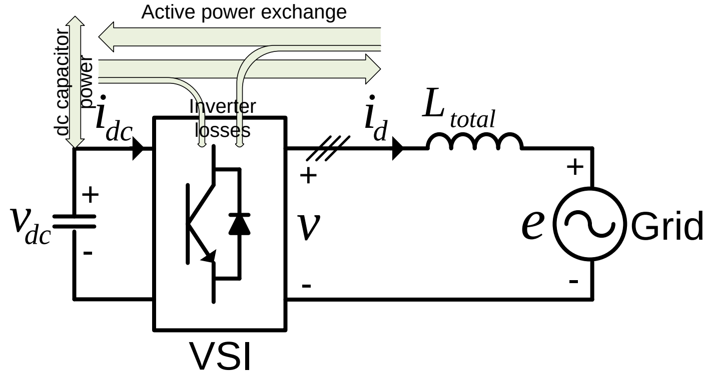

Fig. 2-12 Active power exchange between DC and AC sides of the VSC in order to control the DC link voltage

Furthermore, due to active power exchange between the converter and the grid (Fig. 2-12), dc voltage variations may appear [27][28]. Then, by properly controlling the charging and discharging processes of the dc link capacitors, dc voltage control is achieved. Therefore the regulation of the active power flow plays a key role in achieving the desired dc voltage controllability. Finally, a decrease or increase of converter dc voltage level is obtained by injecting or absorbing active power to/from the grid [29].

Furthermore the variation of the dc link voltage will be discussed from an energy perspective. The VSC energy equilibrium can be expressed as (2.29):

$$P_{fund}\Delta t + P_{harm}\Delta t - P_{loss}\Delta t = \Delta E \tag{2.29}$$

Where:

- P_{fund}- average active power at fundamental frequency
- P_{harm}- average active power at harmonic frequencies
- P_{loss}- system power losses
- ΔE- the amount of energy transferred from or to dc link capacitor in time interval Δt

Knowing that in steady-state operation the dc link voltage is constant, the variation of energy for every fundamental period is $\frac{\Delta E}{\Delta t} = 0$. As a consequence:

$$\begin{gathered} P_{fund} + P_{harm} - P_{loss} = \frac{\Delta E}{\Delta t} \\ P_{fund} + P_{harm} - P_{loss} = 0 \\ P_{fund} = P_{loss} - P_{harm} \end{gathered} \tag{2.30}$$

Taking into consideration (2.30) it can be stated that dc link voltage does not remain constant due to P_{loss} and P_{harm} . Therefore in order to keep it constant to the desired value, the active power at fundamental frequency P_{fund} has to be controlled by the VSI. The system losses mainly appear due to converter losses and filter losses. According with (2.31) P_{harm} is divided into two components [30]:

$$P_{harm} = P_{harm,dc} - P_{harm,ac} \tag{2.31}$$

Where:

- $P_{harm,dc}$ – is a constant component which has to be taken into consideration in dc link voltage control.
- $P_{harm,ac}$ – is a fluctuating component which causes ripple in the dc link voltage. It does not need to be considered in the dc link voltage control because its average value over the fundamental period is usually 0.Therefore $P_{harm,ac}$ can be neglected.

Further on the active power at fundamental frequency P_{fund} in steady-state operation can be presented instantaneously as (2.32) [31]:

$$P_{fund} = P_{loss} - P_{harm,dc} \tag{2.32}$$

By ignoring the losses P_{loss}, the assumption that the active power flow between grid and VSC is equal to the active power on the dc side can be done ($P_{ac} \cong P_{dc}$). Therefore $v \cdot i_d \cong v_{dc} \cdot i_{dc}$, where i_d is the instantaneous current component which produces active power.

Finally it can be stated that through regulation of the direct axis current i_d it is possible to control the active power flow in the VSC and thus the dc link voltage.

2.3 Overview of non-active current compensators

2.3.1 Reactive Power Compensation

Recently, grid integration of large-scale wind power plants has become a challenging task. As it was previously mentioned in chapter 1, high levels of wind power generation can affect the power quality and stability of the grid, since power systems were traditionally built around large synchronous generators directly connected to the grid. Therefore, as these disturbances cannot longer be allowed, TSOs tightened their grid connection demands in order to limit the harmful effect of the high penetration of wind power in the grid. As a result, wind power plants have to behave as conventional power plants, controlling the delivered active and reactive power and providing grid support, in case it is needed, by performing voltage and frequency control. Due to the fact that one of the main grid code compliance difficulties encountered in wind power plants are related to reactive power compensation and voltage control capabilities, external reactive power compensation units such as FACTS devices may be needed at the PCC in order to ensure a dynamic voltage control of the WPP [32]

Flexible AC Transmission Systems (FACTS) and their controllers were introduced in first instance by Hingorani in 1988 [33]. The main functionality of this technology was to enhance the performance of conventional power systems controllers (mechanically switched passive components) by introducing power electronic devices. FACTS controllers provide the capability of dynamically control several power system parameters such as series impedance, shunt impedance, voltage, current, phase angle, etc. obtaining in this way a fast controllability over the active and reactive power flow in a transmission system [34]. Several of the applications where FACTS devices can be located are: power flow control, increase in transmission capacity, voltage control, reactive power compensation, power quality improvement, power conditioning, flicker mitigation, interconnection of renewable generation and storage devices, etc. [35].

In Fig. 2-13, two columns can be easily differentiated between the conventional (mechanically switched) and its correspondent FACTS (static) devices used in controlling transmission system parameters. The main difference between these methods is that from one side, the conventional devices are based on switching in or out passive components such as resistors, inductors, capacitors and transformers by using mechanical switches. On the other hand, FACTS devices switch these elements as well, but by means of using additional power electronics in order to obtain a faster and more accurate performance during steady state and dynamic conditions. With FACTS devices, switching aging of mechanical switches is considerably reduced and therefore a higher dynamic controllability can be achieved [34]. At the same time, FACTS devices can be based on thyristor valves or on the use of voltage source converters (VSC) switching technology. The main advantage in using VSC is that full controllable voltage magnitude and phase can be achieved by using modulation techniques for power electronic devices with turn-off capabilities (GTO thyristors, IGBTs, IGCTs, etc.)[35].

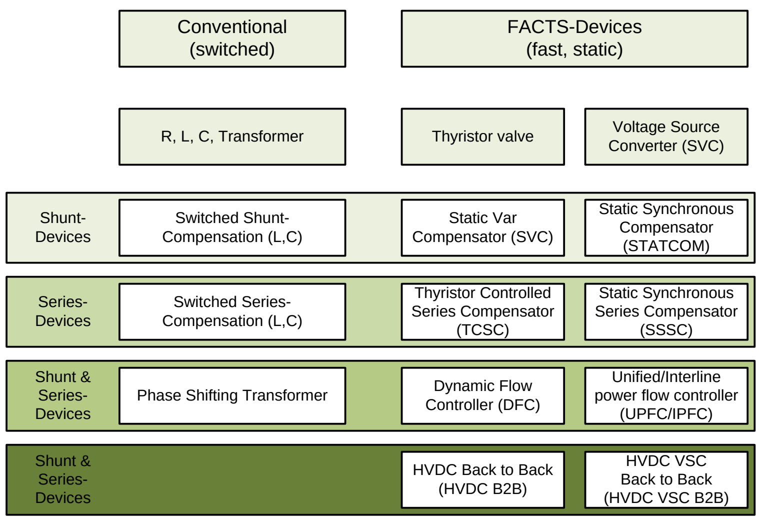

Fig. 2-13 Classification of FACTS Controllers according to their connection and semiconductor devices-type[35]

Another way of FACTS controllers' classification depends on their connection-type within the transmission system. Therefore, in Fig. 2-13 it can be observed that the devices from each column can be found in series, shunt and shunt-series connected with the power system. In the case that current/power flow and damping of the oscillations is needed, the series connection of the FACTS controllers is preferred. On the other hand, shunt connection would be the best solution in case the voltage control at the PCC is pursued, as it would be achieved by injecting reactive power to the connection point. Therefore, series controllers are the most suitable in providing power flow control meanwhile shunt devices provides voltage control at the PCC in a most effective way. Finally, FACTS devices can be found in a combination of shunt-series connection. In this case, the best performance is achieved as it combines all the benefits from both controllers. However, the main problems of these controllers are their high cost [33].

Wind power plants are one of the main applications where FACTS devices can be allocated, by means of using SVC or STATCOM devices as external reactive power compensation and voltage control at the point of connection. As a result, most of the wind power plants can fulfil the grid code requirements.

As one of the topics of this project deals with the use of FACTS devices for WPP applications, the main shunt connected FACTS controllers are presented in the following sections.

Static Var Compensator – SVC

The main characteristic of the Static Var Compensator is that they are built up using thyristor switches, controlling in this case the voltage at the point of connection much faster than mechanical switched passive components (L, C). The SVC is able to inject controllable inductive and/or capacitive output current in order to inject or absorb reactive power. As a consequence of this dynamic reactive power control, the voltage at the PCC is continuously controlled. There are three possible SVC configurations: Thyristor Switched Capacitors (TSC), Thyristor Controlled or Switched Reactors (TCR/TSR) or a combination of both, as it can be observed in Fig. 2-14. It can be stated that the main difference between TCR and TSC are that the first one is continuously controlled by providing the desired firing angle of the antiparallel thyristors, while in the second one the capacitor is just switched on and off. Therefore, by properly controlling the conduction periods of each of the thyristor switches, reactive power compensation can be obtained over a wide range. In Fig. 2-14, the voltage/current characteristic of the SVC is introduced. It can be observed that a determined amount of capacitive or inductive currents will be injected depending on the voltage of the connection point. The slope or droop characteristic around the rated voltage determines the voltage control capability, as if there is a high slope the SVC will be able to control the voltage over a wider range and vice versa.

The main disadvantage of this shunt compensation equipment is the linear relationship between the grid voltage and the current injection capability. Therefore in case of a severe grid voltage drop, the SVC would not be able to inject reactive current, as it is required in order to support the grid under fault conditions.

In order to overcome some of the main SVC technology limitations such as slow time responses, poor dynamic performance and strong relationship between the injected current and the bus voltage, Static Synchronous Compensators (STATCOMs) are introduced as an improved solution in controlling the PCC voltage [5].

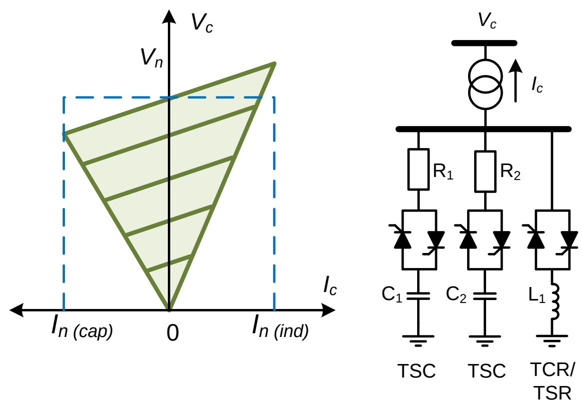

Fig. 2-14 SVC voltage/current characteristic and SVC configurations [5]

STATic synchronous COMpensator – STATCOM

A STATCOM is a shunt FACTS device based on voltage sourced converter technology (VSC), which main purpose is to perform reactive power compensation and voltage control at the PCC. These objectives will be accomplished by injecting or absorbing controlled reactive current to the grid. STATCOM technology can be treated as an ideal synchronous voltage source, as it is capable of generating a three phase voltage with controllable magnitude and phase at its output.

The operating principle of the STATCOM can be described in Fig. 2-15. It will be assumed that the shunt compensator is connected to the grid through an inductance, as it can be seen in Fig. 2-15 (a) and (c), and also that the grid voltage amplitude remains constant and in phase with the compensator voltage (lossless line). In this way, two main operation modes can be clearly defined depending on the sign of the generated current[4]:

- Reactive power absorption- in the case when the converter voltage magnitude is smaller than the grid voltage. Then the voltage drop across the inductor has opposite sign than the converter voltage, therefore the reactive current is flowing from the grid to the STATCOM consuming in this way reactive power (Shown in the phasorial diagram of Fig. 2-15(d) in the inductive operation mode).
- Reactive power generation- a STATCOM has the ability of producing reactive power when its terminal voltage magnitude is greater than the grid voltage. In this way reactive power would be supplied to the grid, as the voltage drop across the line inductor has the same sign as the grid voltage and consequently a positive current (according to the sign criteria adopted in Fig. 2-15 (a) and (c)) is flowing through it. (Shown in the phasorial diagram of Fig. 2-15(d) in the capacitive operation mode).

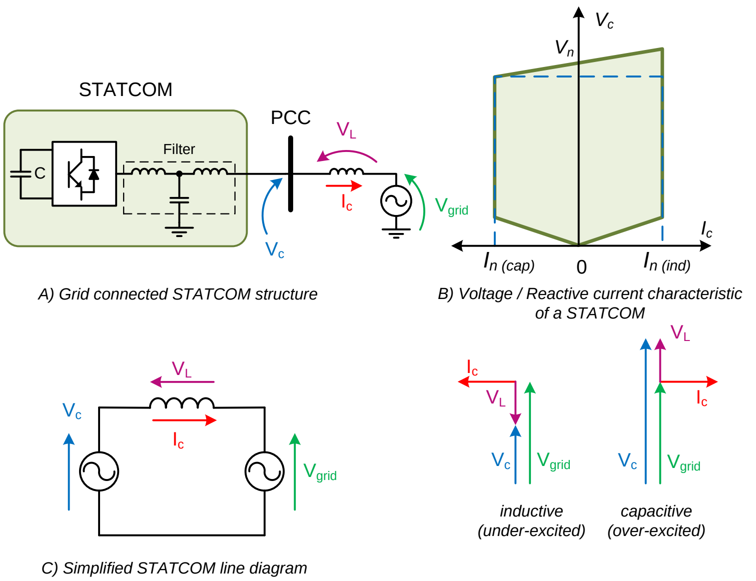

Fig. 2-15 a)Grid connected STATCOM structure, b)STATCOM voltage/current characteristic and c) Simplified STATCOM line diagram and phasorial analysis [5]

The voltage/current characteristic of the STATCOM controller is depicted in Fig. 2-15 (b). It can be observed that the steepness of the slope around the rated voltage is determined by the droop characteristic, e.g. for a greater slope the controller is able to provide reactive power compensation for a wider range of grid voltages. This voltage droop will determine which is the maximum allowable grid voltage variation. Thus, once the maximum voltage variation (typically between ± 0.05pu) has been reached, the STATOM will be providing full reactive power injection or absorption. One of the main advantages that STATCOM provides compared with the SVC is that the reactive current injected is not dependent on the PCC voltage, being able in this case to provide maximum reactive power compensation even under the most severe grid conditions [35].

As this project deals with the implementation of a STATCOM controller for power quality purposes in wind parks, it is worth to point out which are the main functionalities that this FACTS device can provide to the WPP in order to enhance its performance [4]:

- Reactive power compensation under steady state conditions. The reactive power can be provided as a result of a desired reactive power reference, according to a desired output power factor, or according to a specific linear Q/V characteristic function.
- As a consequence of the previous functionality, the PCC voltage can be controlled. It is often appearing in the grid codes as one of the main requirements.
- The compensator output is performing smooth variations, e.g. not stepwise behaviour is obtained, as it is in the case of mechanically switched passive elements.
- It provides a fast dynamic response.
- In case a grid fault is present, STATCOM technology is able to provide maximum reactive power as it is required by the grid codes.

2.3.2 Active Power Filtering

The problems caused by power system harmonics are not something new, this topic have been discussed from the early of 1920's. Nowadays the main harmonic sources are caused by the nonlinear loads like: rotating machines, transformers, arcing devices (arc furnaces) and power electronic converters [17][13]. Due to electronics evolution, every year the price of electronic components has a downward trend favouring their use in all branches. The main users of equipments with nonlinear components can be divided into three groups according with the following table:

Harmonic sources	Main harmonics producer devices	Voltage level applications
Power producer companies (WPP)	Power electronics converters (Ac-Ac) used in wind turbines control	MV-HV
Industry consumers	Power electronics converters (Ac-Ac) used in adjustable speed drives	MV-HV
Home appliances	Ac-Dc converters used in power supply for electric equipments	LV

Table 2-3 Main users of nonlinear loads equipments [16]

Taking into consideration the Table 2-3 presented above, it can be stated that power converters (rectifiers and inverters) are one of the main responsible for the harmonics generation which are troubling power system. The harmonics topic showed an increased interest in the last years since the nonlinear devices cannot be replaced with other type of equipments, having a well defined place in today's technology [36]. The main users of nonlinear components are the industrial consumers and the power producer companies (Table 2-3) [16]. Further on, Fig. 2-16 briefly emphasizes the harmonics propagation into the power system by taking into consideration the WPP, the industrial consumers and the home appliances. Depending on the highest harmonics source and on the distribution system impedances, two main situations may arise:

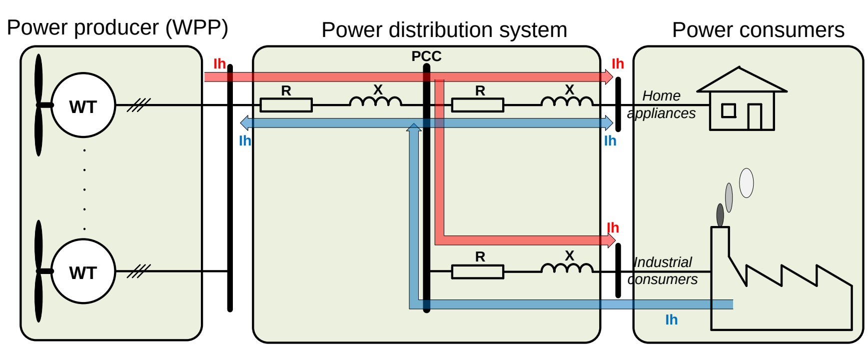

Fig. 2-16 The harmonics propagation into the power system by taking into consideration the WPP, the industrial consumers and the home appliances.

- For the first situation it's considered that the highest harmonic sources are provided by the WPPs. In this case, according with Fig. 2-16, the harmonics flowing directions are marked with red line.

- In the second situation the higher harmonics levels are generated by the industrial consumer. Depending on the distribution line impedances, harmonics can flow into two directions, which are emphasized with blue line.

As a conclusion, it can be stated that in both cases home appliances may be affected by the harmonics. Therefore, even if a consumer is not producing harmonics, it can be affected by other consumers or power producers. Harmonics currents flow through the distribution system seeking the low impedance path. As a consequence, in many cases, industrial consumers were found to be the main responsible for the harmonics sources which affected home appliances.

In order to achieve a high productivity, power quality issues will be taken into account, from consumer point of view. Moreover, from power producer side, the most important factor which ensures customer loyalty is the quality of the delivered power. Any producers do not want to face the responsibility of the customer equipment malfunctioning consequences [15]. In order to mitigate the problems introduced by harmonics, there are two main methods available:

- PF-passive filtering
- AF-active filtering

In WPPs a large number of high power converters are used, therefore the generated output power is distorted by harmonics. By applying one of the above mentioned methods (AF or PF), the injected harmonics can be alleviated in order to accomplish with the required power quality standards.

Passive filters are made of passive components like capacitors, inductors and resistors. They can be usually found connected in parallel, series or in a combination of both (parallel-series) with the non-linear loads/sources.

Taking into consideration that PF are built of passive components, it may cause parallel/series resonance with the system impedance. Due to the system impedance variation, the designed PF resonance frequency varies, making them less effective. Therefore PFs have to be carefully designed. Another important issue which slightly influences PF resonance frequency is the filter parameters variation. This variation has three main causes [17][19]:

- Design tolerance-C (from -5% to 10%) and L (from -3% to 3%)
- Temperature-C (from -2% to 2%) and L (slight variation if the inductor has an air core)
- Aging

Engineers should perform elaborate investigations, before installing passive filters, regarding the possibility of harmonic resonance. Depending on the system complexity, these investigations may arise to relatively high engineering costs. Taking into consideration the main drawbacks presented above, it can be stated that PF may not be the optimal method of dealing with harmonic problems in a complex system. In order to overcome the passive filters drawbacks presented above, active filters may be used.

The active filter (AF) technology is not a novelty, since its basics were clearly defined in 1970's. However, this technology has attracted the attention of power electronics engineers starting only from the recent years, in order to solve the harmonics problems in complex power systems. The Active Filters are based on power electronics converters, and three main categories can be distinguished depending on their connection type to the distribution system:

- Series active power filters-operate as a controllable voltage source
- Shunt (parallel) active power filters-operate as a controllable current source
- Series-Shunt active power filters-are a combination between shunt and series active filters

The shunt active filter, as the name is suggesting, is connected in parallel with the harmonic source, the wind power plant in the studied case (Fig. 2-17 c). The main purpose of the shunt active filter is to inject equal but opposite harmonic compensation current than the harmonic components generated by the WPP. In the following figure, it can be seen that the WPP is injecting a distorted current, which is emphasized with red signal. Therefore, in order to avoid the grid pollution, an active filter is used. As it was previously stated, the AF will inject the needed current (blue signal) in order to counteract the harmonics produced by the WPP. As a result a current with a low harmonic level (green signal) is flowing to the grid. In this case the power quality is improved, by reducing the THD in order to fulfil the grid codes requirements [15, 17, 36].

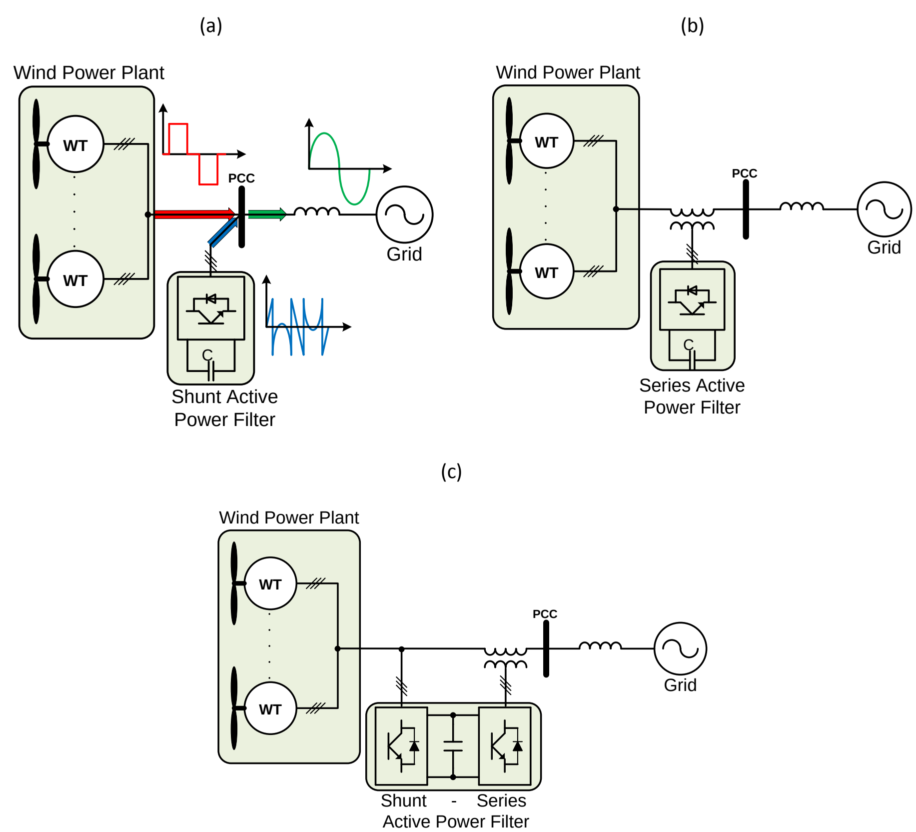

Fig. 2-17Main Active Power Filters connection types: a) Shunt connected AF, b) Series connected AF, c) Shunt-Series Connected AF [15, 36]

As it can be seen in Fig. 2-17 b, the active filter is connected in series with the harmonic source (WPP). The main operation principle of series active filter consists in generating a voltage which has the same frequency and magnitude with the harmonics source voltages generated by the WPP. Therefore a high impedance path is imposed to the current harmonics that needs to be eliminated by the series active power filter. As a conclusion, it can be stated that low harmonic currents will flow from the WPP to the grid.

Finally, Fig. 2-17 c introduces the case when shunt and series connection of the active filters is combined. Therefore, it is providing current filtering (by using shunt active filter) and voltage filtering (by using series active filter). Despite the fact that this configuration is providing the highest power quality performance, it is not attractive from economical point of view.

In the last years several companies have focus their work on power line conditioners in order to improve the power quality of the system [15, 17].

Shunt Active Filter based on voltage detection method

The shunt active filters can be classified depending on their detection signal into two main categories:

- Shunt Active Filters based on current detection
- Shunt Active Filters based on voltage detection

This project deals with a Shunt Active Filter based on voltage harmonics detection method. The use of this approach has been selected as it is a suitable solution in solving electrical power utility problems [AK]. In the studied case, the purpose of the active filter is to damp out the 5th and 7th harmonic voltages produced by the WPP in order to keep them within the allowed limits required by the grid codes [14]. Hence by absorbing 5th and 7th non-active currents the mitigation of harmonic voltages is achieved. Therefore the power quality delivered from the WPP to the grid can be improved.

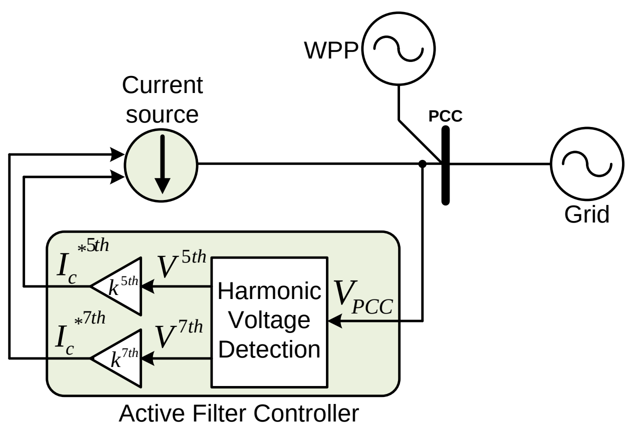

Fig. 2-18 Compensation principle of the Shunt Active Filter based on voltage detection [36]

The compensation principle of the shunt active filter based on voltage detection can be depicted in Fig. 2-18. As it can be observed, the active filter detects the voltage harmonic content at the PCC ($v_{PCC} = v^{1st} + v^{5th} + v^{7th}$), afterwards the compensation current i_c^* is injected according with (2.33).

$$
\begin{aligned}
i_c^{*5th} &= k^{5th} \cdot v^{5th} \\
i_c^{*7th} &= k^{7th} \cdot v^{7th}
\end{aligned}
\tag{2.33}
$$

Where k^{5th} and k^{7th} are the control gains of the Active Filter Controller.

Taking into consideration the above equations, it can be stated that, from external circuit point of view, the active filter has a “resistor” behaviour (1/k) for all harmonic frequencies (5^{th} and 7^{th}). Hence the compensation currents are obtained by considering the detected 5^{th} and 7^{th} harmonic voltages. It is worth to mention that for fundamental frequency, the active filter behaves as an “infinite impedance”, thus having no contribution to the “external circuit” [36].

Therefore, from control point of view an active filter based on voltage detection consist of a feedback control loop between the detected harmonic voltages and the compensation currents.

3. Modeling and Control Design of the Proposed System

This chapter introduces the overall control design of the proposed power conditioner in order to achieve the desired functionalities (STATCOM, Active Filter and Smart STATCOM). Firstly, an accurate model of the system (3L-DNPC and LCL-filter) is required, as a more realistic approach to the laboratory setup behavior will be obtained. Afterwards, the design of the current controllers for each of the desired compensation frequencies (50Hz, 250Hz and 350Hz) is introduced. Furthermore, the voltage controller design is performed in order to keep the DC link voltage constant at the desired value. Additionally, the proposed non-active power reference strategies are presented, which main purpose is to operate under STATCOM and Active Filter operation mode. A novel control strategy is proposed, which simultaneously combines the implementation of STATCOM and Active Filter functionalities in order to provide maximum power quality at the PCC. Finally the simulation results are discussed in order to validate the performance of the control design. In simulation, the control has been implemented in C-code by using S-Function Builder blocks from Matlab/Simulink. The C-code of the controllers is introduced in Appendix B and Appendix C.

3.1 System Modeling

In order to obtain a performant control of the laboratory setup, an accurate system modeling is needed. This section presents the model implementation of 3L-DNPC grid connected converter through an LCL-filter. Additionally the LCL-filter has been designed and successfully modeled according to the desired control specifications. Finally, as it can be depicted in Fig. 3-1 the overall system simulation has been performed by using Matlab/Simulink and Plecs toolbox.

3.1.1 3L-DNPC converter description model

The proposed system, modelled in Fig. 3-1, consists of a three-level DNPC converter connected to the grid, which main purposes are reactive power compensation, control of the PCC voltage and mitigation of the main harmonics produced by the WPP (5^{th} and 7^{th}).

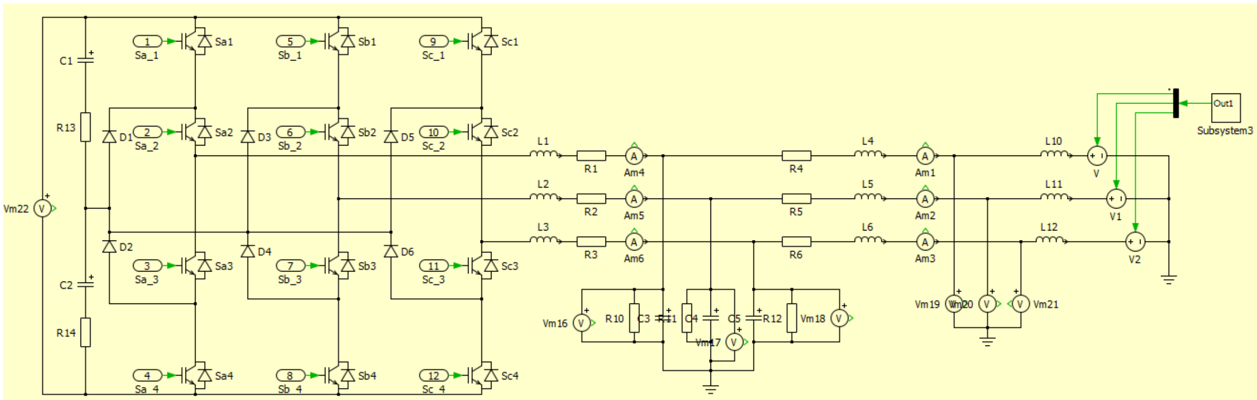

Fig. 3-1 Plecs modelled DNPC converter connected to the grid through an LCL-filter

In order to properly simulate the laboratory setup behaviour, special attention has to be given to the following parameters of the physical setup:

- Converter rated power: S = 20kVA
- Rated grid voltage (L-L RMS): V_{grid} = 400V
- Converter rated current (RMS): I_{conv} = 30A
- DC-link voltage: V_{DC} = 700V
- Switching Frequency: F_{sw} = 3kHz

Due to the fact that the proposed system is designed for high power applications, the use of a three-level converter is necessary, as it allows connection to higher voltage ranges (than 2L converter), in order to achieve high control performances for 5^{th} and 7^{th} harmonic using low switching frequency. As a consequence, a lower THD is obtained and a filter of smaller dimensions is required [15, 18]. Taking [18] into consideration, the used switching frequency for a 2LC should be at least ten times bigger than the highest harmonic bandwidth that has to be controlled. Due to the fact that the necessary switching frequency for controlling a certain harmonic bandwidth in 3LC is lower than in 2LC, the starting point in choosing the switching frequency was selected to be 3.5kHz (3.1).

$$F_{sw} = 10 \cdot f_{7th} \tag{3.1}$$

Where:

- F_{sw} – converter switching frequency
- f_{7th} – is the 7^{th} harmonic frequency(350Hz)

By testing the system performance it has been observed that the minimum switching frequency required, in order to achieve high controllability in 7^{th} harmonic voltage compensation, is 3kHz.

In order to obtain the desired converter behaviour, a suitable set of duty-cycles has to be provided to the IGBTs. Therefore, in this specific case space vector modulation (SVM) is used. As it was stated in section 2.1, the operation of each inverter leg can be represented by three switching states P,0 and N. Taking into consideration that is a three phase converter (which implies the use of three legs), a total of 27 possible combinations can be achieved. In Table 3-1 the 27 possible combinations of switching states are listed. According with the mentioned table, the v_α and v_β voltages are calculated by using (3.2).

$$\begin{bmatrix} v_\alpha \\ v_\beta \end{bmatrix} = \frac{2}{3}\begin{bmatrix} 1 & -\frac{1}{2} & -\frac{1}{2} \\ 0 & \frac{\sqrt{3}}{2} & \frac{\sqrt{3}}{2} \end{bmatrix} \cdot \begin{bmatrix} v_{aN} \\ v_{bN} \\ v_{cN} \end{bmatrix} \tag{3.2}$$

It is worth to mention that several combinations are redundant, producing the same voltage vector at the output of the converter (Table 3-1 from V_1 to V_6). In addition the 0 output voltage can be achieved by applying one of the three voltage vectors (PPP, 000 or NNN). Therefore it can be stated that 19 active voltage vectors can be applied to the three-phase system.

Taking into consideration that the main harmonic standards have more restrictive requirements in limiting the even current harmonic injection into the grid, this project deals with the use of even harmonic cancellation SVM technique. Fig. 3-2(a) emphasizes with the depicted arrows the voltage vector sequences that should be followed in order to achieve desired purpose [18]. By dividing the α-β plane in sectors of 60^0, six different sectors are obtained. Further on, as it can be seen in Fig. 3-2(b), each sector has been divided into six small regions. All these sectors are used for implementing the modulation strategy. Furthermore, the required voltage vector (V_{ref}) is obtained by using the three nearest stationary vectors (V_0,V_1 and V_2) to synthesize it. Therefore, according with Fig. 3-2(b), when the reference vector is laying in region 2a of sector I, the reference vector can be constructed as:

$$\vec{V}_{ref}T_s = \vec{V}_0T_0 + \vec{V}_1T_1 + \vec{V}_2T_2$$
$$T_s = T_0 + T_1 + T_2 \tag{3.3}$$

Where T_s is the sampling period, T_0, T_1 and T_2 are the dwell times for V_0, V_1 and V_2.

(a) **(b)**

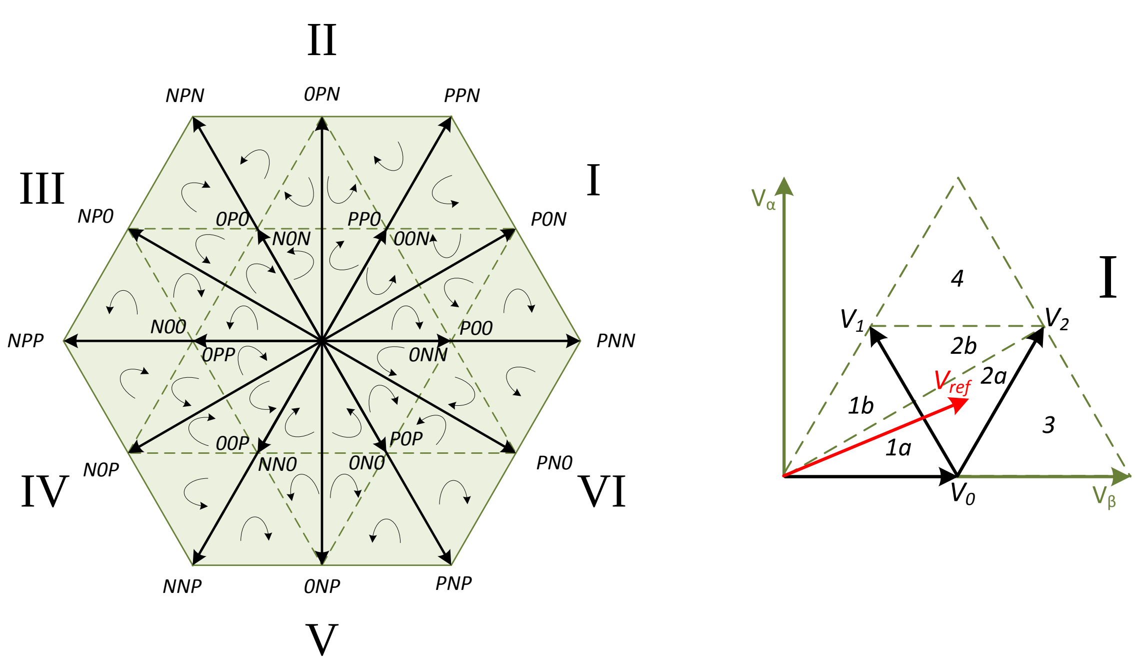

Fig. 3-2 a) SVM diagram emphasizing the voltage vector sequences for even harmonic cancellation, b) Zoom of the first SVM diagram sector [18]

Vector		Phase a	Phase b	Phase c	V_α	V_β
V1	V1a	P	0	0	$+\frac{V_{DC}}{3}$	0
	V1b	0	N	N		
V2	V2a	P	P	0	$+\frac{V_{DC}}{6}$	$+\frac{V_{DC}\sqrt{3}}{6}$
	V2b	0	0	N		
V3	V3a	0	P	0	$-\frac{V_{DC}}{6}$	$+\frac{V_{DC}\sqrt{3}}{6}$
	V3b	N	0	N		
V4	V4a	0	P	P	$-\frac{V_{DC}}{3}$	0
	V4b	N	0	0		
V5	V5a	0	0	P	$-\frac{V_{DC}}{6}$	$-\frac{V_{DC}\sqrt{3}}{6}$
	V5b	N	N	0		
V6	V6a	P	0	P	$+\frac{V_{DC}}{6}$	$-\frac{V_{DC}\sqrt{3}}{6}$
	V6b	0	N	0		
V7		P	N	N	$+\frac{2V_{DC}}{3}$	0
V8		P	0	N	$+\frac{V_{DC}}{2}$	$+\frac{V_{DC}\sqrt{3}}{6}$
V9		P	P	N	$+\frac{V_{DC}}{3}$	$+\frac{V_{DC}\sqrt{3}}{3}$
V10		0	P	N	0	$+\frac{V_{DC}\sqrt{3}}{3}$
V11		N	P	N	$-\frac{V_{DC}}{3}$	$+\frac{V_{DC}\sqrt{3}}{3}$
V12		N	P	0	$-\frac{V_{DC}}{2}$	$+\frac{V_{DC}\sqrt{3}}{6}$
V13		N	P	P	$-\frac{2V_{DC}}{3}$	0
V14		N	0	P	$-\frac{V_{DC}}{2}$	$-\frac{V_{DC}\sqrt{3}}{6}$
V15		N	N	P	$-\frac{V_{DC}}{3}$	$-\frac{V_{DC}\sqrt{3}}{3}$
V16		0	N	P	0	$-\frac{V_{DC}\sqrt{3}}{3}$
V17		P	N	P	$+\frac{V_{DC}}{3}$	$-\frac{V_{DC}\sqrt{3}}{3}$
V18		P	N	0	$+\frac{V_{DC}}{2}$	$-\frac{V_{DC}\sqrt{3}}{6}$
V19		P	P	P	0	0
		0	0	0		
		N	N	N		

Table 3-1 Available switching states for 3L-DNPC converters [18]

It is worth to mention that OFF-ON-OFF or ON-OFF-ON sequences will be applied to the converter IGBTs during one switching period. Therefore, in order to obtain a suitable controllability of the switching behavior, the sampling frequency has been selected to be twice the switching frequency. In this way an update of the switching states and dwell times calculation will be provided at the beginning and in the middle of every switching period. Then, the used sampling frequency is 6kHz.

Due to the fact that the study of the modulation techniques is not within the objectives of the project, the C-code implementation of the SVM is introduced in Appendix D

3.1.2 LCL – Filter description model

The three-level NPC converter is connected to the grid through a passive LC filter in order to meet harmonic current injection requirements [9]. It has been assumed that the converter is connected to a higher voltage line, therefore a step-up transformer has been used. It has been considered that the value of the series impedance of this transformer and the inductive impedance of the grid are 6% and 4% of the base impedance respectively. Hence, the modelled system is represented by the LCL filter shown in Fig. 3-3.

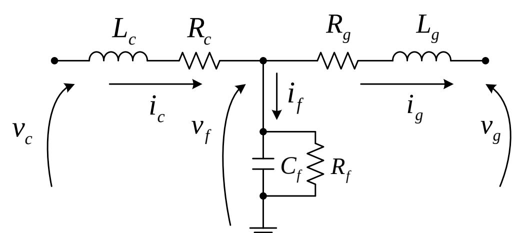

Fig. 3-3 Single-phase LCL filter representation

Where L_c and R_c are the converter side inductance and its series resistance, L_g and R_g are the grid side inductance with its series resistance and C_f is the capacitor bank, which is connected to a parallel resistance R_f. The converter, capacitor and the grid currents are represented by i_c, i_f and i_g respectively. Furthermore the converter, capacitor bank and grid voltages are represented by v_c, v_f and v_g. Based on Kirchhoff's laws, the filter model can be expressed by using the equations in (3.4), (3.5), (3.6) and (3.7).

$$i_c - i_g - i_f = 0 \tag{3.4}$$

$$v_c = L_c \frac{di_c}{dt} + R_c i_c + v_f \tag{3.5}$$

$$v_f = L_g \frac{di_g}{dt} + R_g i_g + v_g \tag{3.6}$$

$$i_f = C_f \frac{dv_f}{dt} + \frac{v_f}{R_f} \tag{3.7}$$

The model in Laplace domain can be express as:

$$i_c - i_g - i_f = 0 \tag{3.8}$$

$$v_c - v_f = i_c(sL_c + R_c) \tag{3.9}$$

$$v_f - v_g = i_g(sL_g + R_g) \tag{3.10}$$

$$v_f = i_f \frac{R_f}{1 + sC_f R_f} \tag{3.11}$$

Taking into consideration the previous equations, the filter transfer function, used in overall system simulation, is obtained by defining the converter voltage as the input and the grid current as the output of the system, $F_{LCL} = \frac{i_g}{v_c}$ .The grid voltage is assumed to be an ideal voltage source and it represents a short-circuit for harmonic frequencies. Then, this parameter is set to zero for filter analysis ($v_g = 0$).

Taking into consideration equations (3.10) and (3.11) the filtered current can be expressed in function of grid current:

$$i_f = i_g \frac{s^2 C_f L_g R_f + s\left(C_f R_g R_f + L_g\right) + R_g}{R_f} \tag{3.12}$$

From equation (3.8) and (3.10), i_c and v_f are obtained. The above calculated expressions are replaced in equation (3.9), therefore the following form is obtained:

$$v_c = i_g(sL_g + R_g) + (i_g \frac{s^2 C_f L_g R_f + s\left(C_f R_g R_f + L_g\right) + R_g}{R_f} + i_g)(sL_c + R_c) \tag{3.13}$$

Finally the filter transfer function between the grid current and converter voltage is obtained in (3.14).

$$\begin{gathered} F_{LCL} = \frac{I_g(s)}{V_c(s)} = \frac{K}{s^3 + \lambda_2 s^2 + \lambda_1 s + \lambda_0} \\ K = \frac{R_f}{L_c C_f R_f L_g} \\ \lambda_2 = \frac{C_f R_f R_g L_c + C_f R_f R_c L_g + L_g L_c}{L_c L_g C_f R_f} \\ \lambda_1 = \frac{R_c R_g C_f R_f + R_c L_g + R_g L_c + R_f L_c + R_f L_g}{L_c L_g C_f R_f} \\ \lambda_0 = \frac{R_g R_c + R_f R_c + R_f R_g}{L_c L_g C_f R_f} \end{gathered} \tag{3.14}$$

As the grid side inductance has been previously determined, L_c and C_f parameters of the filter will be obtained according to a desired resonance frequency. Taking into consideration that the highest current control bandwidth is 350 Hz (7th harmonic) and the switching frequency was chosen at 3 kHz, the LCL filter resonant frequency was selectively placed at 1.2 kHz in order to reduce the current harmonics and still be high enough not to limit the control system bandwidth.

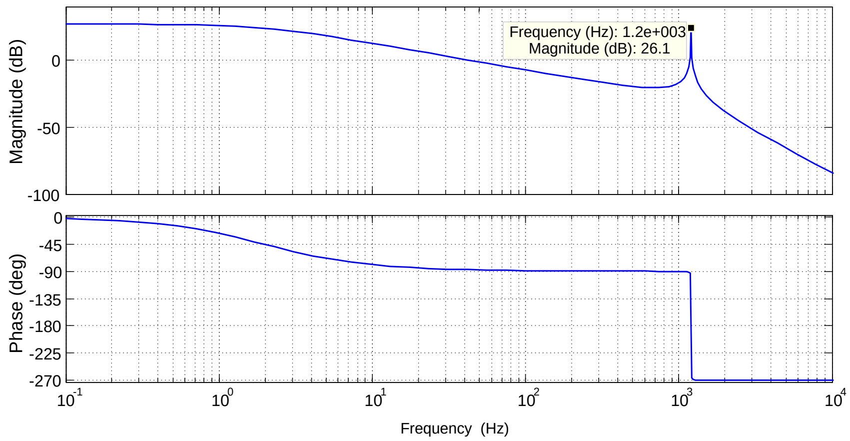

Fig. 3-4 Bode diagram of the LCL filter for the proposed parameters

The bode plot of the LCL filter is depicted in Fig. 3-4. It can be seen, that the magnitude gain corresponding to 3 kHz is able to mitigate the switching frequency harmonics, and the resonant frequency is higher than the maximum controller bandwidth. Moreover, it is worth to note that the filter reactive power has a direct impact on the converter rating, since the converter must provide the reactive power injected into the grid plus the reactive power of the filter. Taking into consideration that the STATCOM is the main functionality of the system, the desired operating point is at 50 Hz. Therefore, in this case it is possible to achieve zero reactive power consumption by properly designing the series inductances and parallel capacitor. As it can be observed in Fig. 3-4 the magnitude at fundamental frequency is close to 0dB, which implies minimum reactive power consumption. In this way the current transfer to the grid can be achieved with a minimum converter effort. The used filter parameters can be found in Table 3-2.

$L_c = 1.44mH$	$R_c = 20m\Omega$
$L_g = 2.24mH$	$R_g = 25m\Omega$
$C_f = 20\mu F$	$R_f = 79.5k\Omega$

Table 3-2 LCL filter parameters

Taking into consideration that the model will be implemented on a digital processor, the discrete transfer function of the filter is required in order to properly design the control of the system. Therefore, in (3.17) the discrete transfer function is introduced by using the zero order hold discretization method from the Matlab “c2d” command.

$$H_{LCL}[z] = \frac{0.01104z^2 + 0.04059z + 0.01101}{z^3 - 1.611z^2 + 1.61z - 0.9957} \tag{3.15}$$

The final transfer function that will be considered (3.16), is obtained by multiplying (3.17) with a sample delay, which represents the sampling plus calculation time delay introduced by the processor. In this way a more accurate approach to the real system behaviour is achieved.

$$F_{LCL}[z] = H_{LCL}[z] \cdot \frac{1}{z} \tag{3.16}$$

3.2 Current Control System Design

The control of the grid currents injection plays a key role in achieving the desired converter functionalities, since the proposed system is based on a three-level DNPC converter shunt connected to the grid through an LCL filter. Thus, by properly controlling the current, the injection of a determined active and reactive power set point is ensured.

In order to achieve the desired behaviour of the current control system, proportional plus resonant controllers will be used, since, as stated in chapter 2, they offer an accurate and selective control by providing infinite gain for the desired resonant frequencies. Hence, stationary reference frame (αβ) signals can be controlled using this controller type. In (3.17) the transfer function of the proportional plus resonant controller is introduced.

$$C(s) = K_p + \frac{K_i s}{s^2 + \omega_g^2} \tag{3.17}$$

Where K_p is the proportional term, K_i represents the integral term and ω_g is the AC frequency at which the controller provides infinite gain (usually the grid frequency for 50Hz controllers). In Fig. 3-5 (a) the time response of the controller is introduced when a sinusoidal signal with frequency equal to the resonant frequency of the controller is provided as an input.

(a)

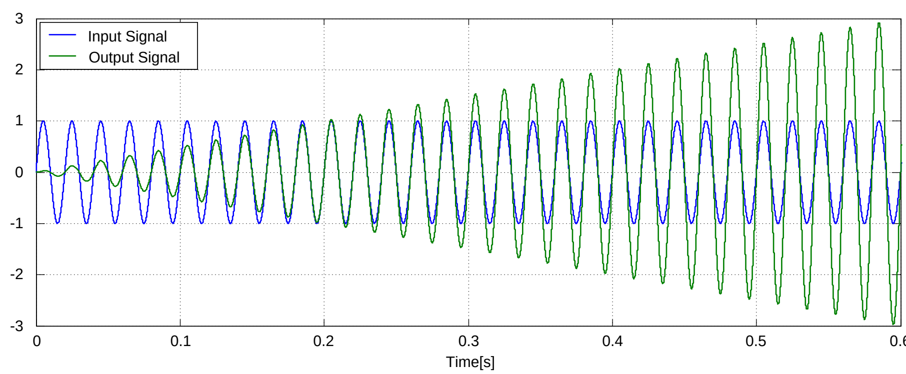

(b)

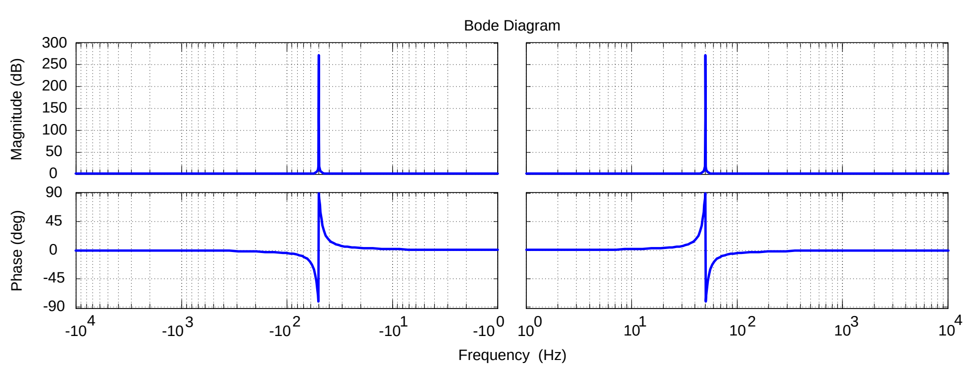

Fig. 3-5 a) Resonant current controller time response, b) Resonant current controller frequency response [24]

Therefore it can be stated that the resonant controller acts as an integrator for sinusoidal signals. Furthermore, the bode response is shown in Fig. 3-5 (b), and it can be observed that an infinite gain is provided for the tuning frequency of the controller, which in this specific case is 50Hz [19, 24].

Current controllers for fundamental, 5th and 7th harmonic frequencies are required as the purpose of this project deals with the implementation of a power conditioner based on a STATCOM which also performs as an Active filter for 5th and 7th harmonics. As a result, a PCC voltage power quality improvement will be achieved by independently controlling the injection of non-active currents into the grid. The proposed current control structure is presented in Fig. 3-6, in which an independent control for each of the specified frequencies can be found.

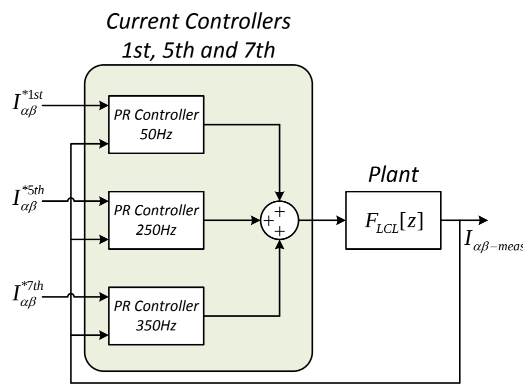

Fig. 3-6 Proposed Overall current control loop diagram

Where $I_{\alpha\beta}^{*1st}$, $I_{\alpha\beta}^{*5th}$ and $I_{\alpha\beta}^{*7th}$ are the reference currents for fundamental, 5th and 7th harmonic frequencies in αβ frame, $I_{\alpha\beta-meas}$ is the measured grid current and $F_{LCL}[z]$ is the transfer function of the filter (plant) plus the sampling delay (sampling + calculation time of the processor) that was obtained from the section 3.1.2, in which the converter voltage and grid current are its input and output parameters respectively. Additionally, it is worth to mention that a control loop as the one shown in Fig. 3-6 will be identically used in alpha and beta axes.

The proposed current control algorithm will be designed in discrete time since the control structure will be implemented in the laboratory setup by using a digital processor. By considering that a pole in continuous time domain is placed in discrete time as $z = \exp(s\Delta t)$, the pole from equation (3.17) placed at $s = \pm j\omega_g$ is mapped in z-domain as described in the following equations:

$$s = \pm j\omega_g \text{ is mapped as } z = e^{(\pm j\omega_g \Delta t)} = cos(\omega_g \Delta t) \pm jsin(\omega_g \Delta t) \tag{3.18}$$

$$\begin{aligned} &[z - cos(\omega_g \Delta t) - jsin(\omega_g \Delta t)][z - cos(\omega_g \Delta t) + jsin(\omega_g \Delta t)] \\ &= z^2 - 2cos(\omega_g \Delta t)z + 1 \end{aligned} \tag{3.19}$$

According to (3.18) and (3.19), it can be stated that the poles from (3.18) are obtained by using the result of (3.19) as the denominator equation for the discrete time current controller. In this case the discrete resonant controller transfer function is given in (3.20).

$$C[z] = K\frac{z^2 + \alpha_1 z + \alpha_2}{z^2 - 2cos(\omega_g \Delta t)z + 1} \tag{3.20}$$

Where K and the zeros of the controller transfer function are the design parameters, and Δt is the sampling period.

Finally, each of the implemented controllers are tuned individually in order to fulfil the required specifications for the different compensation frequencies. Therefore, the design parameters obtained for controlling 50Hz, 250Hz and 350Hz are described in the following subsections.

3.2.1 Fundamental Frequency Current Controller Design

The design parameters have been obtained by introducing the controller transfer function given in (3.20) and the filter transfer function $F_{LCL}[z]$ in the closed loop structure depicted in Fig. 3-7. In this figure, it is relevant to observe that the tuning frequency of the resonant controller is the one corresponding to 50Hz. Further on, the proposed loop is introduced in MATLAB/Sisotool toolbox in order to determine the gain of the system (K) and the placement of the controller zeros, which correspond to a desired dynamic response of the system.

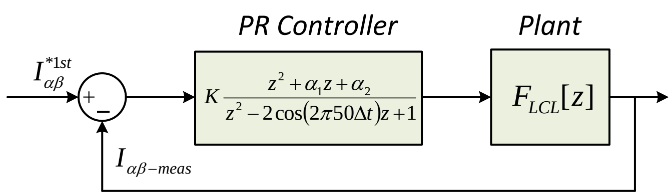

Fig. 3-7 50Hz current controller closed loop diagram

In the study case, the design specifications are based on obtaining a very selective control for 50Hz and a settling time smaller than 20ms, as the grid codes require that in case of severe grid voltage variations rated reactive power has to be injected in less than one fundamental frequency period [37]. Then special attention is given in order to fulfil these two requirements. Thus, the obtained design parameters for the 50Hz current controller are given in the transfer function introduced in (3.21).

$$C[z] = 2.1704\frac{z^2 - 1.8875z + 0.8904}{z^2 - 1.9973z + 1} \tag{3.21}$$

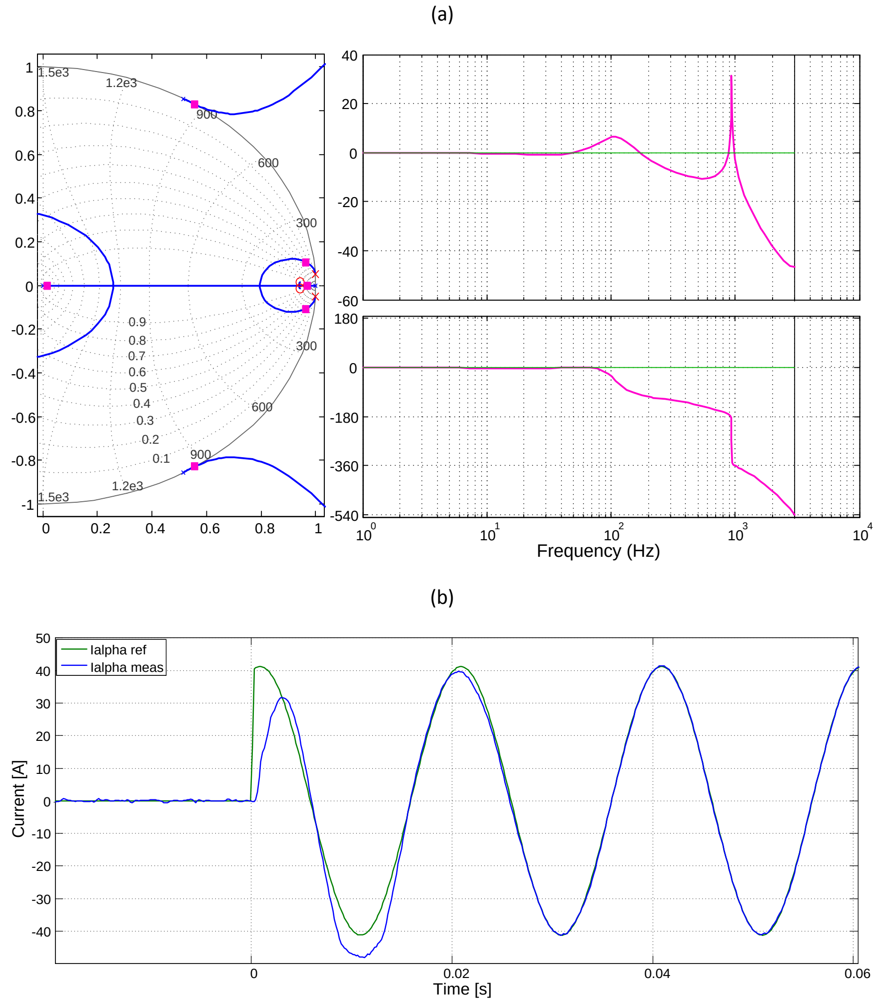

Fig. 3-8 (a) Root-locus and closed loop bode response for 50Hz current control design parameters. (b) Current alpha reference and measured obtained in the experimental results

In Fig. 3-8(a) the pole placement and closed loop bode response are obtained in order to determine the response of the system when the controller specified in (3.21) is used. From this figure, it can be deducted that the system is stable, as all the closed loop zeros and poles are placed within the unity circle, and that the bandwidth of the system is around 60Hz. Therefore it can be stated that 50Hz AC signals will be selectively controlled by using the proposed resonant current controller. Furthermore, Fig. 3-8(b) shows that the system is capable of providing a step from zero to the rated current within 20ms, in case the designed controller is implemented in the laboratory setup.

3.2.2 5th Harmonic Current Controller Design

In this case, the same control loop as the one introduced in Fig. 3-7 is used when controlling 5th harmonic currents. The only noticeable difference is that the tuning frequency of the resonant controller corresponds to 250Hz. Then, as it was presented in the previous section, the gain and the zeros of the controller have to be determined in order to obtain the desired system dynamics. The design specifications in this case are mainly based on obtaining a very selective control, since a minimum settling time for the injection of 5th harmonic currents is not required by the grid codes. As a result

250Hz AC currents can be controlled without affecting other frequency signals. Equation (3.22) shows the proposed current controller design parameters. Additionally, the root-locus and closed loop bode response of the described system is depicted in Fig. 3-9(a) by using (3.22) as the transfer function of the resonant controller.

$$C[z] = 2.3071\frac{z^2 - 1.8428z + 0.8851}{z^2 - 1.9318z + 1} \tag{3.22}$$

According to Fig. 3-9(a), it can be stated that the system is stable, as the closed loop poles and zeros are placed in the unity circle (root-locus) and that a selective control will be achieved for 250Hz control signals (closed-loop bode response). Finally, the proposed controller is implemented in the laboratory setup. Fig. 3-9(b) shows the dynamic behaviour of the proposed 5th harmonic current controller when a step from zero to rated current is provided in time zero seconds.

(a)

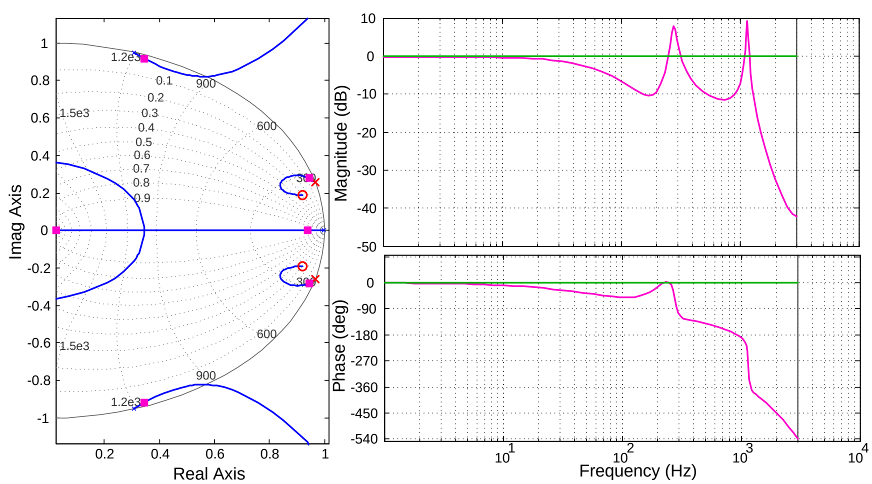

(b)

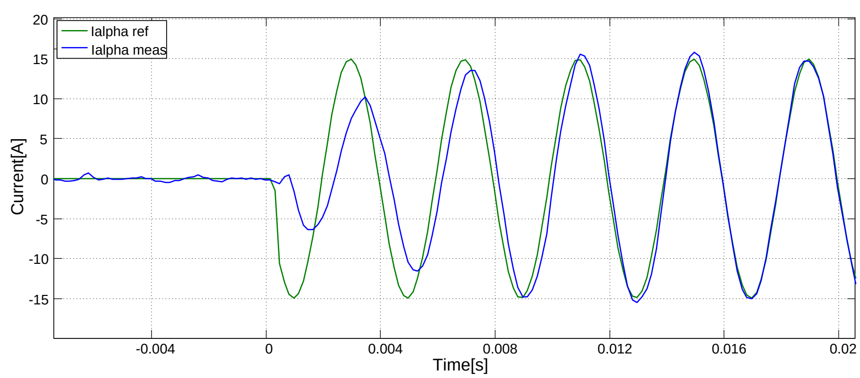

Fig. 3-9 8(a) Root-locus and closed loop bode response for 250Hz current control design parameters. (b) Current alpha reference and measured obtained in the experimental results

3.2.3 7th Harmonic Current Controller Design

Finally the tuning parameters have also been obtained for controlling 7th harmonic currents by using the same method described in section 3.2.1 and considering 350Hz as the tuning frequency for the resonant controller. In this case, similar design specifications as in the case of 5th harmonic controller are required. Thus, the controller should perform a selective control for 7th harmonic currents in order not to influence the control of other current frequency signals. Then the design specifications are mainly based on obtaining a very selective control, since a minimum settling time for the injection of 7th harmonic currents is not required by the grid codes.

$$C[z] = 3.2007\frac{z^2 - 1.78917z + 0.853158}{z^2 - 1.8672z + 1} \tag{3.23}$$

Equation (3.23) introduces the tuning parameters of the 350Hz resonant controller. Further on, the system performance is analyzed in Fig. 3-10 where the root-locus, closed loop bode and time response for the laboratory implementation are provided. Fig. 3-10(a) shows that the system is stable and selective for 350 Hz signals, by using the root-locus and closed loop bode diagram respectively. Finally, the time response of the system is shown in Fig. 3-10(b) where a step from zero to the rated current is provided in time zero seconds.

(a)

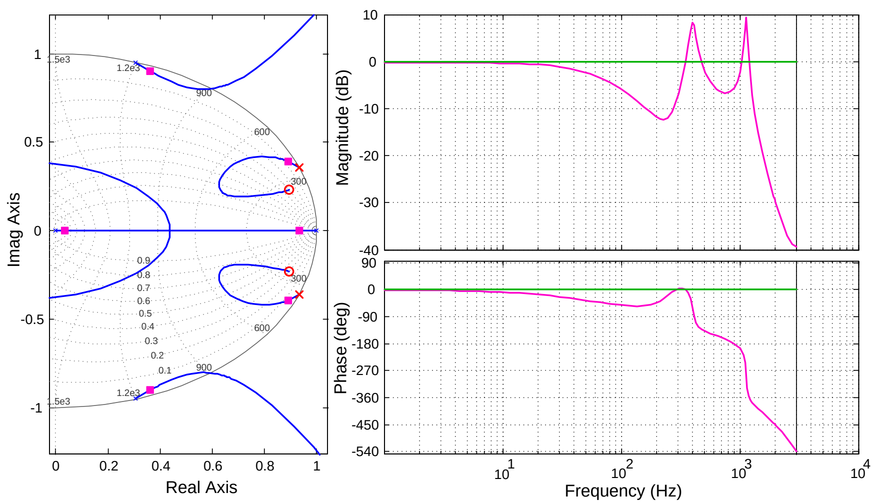

(b)

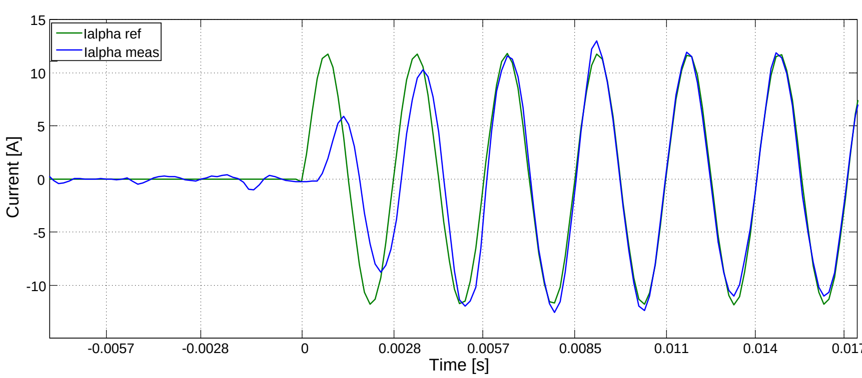

Fig. 3-10 (a) Root-locus and closed loop bode response for 350Hz current control design parameters. (b) Current alpha reference and measured obtained in the experimental results

As a final conclusion, it can be stated that each of the controllers have been properly designed, as their response was tested in the laboratory with successful results. It is worth to mention that all three controllers are able to work simultaneously, without interfering between them.

3.3 Voltage Control Design

Since the converter is operating without an external DC voltage source, the DC-link voltage control is needed in order to achieve the required non-active currents controllability. As it was stated in section 2.2.4 the desired DC voltage can be obtained by managing the active power exchange between the DC and AC sides of the converter. Therefore, according with Fig. 3-11 the DC voltage controllability is achieved by modifying the active power reference. Further on by using IARC, the active and reactive power command signals are translated into α and β components of the reference current for the fundamental current controllers [31].

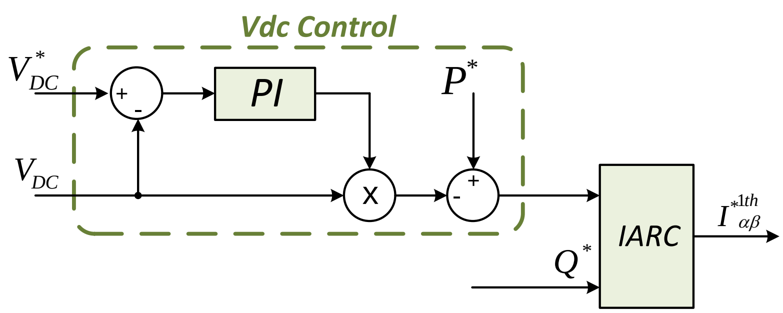

Fig. 3-11 Structure of DC-voltage Control schematic

Finally by regulating the direct axis current i_d it is possible to control the active power flow in the VSC and thus the DC link voltage.
By considering a lossless system (converter and filter losses are neglected) the assumption that $i_d = i_{dc}$ can be made. Therefore the plant transfer function is obtained by defining $i_d (= i_{dc})$ as the input and the DC-link voltage v_{dc} as the output of the system $P_{dc}(s) = \frac{v_{dc}}{i_d}$ [31, 38].

Further on, from the conventional equation (3.24) which describes the relation between capacitor current and voltage, the transfer function is obtained:

$$i_{dc} = C\frac{dv_{dc}}{dt} \Longrightarrow v_{dc} = \frac{1}{C}\int i_{dc}dt \tag{3.24}$$

By considering $i_d = i_{dc}$ and applying Laplace transform to (3.24), the plant transfer function has the following form:

$$P_{dc}(s) = \frac{v_{dc}}{i_d} = \frac{1}{Cs} \tag{3.25}$$

The discretization of the previous equation is given in (3.26).

$$P_{dc}[z] = \frac{\Delta t}{C(z-1)} \tag{3.26}$$

Where Δt is the sampling period.

Due to the fact that the control signal is a dc variable, a PI controller is used in order to achieve the desired system response. The PI controller transfer function is showed in (3.27) by considering the error $ev_{dc}\ (v_{dc}^{*} - v_{dc})$ as the input and the i_d as the output of the system, $[z] = \frac{i_d}{ev_{dc}}$.

$$C[z] = K\left(1 + \frac{T_i}{z-1}\right) = \frac{\alpha_1 z + \alpha_2}{z-1} \tag{3.27}$$

As it can be seen this controller has one pole at z = 1, therefore only by changing the controller zero, the path of the closed loop poles can be modified. By taking into consideration the controller transfer function and the discrete transfer function of the plant, the DC-voltage design loop is shown in Fig. 3-12.

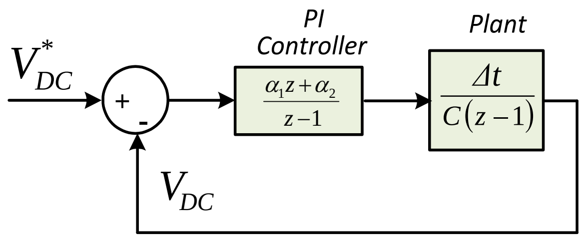

Fig. 3-12 Voltage control design loop

The controller design has been done in Matlab/Sisotool by placing the zero in order to locate the closed loop poles at the desired position. Finally, the obtained PI controller design parameters are given in (3.28).

$$C[z] = \frac{0.2484\,z - 0.2474}{z-1} \tag{3.28}$$

In Fig. 3-13(a) the root-locus and bode diagram show that the system is stable and selective for low frequency signals. Finally, the step response of the system is depicted in Fig. 3-13(b) and it can be stated that, according to the design requirements, a slower stabilization time is obtained than in the inner current loop.

(a)

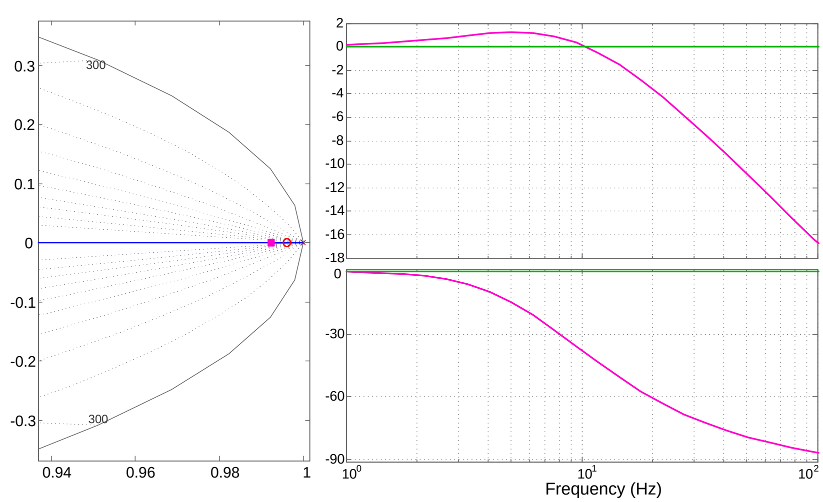

(b)

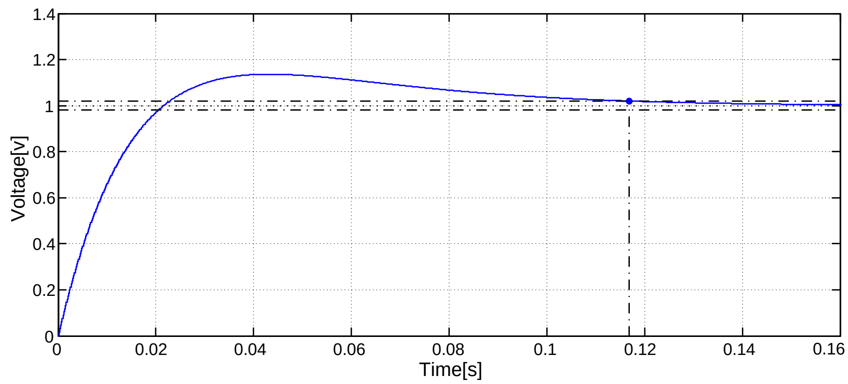

Fig. 3-13 (a) Root-locus and closed loop bode response for the PI voltage control design parameters. (b) DC voltage control system step response

3.4 Proposed non-active power reference strategy

The main contribution of this project deals with the control implementation of a power conditioner based on a STATCOM which is able to perform as an Active Filter for 5th and 7th harmonics. Besides that, the concept of Smart-STATCOM is introduced, as depending on the grid voltage conditions the system is self-controlled. Thus, deciding at any instant the amount of compensation currents needed in order to provide maximum PCC power quality according to the limits of the system. The improvement of the power quality (voltage quality) will be achieved by absorbing reactive currents for each of the harmonic frequencies (1st, 5th and 7th). The implementation of three operation modes can be clearly defined. The STATCOM operation mode, which is the main functionality of the system, is responsible of the reactive power compensation and control of the PCC voltage by injecting or absorbing non-active fundamental frequency currents. Besides that, the power quality at the PCC can be improved when the system is operating in the Active Filter mode. In this way, the harmonic voltages are mitigated by controlling 5th and 7th non active currents. Finally, the Smart-STATCOM operation mode introduces a novel control strategy which determines the most suitable combination of STATCOM and Active Filter functionalities in order to achieve maximum power quality at the PCC.

In the proposed control strategy structure, the system uses as measurements:

- $Igrid_{abc}$ – the grid current is used as a feedback signal for the resonant current controllers loop.
- $Vgrid_{abc}$ – the grid voltage is used for synchronization and harmonic detection for fundamental, 5th and 7th harmonics.
- V_{DC} – the DC- voltage as a feedback in order to control the converter DC – link.

In order to achieve the desired system functionalities, several controllers are used: a PI controller which manage the DC voltage control and three resonant current controllers for fundamental, 5th and 7th harmonic frequencies. Hence, an accurate current control will be achieved, as the current controller poles will be placed to provide infinite gain for 50Hz, 250Hz and 350Hz respectively (section 3.2).

The synchronization method used in this control strategy is based on a multiple SOGI frequency locked loop algorithm. As a result, the fundamental, 5^{th} and 7^{th} grid frequencies are continuously estimated for online tuning of the resonant controllers. Additionally, this grid synchronization method is able to detect the grid voltages for each of the specified harmonic frequencies (section 2.2.1). In order to achieve the desired PCC voltages, the reference currents will be obtained by implementing a droop control algorithm which is using the detected voltages as a feedback.

Finally the overall simulation has been implemented by using Matlab/Simulink and Plecs toolbox in order to perform an accurate system prediction before implementing it in laboratory.

3.4.1 STATCOM Operation Mode

In case the system is performing in STATCOM operation mode, the non-active fundamental currents are accurately controlled in order to perform reactive power compensation and control of the PCC voltage.

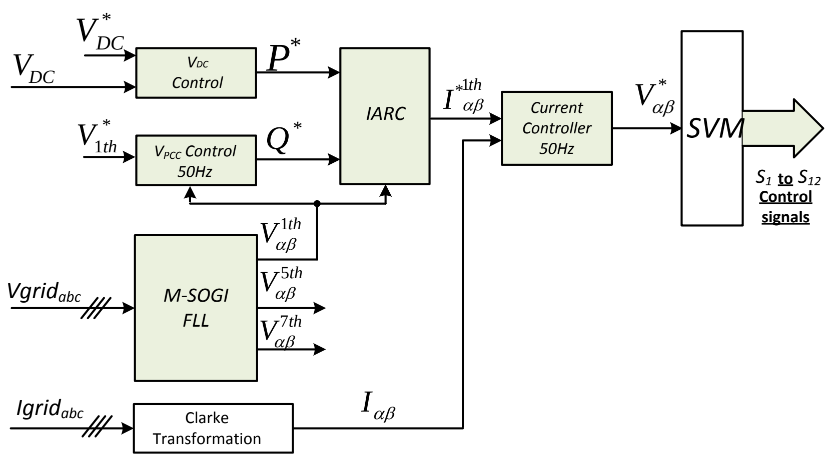

Fig. 3-14 STATCOM control strategy structure

Fig. 3-14 introduces the implemented structure for the STATCOM control strategy, where it can be observed that one inner and two outer control loops are used. The inner control loop, in this case the PR current controller for fundamental frequency, has the functionality of injecting or absorbing a desired amount of current according to a characteristic dynamics. Moreover the outer control loops consist of:

- The DC-link Voltage control – a PI controller as the one introduced in section 3.3 is used in order to regulate the energy exchange between the DC and AC sides of the converter.
- The PCC voltage control – this control loop is based on the implementation of a droop controller, as depending on the PCC voltage variation the system should inject a desired amount of Q according to the required droop characteristic (Fig. 3-15).

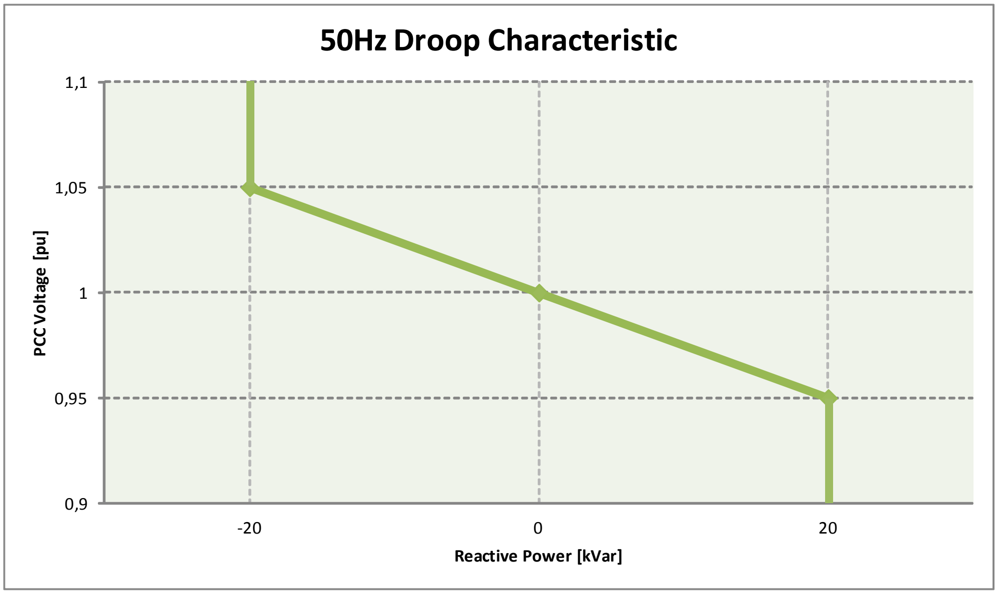

Fig. 3-15 Droop Controller for fundamental PCC voltage control

The implemented droop controller has the following form [19]:

$$V - V_0 = -k_{50}(Q - Q_0) \tag{3.29}$$

Where:

- V – is the measured fundamental PCC voltage
- V_0 – is the rated RMS line to ground fundamental PCC voltage(230V)
- Q – the reactive power reference to be injected to the grid determined by the droop controller
- Q_0 – the set point for reactive power injection at the rated conditions (0Var for 230V)
- k_{50} – is the droop controller gain calculated according with the slope from the Fig. 3-15 .

Once the active and reactive power references have been obtained by using the above mentioned controllers, the IARC is used in order to provide the reference for the current controllers. In this way the system is injecting the required non-active currents in order to contribute to the PCC voltage control.

In order to test the STATCOM operation mode, a simulation of the control diagram introduced in Fig. 3-14 has been implemented. The STATCOM functionality will be validated by considering the test scenarios introduced in Table 3-3. In this case the system behaviour is observed when grid voltage variations are introduced.

Test Scenario	Time Duration [s]	PCC voltage [pu]	Reactive power [kVar]
1	0 to 0.08	0.95	20
2	0..08 to 0.16	1	0
3	0.16 to 0.24	1.05	-20
4	0.24 to 0.3	1	0

Table 3-3 Test scenarios used in simulation in order to validate the STATCOM operation mode

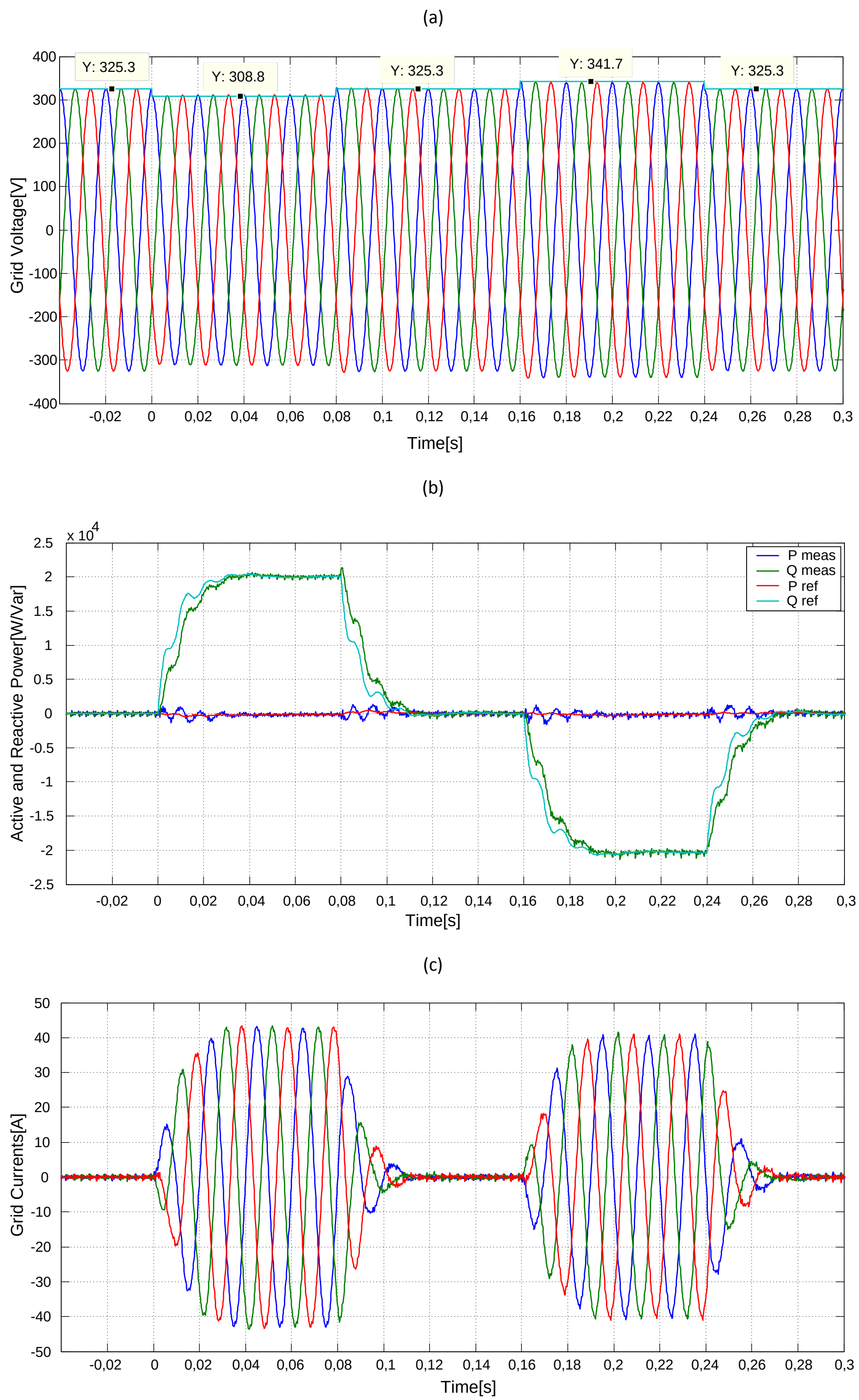

Fig. 3-16 Simulation results of STATCOM operation mode when PCC voltage variations are provided. (a)Measured Voltage at the PCC, (b) Active and Reactive Power Measured and References, (c)Measured Grid Currents

As it can be seen in Fig. 3-16, in the present simulation test, rated reactive power is absorbed or injected to the grid when a voltage variation of approximately 5% is present at the PCC (Fig. 3-16(a)). According to Fig. 3-16 (b), it can be stated that the system is injecting rated reactive power within 20ms when a step from 0 to 20 kVar is provided. In this case, the STATCOM is following the German EON Netz grid codes, which establish that the required time for injecting full reactive power under fault conditions has to be within 20ms [37]. As it was expected the rated current is injected into the grid when the system is providing rated reactive power (Fig. 3-16 (c)).

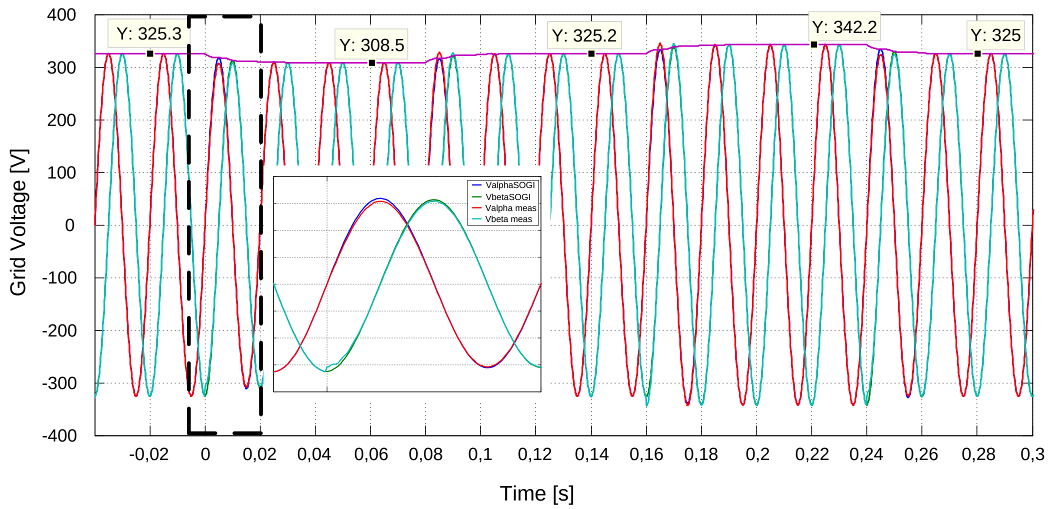

Fig. 3-17 Simulation results of the SOGI-QSG performance in alpha/beta frame

Fig. 3-17 emphasize the fundamental grid voltage detected by the MSOGI-FLL. It can be observed that a fast stabilization time is achieved when voltage variations are present into the grid. This signal is used as a feedback for the droop controllers in order to determine the amount of compensation current to be injected for contributing to the PCC voltage control.

Taking into consideration the simulation results, it can be stated that the STATCOM is improving the power quality of the system by providing grid voltage support and reactive power compensation.

3.4.2 Active Filter Operation Mode

When the system is performing in Active Filter operation mode, the power quality at the PCC can be improved, (through harmonic voltage mitigation) by controlling 5th and 7th non active currents.

The implemented structure for Active Filter control strategy can be depicted in Fig. 3-18, where it can be observed that two extra current controllers are introduced for 5th and 7th harmonic frequencies. Furthermore, droop controllers for each of the specified frequencies (250Hz and 350Hz) are implemented in order to provide the required non-active currents to achieve high controllability of the PCC harmonic voltages. It is worth to mention that in this case the reactive power reference for fundamental frequency is set to zero, as the purpose of the Active Filter functionality is to compensate 5th and 7th harmonic voltages. Therefore zero fundamental non-active current is injected. Further on the M-SOGI FLL plays an important role in detecting the 5th and 7th harmonic content of the PCC voltages.

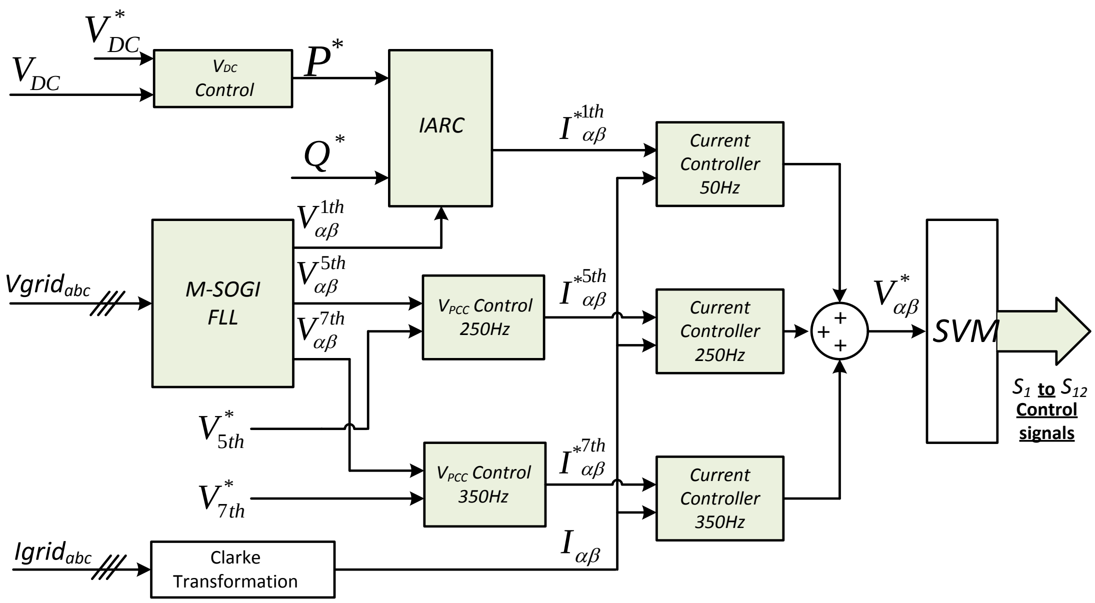

Fig. 3-18 Active Filter control strategy structure

These detected harmonic voltages will be used as a feedback for the droop controllers. The implemented droop controllers characteristic depicted in Fig. 3-19, has been designed in order to keep the harmonic voltages within the allowed limits (6% for 5th and 5% for 7th) specified in the grid codes.[ref] Then, in case the harmonic content at the PCC is higher than the permitted limits, rated non-active currents are injected for 5th and 7th harmonic frequencies.

The rated current injection for 5th and 7th harmonic can be obtained by taking into consideration the attenuation provided by the filter for these specific frequencies (see bode from Fig. 3-4) and the maximum voltage that can be provided at the ac terminals of the converter. The obtained gains (G_{250} and G_{350}) resulting from the filter's bode magnitudes (M_{250} = -14.8 and M_{350} = -16.6) are 0.18 and 0.147 for 5th and 7th harmonics frequencies respectively. Due to the fact that the maximum output voltage of the converter is 404V (when 700V are applied on the dc link), additional 79V can be provided in order not to enter in the overmodulation range. Therefore, by fully deploying this additional voltage and considering the above mentioned gains (G_{250} and G_{350}), the rated 5th and 7th harmonic currents are determined in (3.30).

$$\begin{aligned} I_{5th} &= 79 \cdot 0.18 = 14.22\,A \\ I_{7th} &= 79 \cdot 0.147 = 11.6\,A \end{aligned} \tag{3.30}$$

Then, I_{5th} = 14A and I_{7th} = 12A are considered as the rated harmonic currents for the proposed system.

(a)

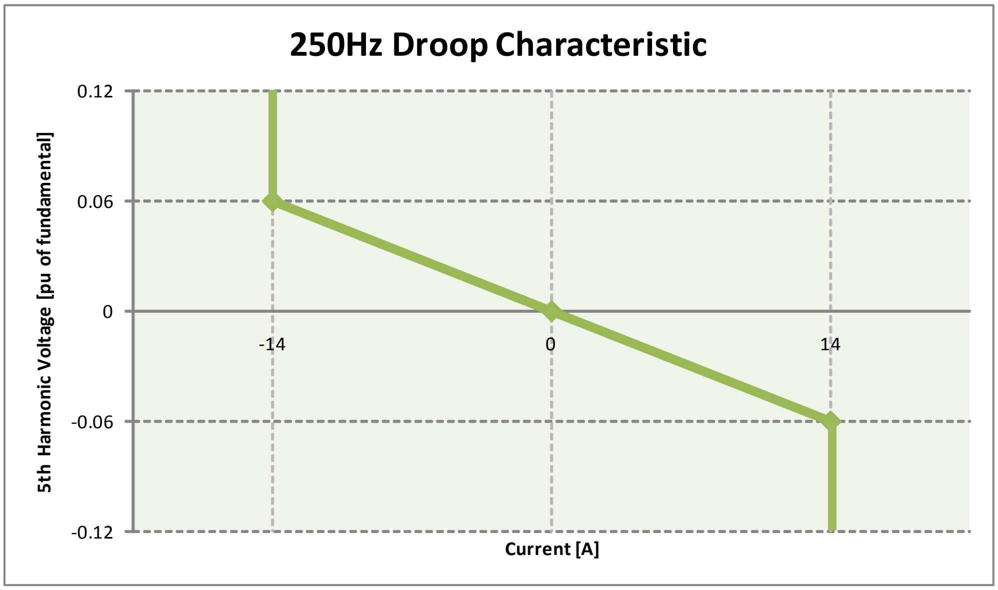

(b)

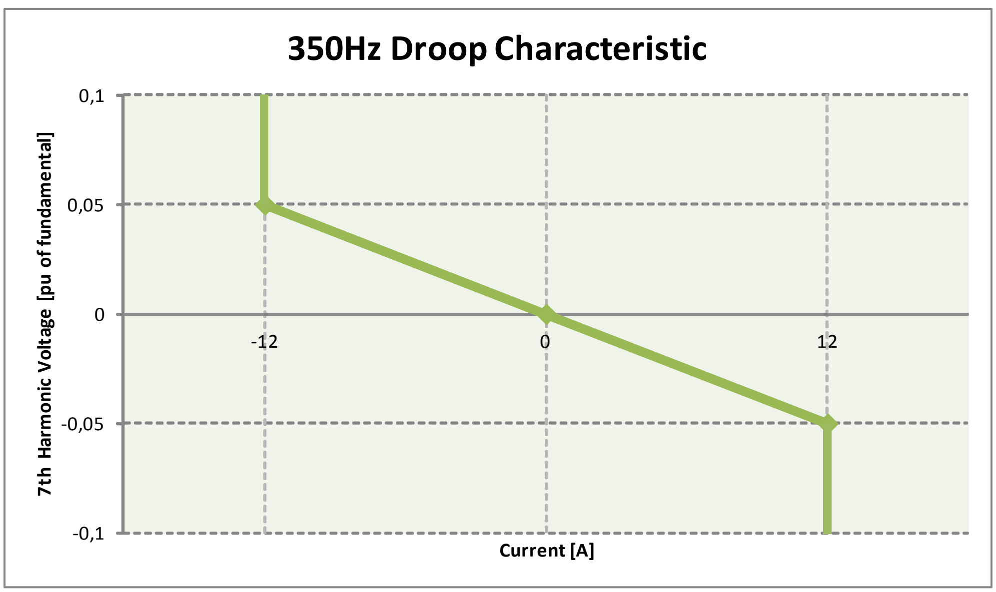

Fig. 3-19 Droop Controllers characteristic for 5th (a) and 7th (b) harmonic voltages

A simulation of the control diagram introduced in Fig. 3-18 has been implemented in order to test the Active Filter operation mode. The simulation has been performed by applying a harmonic grid voltage distortion at the PCC. As it can be seen in Fig. 3-20(a-b), the PCC voltage before harmonic currents compensation is:

- V_{1th} = 1pu
- V_{5th} = 0.08 pu
- V_{7th} = 0.08 pu

with a THD of 11.28%.

(a)

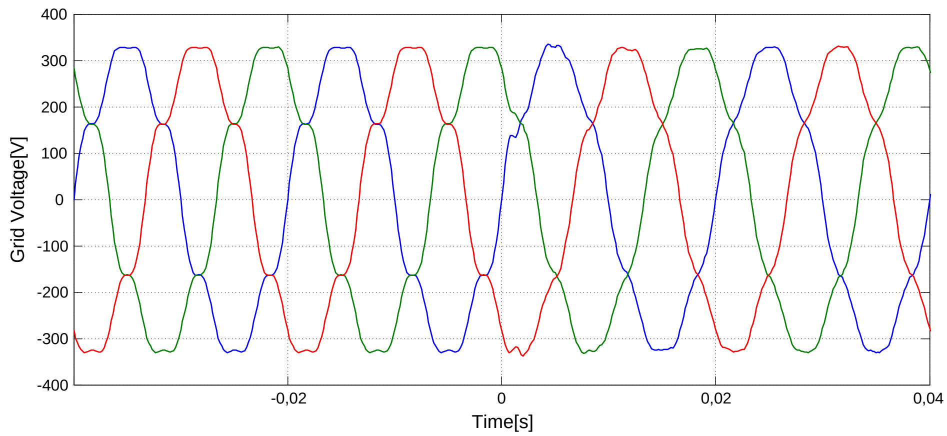

(b)

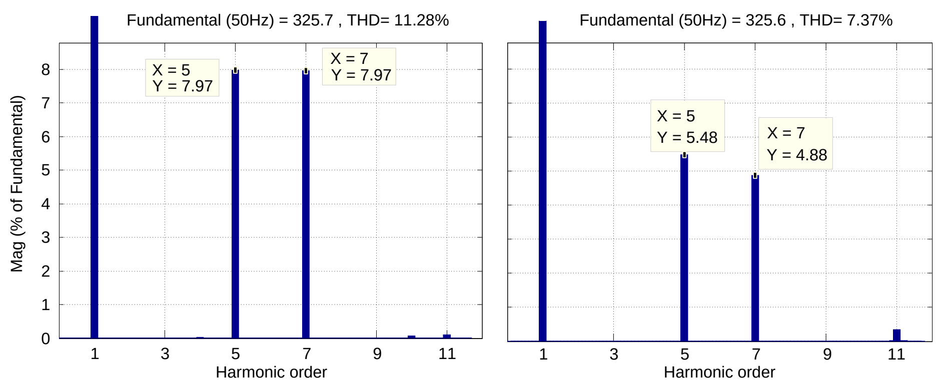

Fig. 3-20 Simulation results of Active Filter operation mode when rated 5th and 7th harmonic voltages are compensated at t = 0 seconds. (a)Measured voltage at the PCC, (b)FFT analysis of the PCC measured voltages before and after current harmonics compensation,

In order to have a better visual comparison of the voltage quality improvement, the Active Filter functionality has been enabled in time 0 seconds (Fig. 3-20 (a)). In this case the harmonic voltage distortion is detected at the PCC and the droop controllers inject the required compensation harmonic non-active currents (Fig. 3-21 (a-b)) in order to keep the harmonic voltages within the allowed limits (6% for 5th and 5% for 7th) [EON gc]. The voltage harmonic compensation effect can be clearly observed in Fig. 3-20(b), which shows the voltage harmonic spectrum before (left-side) and after (right-side) enabling the Active Filter functionality. Finally, the PCC harmonic voltages are reduced to:

- V_{5th} = 0.0548 pu (< 6%)
- V_{7th} = 0.0488 pu (< 5%)

and the THD is reduced to 7.37%.

(a)

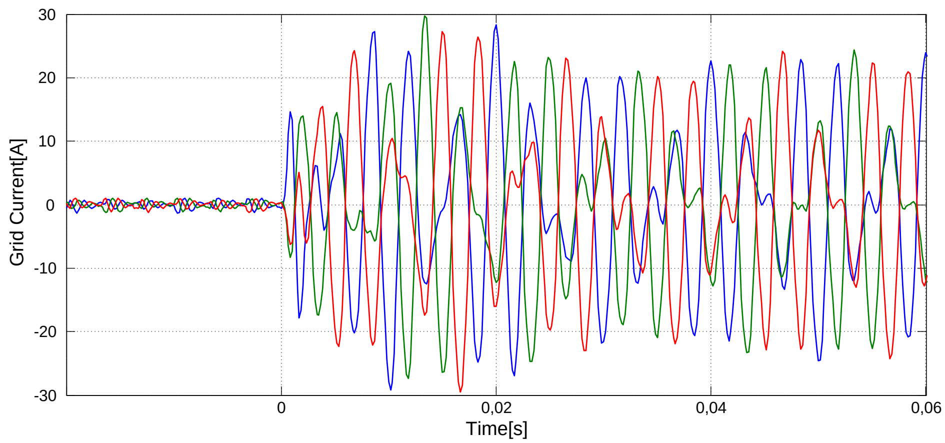

(b)

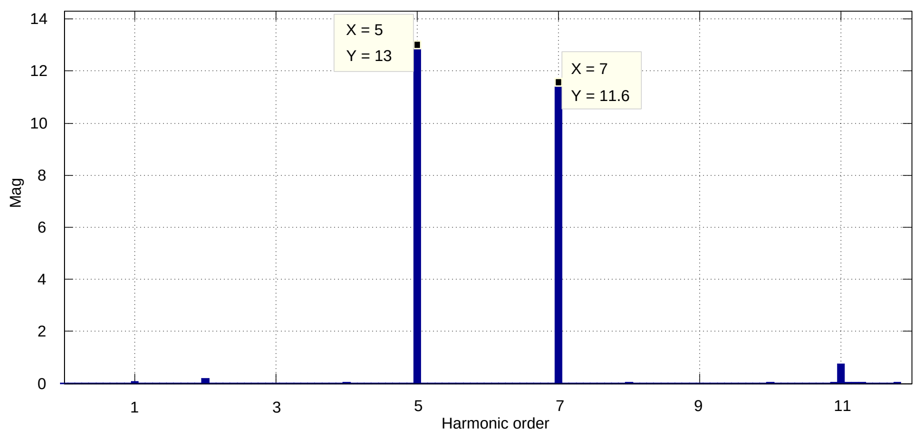

Fig. 3-21 Simulation results of Active Filter operation mode when rated 5th and 7th harmonic voltages are compensated at t = 0 seconds.
(a)Measured Grid Currents, (b)FFT analysis of the measured grid current,

As a conclusion, a reduction of 3.91% in THD has been achieved, resulting in a PCC voltage quality improvement shown in Fig. 3-20(a-b). In this specific case the rated harmonic currents are injected at the PCC (Fig. 3-21). Therefore voltage harmonic mitigation has been achieved by compensating non-active currents.

3.4.3 Smart-STATCOM Operation Mode

In Smart-STATCOM operation mode (presented in Fig. 3-22) a Smart Power Management Control Strategy is introduced, which is responsible of deciding the amount of fundamental and harmonic non-active currents (5^{th} and 7^{th}) to be injected depending on the voltage variations and harmonic content of the grid.

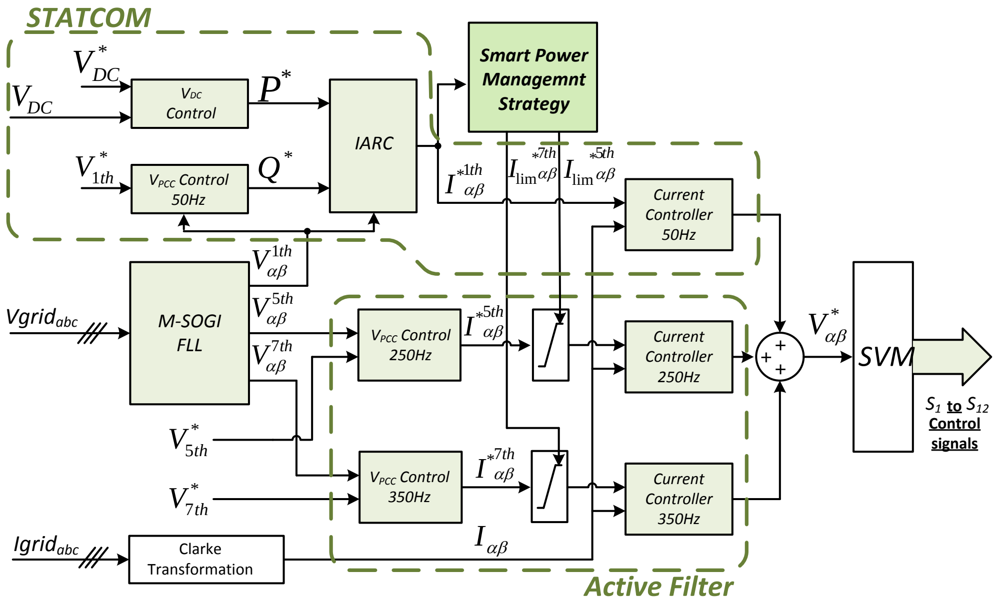

Fig. 3-22 Smart-STATCOM control strategy structure

As described in Fig. 3-23, this control structure has been designed providing compensation priority to the STATCOM functionality, mitigating harmonic voltages only when the rated current of the converter is not fully used in compensating the reactive power. Therefore, when a voltage variation appears at the PCC the desired non-active fundamental current is injected in order to provide grid support. The difference between the rated current and the injected fundamental current defines the current reserve ($I_{reserve}$) of the converter. Then, by managing the converter current reserve, the limitation for 5th and 7th harmonic currents is provided in order to keep all the time the maximum current combination within the converter rating. Finally, the 5th and 7th current limits are obtained according to the specified sharing gains (SG). These gains have been calculated taking into consideration the maximum allowed harmonic voltages present in [14].

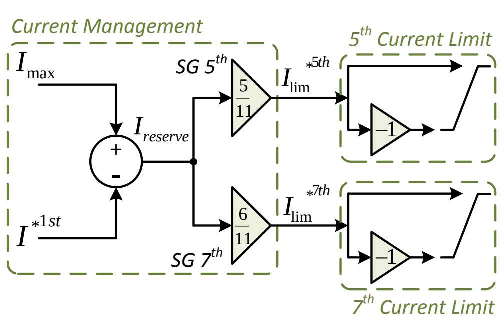

Fig. 3-23 Smart power management strategy

In order to simulate the Smart-STATCOM operation mode, grid voltage variations and harmonic distortion are introduced. Therefore, the 5th and 7th harmonic voltage content is set at 8% of the fundamental rated voltage; meanwhile the amplitude of the fundamental voltage is decreased according to the following test scenarios shown in Table 3-4.

Test Scenario	Time Duration [s]	PCC voltage (fundamental) [pu]
1	0 to 0.08	1
2	0..08 to 0.16	0.98
3	0.16 to 0.24	0.97
4	0.24 to 0.32	0.95

Table 3-4 Test scenarios used in simulation in order to validate the Smart-STATCOM operation mode

(a)

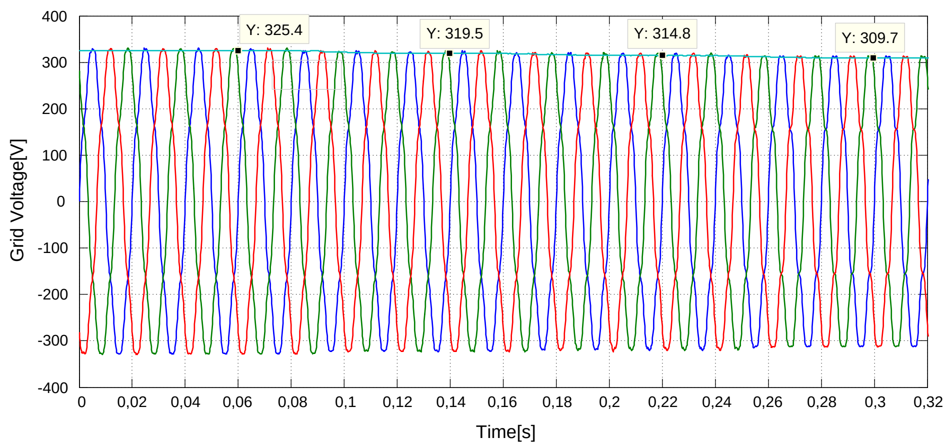

(b)

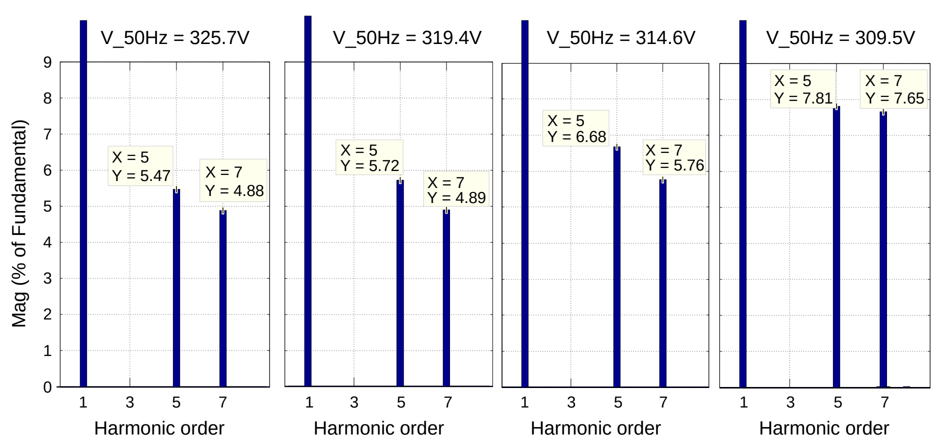

Fig. 3-24 Simulation results of Smart – STATCOM operation mode when PCC voltage variations and harmonic distortion are provided. (a) Measured voltage at the PCC, (b) FFT analysis of the PCC measured voltages

According to the obtained simulation results (Fig. 3-24, Fig. 3-25), in the period between 0 and 0.08 seconds, the Smart-STATCOM system is performing in Active Filter operation mode, as the rated fundamental grid voltage is measured at the PCC. Afterwards, by gradually decreasing the fundamental grid voltage, the STATCOM functionality is progressively introduced. This effect can be clearly observed in the test scenarios 2 and 3 from Fig. 3-25(a) and (b), when the proposed system is performing both STATCOM and Active Filter functionalities.

Finally, in the last test scenario, the system is purely performing in the STATCOM operation mode. In this case, the rated converter current is used in reactive power compensation due to the fact that the fundamental voltage is decreased to the minimum allowed limit (0.95pu). Therefore no current reserves are available for compensating harmonic voltages.

(a)

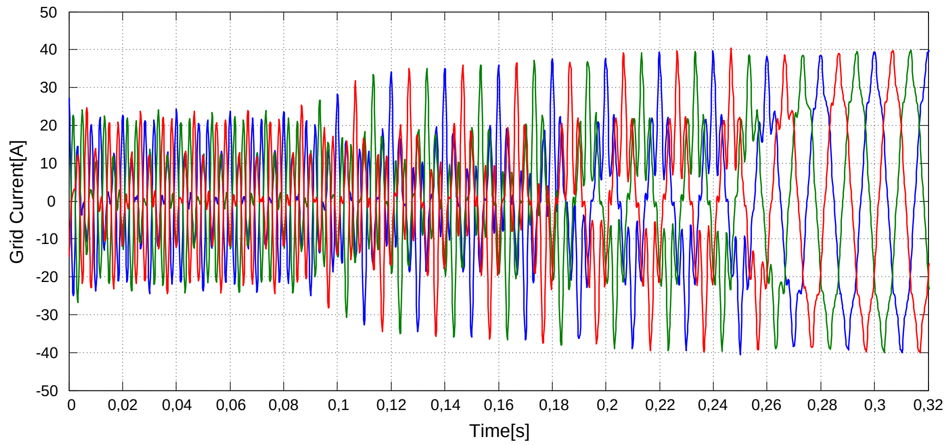

(b)

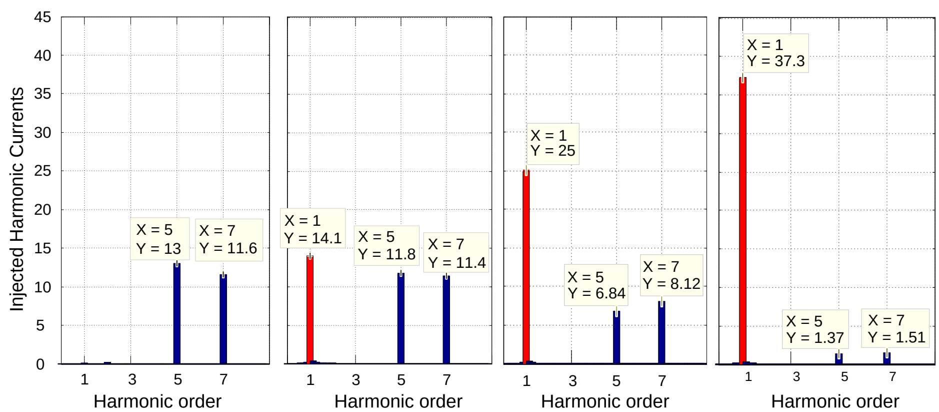

Fig. 3-25 Simulation results of Smart – STATCOM operation mode when PCC voltage variations and harmonic distortion are provided. (a) Measured Grid Currents, (b) FFT analysis of the measured grid current.

As a conclusion the Smart-STATCOM control strategy is self-controlled being able to provide compensation priority to the STATCOM operation mode, mitigating harmonic voltages only when the rated current of the converter is not fully used in compensating the reactive power. In this way the most suitable combination of STATCOM and Active Filter functionalities is obtained in order to achieve maximum power quality at the PCC.

4. Laboratory Implementation

This chapter presents the laboratory implementation of the proposed control strategies described in the previous chapter. It is worth to mention that identical system conditions and controller parameters have been considered as the ones specified in chapter 3. Therefore the achievement of similar laboratory results as in the simulations is expected. Furthermore, the main laboratory setup components are introduced in order to achieve a better understanding of the system behavior. Finally, the obtained laboratory results have been used to validate the system performance in STATCOM, Active Filter and Smart-STATCOM operation modes.

4.1 Laboratory setup description

The laboratory setup consists of a three-level DNPC converter connected to a grid simulator through a LCL filter. The purpose of the grid connected converter is to instantaneously inject the required amount of compensation non-active currents in order to provide maximum PCC voltage quality according to the rated parameters of the system. An LCL filter is used to meet harmonic current injection requirements. Furthermore, the voltage distortion introduced by the WPP (5^{th} and 7^{th} harmonics) is provided to the PCC by using a California Instruments grid simulator. In this way the described system functionalities (STATCOM, Active Filter and Smart-STATCOM) can be tested. Finally the desired system controllability is achieved by implementing the designed control algorithm using a dSPACE 1006 which includes a DS5101 FPGA board. The laboratory setup schematic and its physical implementation are introduced in Fig. 4-1(a) and (b) respectively.

(a) (b)

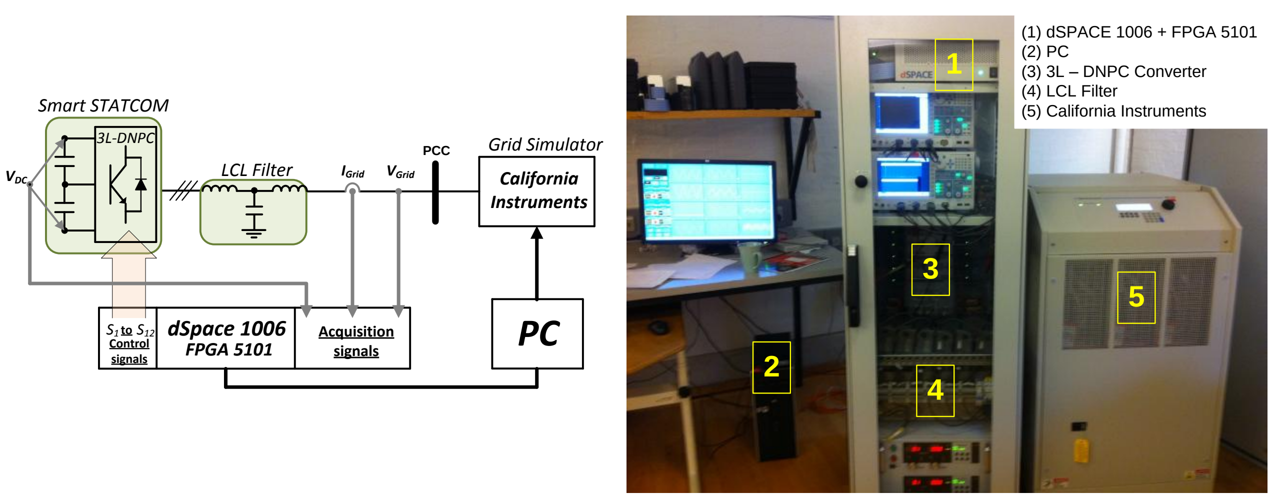

Fig. 4-1 (a) Laboratory setup schematic of the proposed power conditioner system(STATCOM+AF); (b)Laboratory implementation of the proposed system

According with Fig. 4-1(b), the main components of the laboratory setup are:

(1) dSPACE 1006 + FPGA 5101 board - Control Implementation

The proposed digital control algorithm, which was previously described in section 3.4, has been implemented in the laboratory setup by using a dSPACE DS1006 system. This system is based on one central processor, which is responsible of performing all the required calculations needed in measuring, monitoring and control of the system parameters. The interaction between the physical system and the control unit is achieved by using I/O boards. This I/O ports will be in charge of acquiring the measured signals from the LEM boxes (currents and voltages) and sending the IGBT control signals resulting from the control unit calculations. Furthermore, the central processing unit is directly programmed in C-code language, as it allows more precise controllability than building the system from Matlab/Simulink. Additionally a DS5101 Digital Waveform Output (DWO) board, based on FPGA, is responsible of providing the firing pulses for each IGBT (12 separately control signals) as well as performing the sampling period synchronization. Therefore, taking the measurements and control constants as inputs, the main processing board is able of calculating the dwell times needed for each IGBT. Further on, these times are provided as an input to the DS5101 board which generates the firing pulses by using a high precision timer. In addition, this board is producing an interruption to the main processor when a new sampling period is appearing. The FPGA based board is programmed by using a particular DWO language developed for this specific case.

One of the main advantages in implementing the proposed control strategy in a dSPACE system is the ability of real time controlling and monitoring the system behaviour.

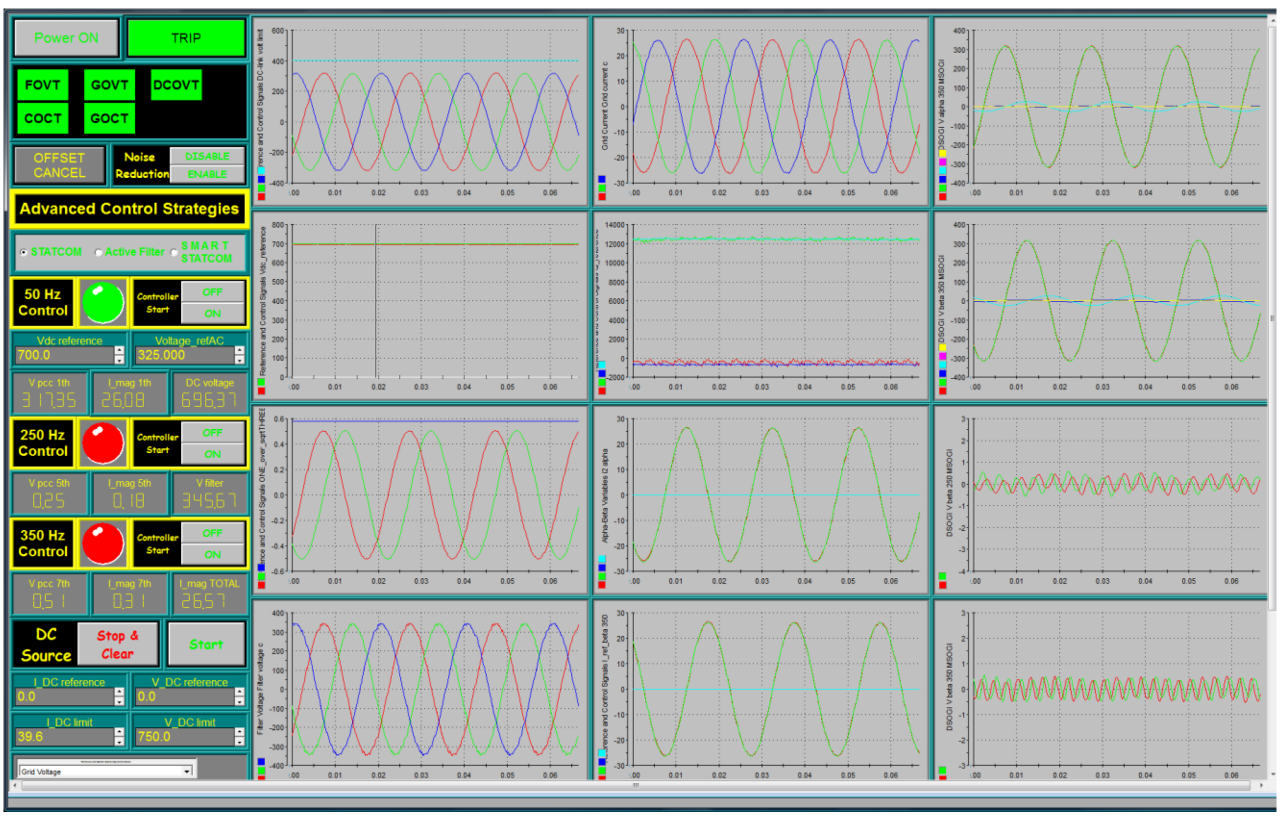

Fig. 4-2 dSPACE Control Desk Interface

The control parameters can be modified in real time by using the Control Desk Interface introduced in Fig. 4-2. According with the previous figure, two sections can be easily identified. The left side column shows the control interface which allows the user to interact with the system, while the right side presents the online monitoring of the control signals. Furthermore the main control commands of the system interface are:

- Power ON button and TRIP display – This control variables represent the Enable and Reset signal of the converter, together with the software trip displays.
- Advanced Control Strategies selector – This control command allows the selection of the system operation mode: STATCOM, Active Filter and Smart-STATCOM.
- 50Hz Current Control button – The main functionality of this command is to enable and disable the current control for fundamental frequency. Additionally it is worth to mention that DC-link voltage reference is provided through a numerical input button. Initially, the grid voltage is slowly increased to its rated value in order to charge the DC-link voltage to 560V. Afterwards, the 50Hz controller is enabled and the DC-link voltage reference is increased to the rated value of 700V.
- 250Hz and 350Hz Current Control buttons – The Enable and Disable signals for the 5^{th} and 7^{th} harmonic current controllers is provided by these specific buttons.

(2) 3L-DNPC converter

The physical converter used in the laboratory setup (Fig. 4-3 b-c) can be represented by the schematic introduced in Fig. 4-3a. As it can be seen the 3L-DNPC converter is built by using two IGBT modules for each phase. An IGBT module consist of two series connected transistors with a middle point and gate control access. As it can be observed in Fig. 4-3b, the used IGBT modules are connected between them by using three plates, corresponding to the negative (N), positive (P) and zero (0) voltages of the DC-link. Each gate-driver is receiving two control signals (one for each power transistor), by using optical cable transmission from the dSPACE. Finally, the rated parameters of 3L-DNPC converter are introduced as follows:

- Converter rated power: S = 20kVA
- Rated grid voltage (L-L RMS): V_{grid} = 400V
- Converter rated current (RMS): I_{conv} = 30A
- DC-link voltage: V_{DC} = 700V
- Switching Frequency: F_{sw} = 3kHz

(a)

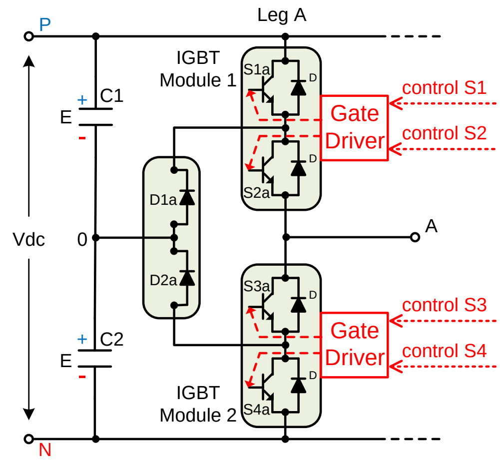

(b)

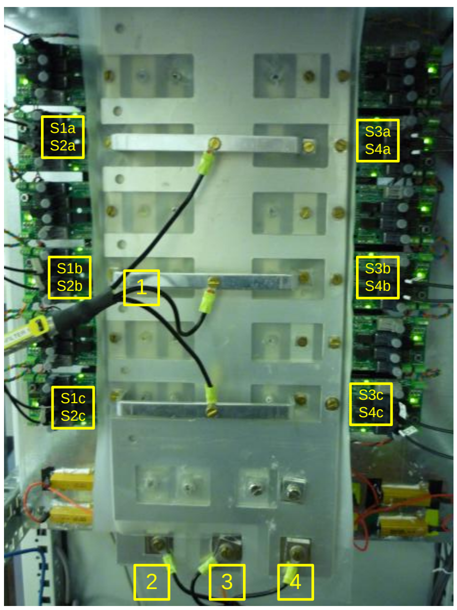

(1)3phase output voltage, (2) Positive DC-link Plate, (3) Neutral DC-link Plate, (4) Negative DC-link Plate

(c)

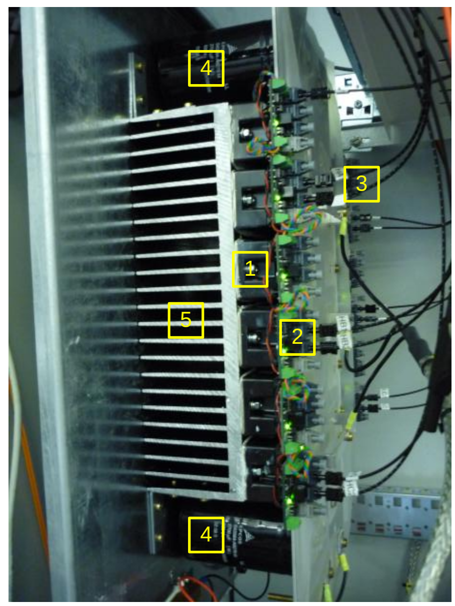

(1) IGBT Module, (2) gate driver, (3) optical control signals, (4) DC-link capacitors, (5) heat sink

Fig. 4-3 (a) Laboratory 3L-DNPC converter schematic,(b) laboratory 3l-DNPC physical setup front view, (c) laboratory 3l-DNPC physical setup profile view

(3) LCL-Filter

A three phase LCL filter is needed in order to fulfill the harmonic current injection requirements. The line filter is implemented according with the specified parameters from section 3.1.2. In order to achieve the desired functionalities of the laboratory setup, the initially available LCL-filter was modified, as the resonant frequency of the filter (≅ 455Hz) was closely placed to the desired control bandwidth (350Hz). Therefore in order to increase the resonant frequency in the most cost effective way, the filter capacitor has been decreased from the initial value of 133uF to 20uF. In this way the desired resonant frequency has been selectively placed at 1.2kHz, as this value corresponds to the 24th harmonic frequency (triplen harmonic) and it is placed far away from the main characteristic harmonics.

(4) Grid Simulator

In a real system application, (when the power conditioner is shunt connected to the WPP) the PCC voltage is distorted by the injection of harmonic currents from the WPP. Therefore, the PCC voltage in the laboratory setup has to be distorted in order to emulate these conditions. A better approach to the real system behavior can be obtained when the voltage distortion introduced by the WPP (5th and 7th harmonics in this specific case) is provided to the PCC by using a California Instruments grid simulator. Thus, the described STATCOM, Active Filter and Smart-STATCOM functionalities can be tested.

The California Instruments grid simulator offers the possibility to program the desired output voltage conditions, by using dedicated software for this application (MX30-GUI). As a result several variations of the grid parameters (amplitude of fundamental, 5th and 7th harmonic voltages) are provided in order to test the dynamic performance of the system. A print-screen of the programmable control interface is introduced in Fig. 4-4.

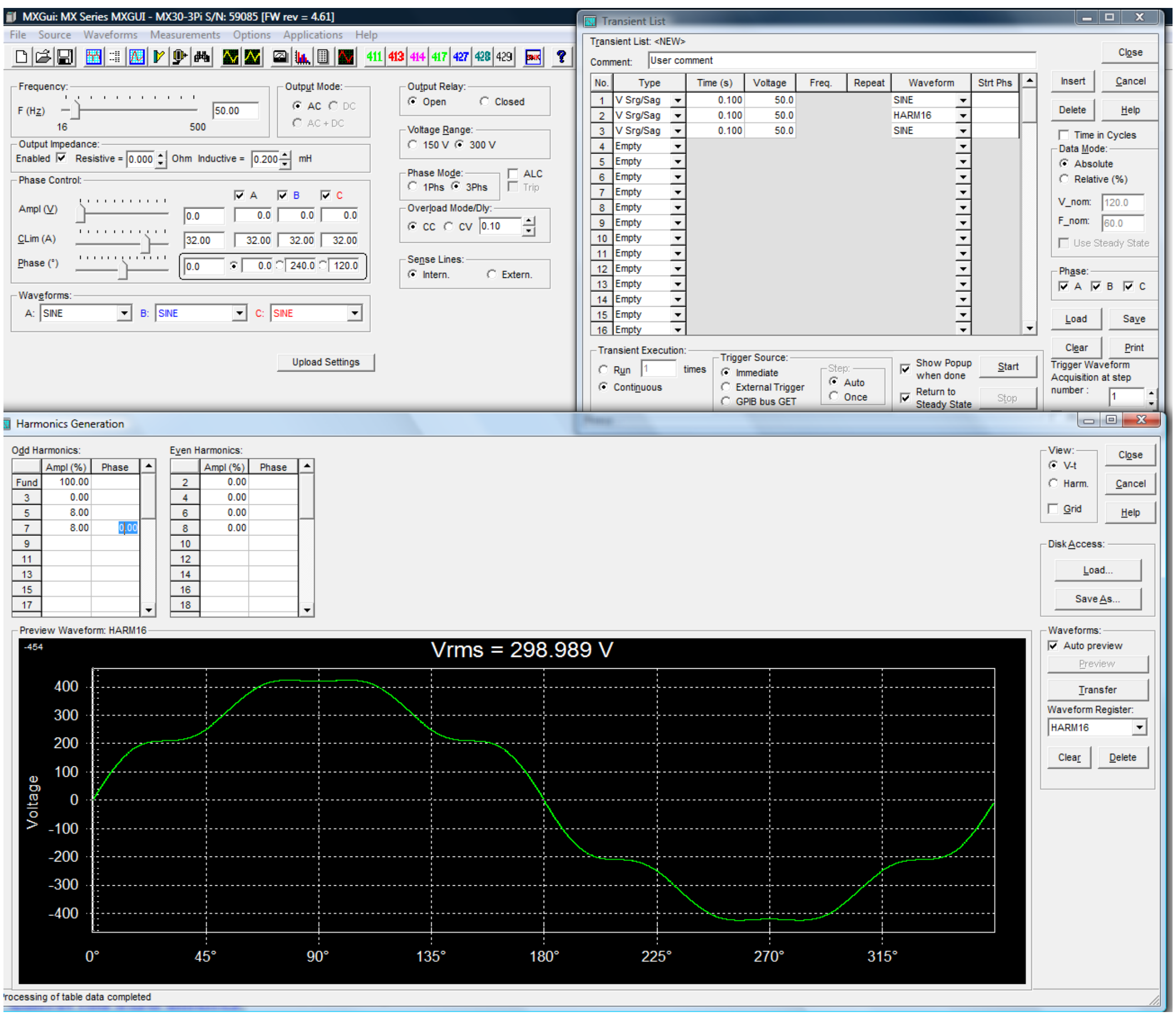

Fig. 4-4 California Instruments Control Interface

4.2 Experimental Results in STATCOM Operation Mode

In this section the laboratory setup is tested in STATCOM operation mode. As the purpose of this functionality is to provide PCC fundamental voltage control, its performance is analyzed when voltage variations are appearing into the grid. Therefore, these grid voltage variations are introduced by the grid simulator (California Instruments). In order to emphasize the dynamic response of the system, the test scenarios introduced in Table 4-1 are provided. Where 1pu is 230V $RMS_{phase-neutral}$.

Test Scenario	Time Duration [s]	PCC voltage [pu]	Reactive power [kVar]
1	0 to 0.06	0.95	20
2	0..06 to 0.1	1	0
3	0.1 to 0.16	1.04	-20
4	0.16 to 0.2	1	0

Table 4-1 Test scenarios used in laboratory in order to validate the STATCOM operation mode

According to the obtained results introduced in Fig. 4-5(a-b-c), it can be observed that in case a voltage variation of approximately ±0.05pu is present at the PCC, rated reactive power (and current) is injected (Test Scenario 1) or absorbed (Test Scenario 2) to the grid. In this case, the proposed STATCOM operation mode follows the German EON Netz grid codes, as a step from 0 to 20kVar is provided within 20ms (Fig. 4-5b) [37].

Taking into consideration the laboratory results, it can be stated that the STATCOM is improving the power quality of the system by providing grid voltage support and reactive power compensation.

(a)

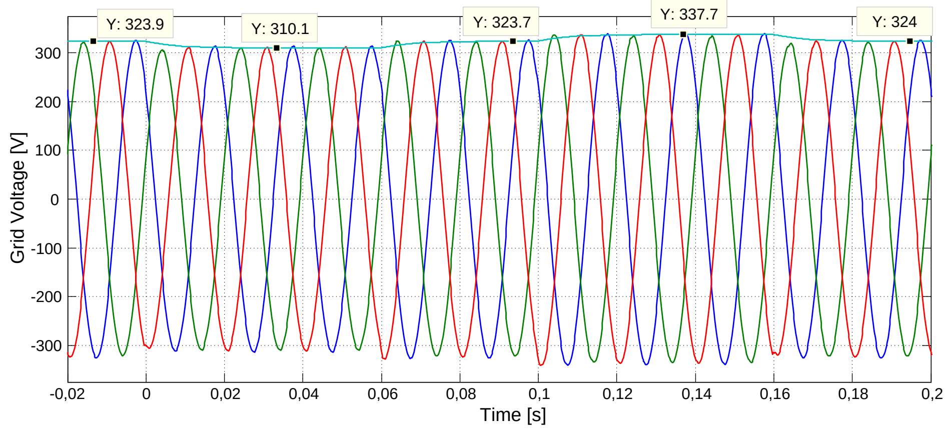

(b)

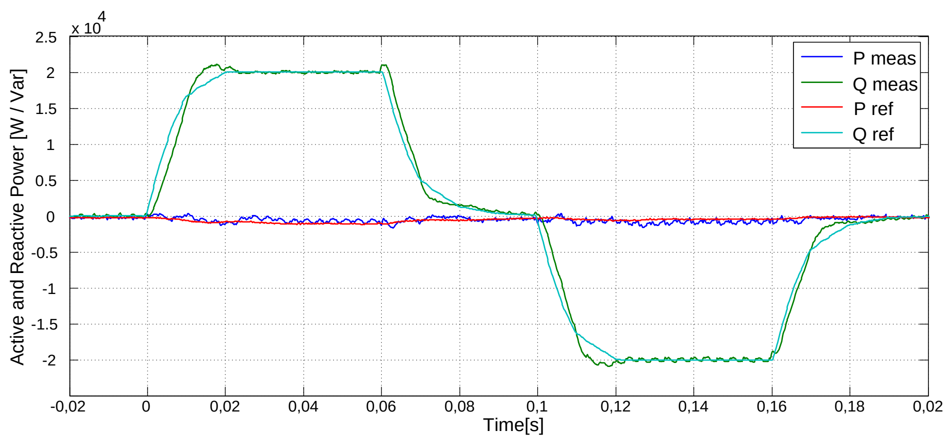

(c)

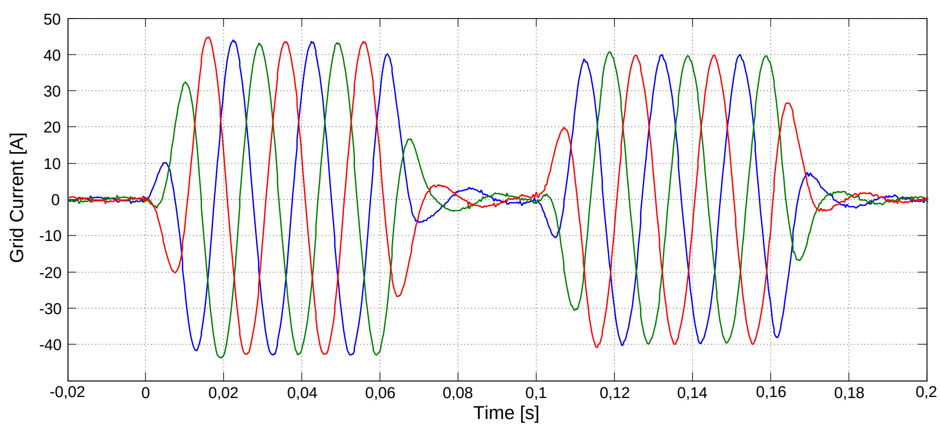

Fig. 4-5 Laboratory results of STATCOM operation mode when PCC voltage variations are provided. (a)Measured Voltage at the PCC, (b) Active and Reactive Power Measured and References, (c)Measured Grid Currents

4.3 Experimental Results in Active Filter Operation Mode

The laboratory test has been performed by using the California Instruments grid simulator in order to provide a harmonic grid voltage distortion at the PCC. Fig. 4-6(a-b) shows that the PCC harmonic voltage content before enabling the Active Filter functionality is :

- V_{1th} = 1pu (230V $RMS_{phase\text{-}neutral}$)
- V_{5th} = 0.08 pu
- V_{7th} = 0.08 pu

with a THD of 11.32%.

Once the active filter functionality has been activated (at time 0s), the voltage quality improvement can be observed in Fig. 4-6a-b.

(a)

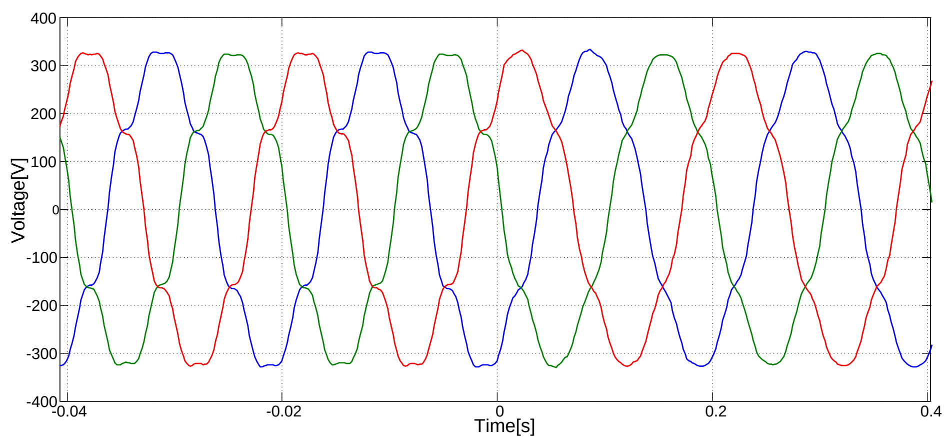

(b)

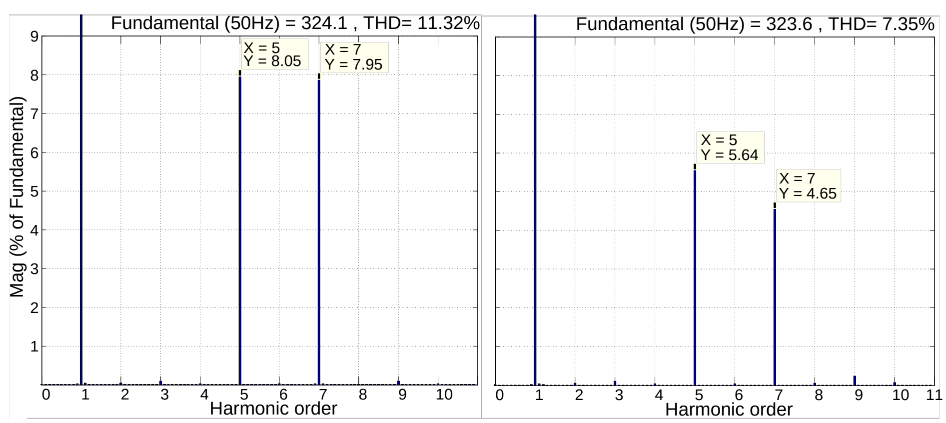

Fig. 4-6 Laboratory results of Active Filter operation mode when rated 5th and 7th harmonic voltages are compensated at t = 0 seconds. (a)Measured voltage at the PCC, (b)FFT analysis of the PCC measured voltages before and after current harmonics compensation,

By performing in Active Filter operation mode, the inverter is injecting the necessary non-active currents (Fig. 4-7a-b) in order to mitigate the harmonic voltages within the allowed limits (6% for 5th and 5% for 7th) Fig. 4-6(b) [14]. Therefore, the PCC harmonic voltages are reduced to:

- V_{5th} = 0.0564 pu (< 6%)
- V_{7th} = 0.0465 pu (< 5%)

and the THD is reduced to 7.35%.

(a)

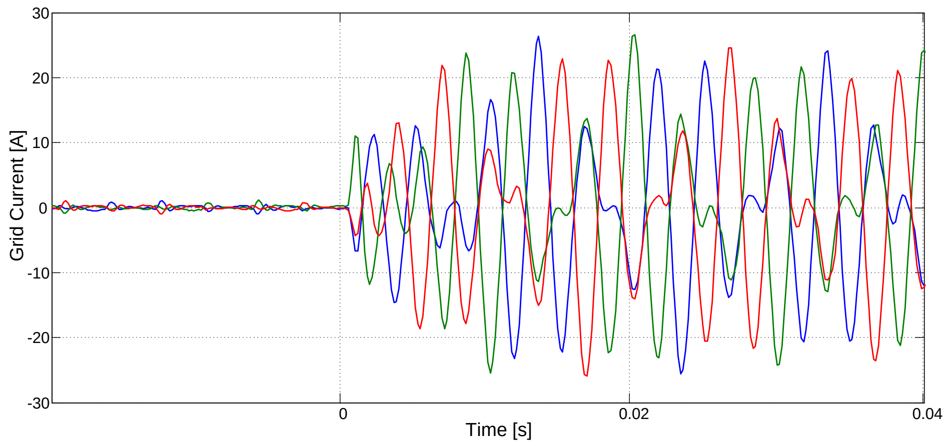

(b)

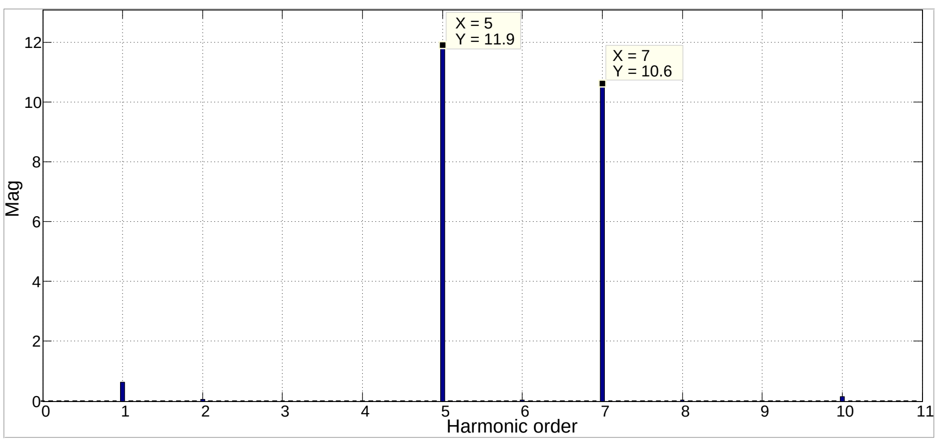

Fig. 4-7 Laboratory results of Active Filter operation mode when rated 5^{th} and 7^{th} harmonic voltages are compensated at t = 0 seconds. (a)Measured Grid Currents, (b)FFT analysis of the measured grid current,

Finally, it is worth to note that a power quality improvement has been achieved, by obtaining a reduction of 3.98% in voltage THD.

4.4 Experimental Results in Smart-STATCOM Operation Mode

In this case the Smart-STATCOM operation mode is tested in the Laboratory setup in order to validate the proposed control strategy in section 3.4.3. The system behaviour is analysed when grid voltage variations and harmonic distortion are provided to the PCC by the California Instruments grid simulator. Therefore, the 5^{th} and 7^{th} harmonic voltage content is set at 8% of the fundamental rated voltage while the amplitude of the fundamental voltage is changed according to the following test scenarios:

Test Scenario	Time Duration [s]	PCC voltage (fundamental) [pu]
1	0 to 0.06	1
2	0..06 to 0.12	0.98
3	0.12 to 0.18	0.97
4	0.18 to 0.24	0.95

Table 4-2 Test scenarios used in laboratory in order to validate the Smart-STATCOM operation mode

(a)

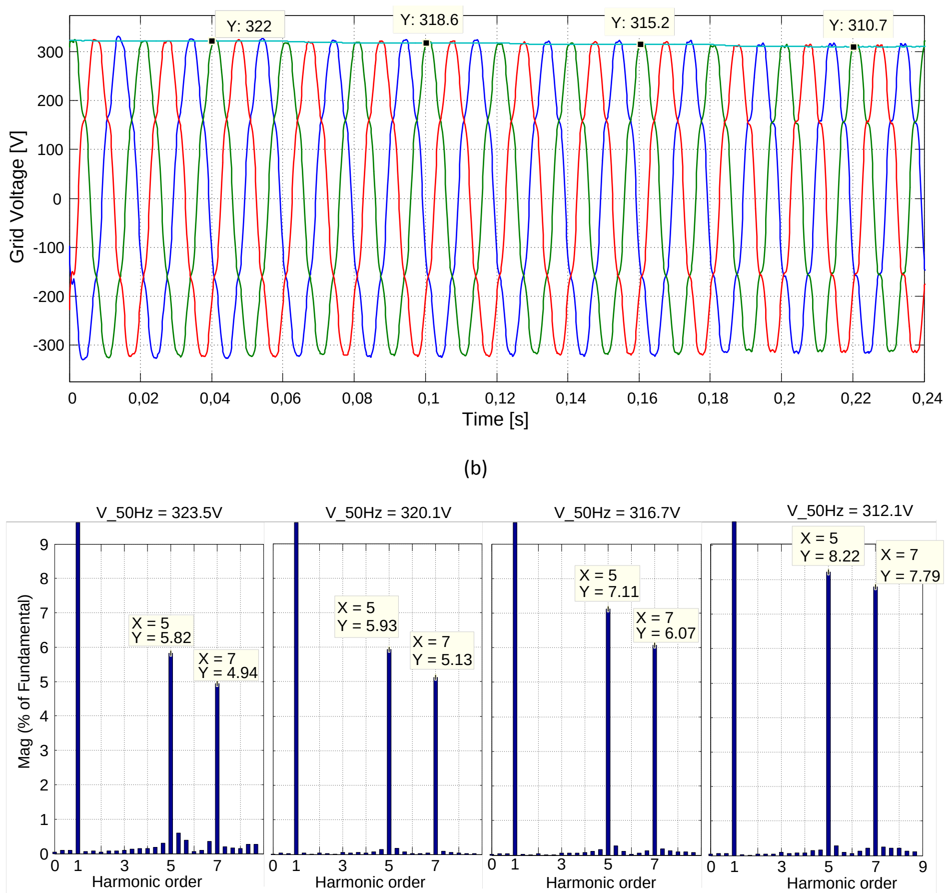

Fig. 4-8 Laboratory results of Smart – STATCOM operation mode when PCC voltage variations and harmonic distortion are provided. (a) Measured voltage at the PCC, (b) FFT analysis of the PCC measured voltages

As it can be observed in Fig. 4-8 and Fig. 4-9, in the first test scenario (from 0 to 0.06 s) the Smart-STATCOM system is performing in Active Filter operation mode, as rated fundamental voltage is measured. Due to the fact that fundamental PCC voltage control is not required, the total current injection capability is used in providing voltage harmonic compensation. Therefore, Fig. 4-9a-b shows that mainly 5^{th} and 7^{th} harmonic currents are injected to the grid. Comparing the obtained results for this specific case with the results from the Active Filter operation mode (section 4.3), it can be stated that the system shows a similar behaviour, e.g. reducing in both cases the harmonic voltages to the allowed limits.

(a)

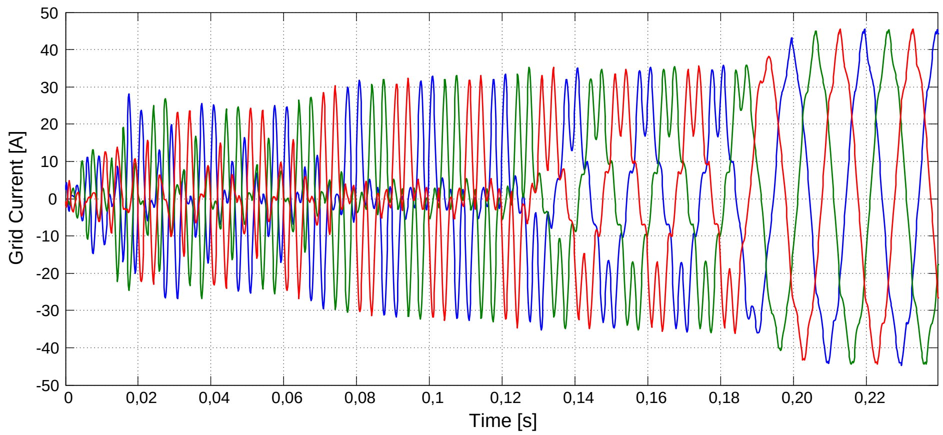

(b)

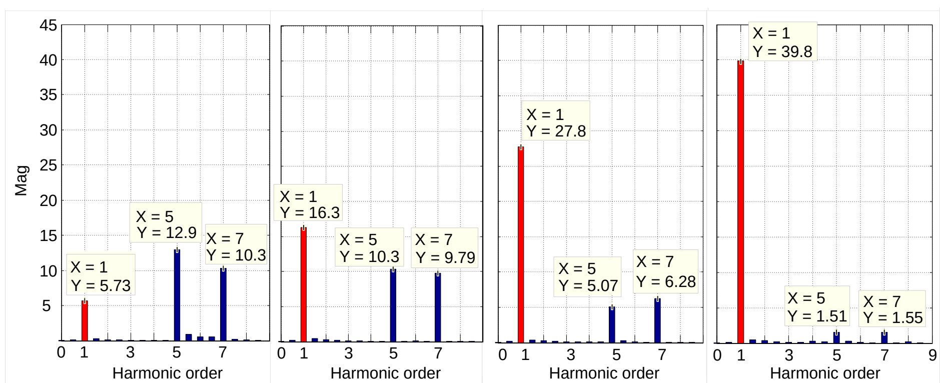

Fig. 4-9 Laboratory results of Smart – STATCOM operation mode when PCC voltage variations and harmonic distortion are provided. (a) Measured Grid Currents, (b) FFT analysis of the measured grid current.

Afterwards, the STATCOM operation mode is progressively introduced by gradually decreasing the fundamental grid voltage. This effect can be clearly observed in the test scenarios 2 and 3 from Fig. 4-8 and Fig. 4-9, when the proposed system is performing both STATCOM and Active Filter functionalities. The main difference between the obtained results of the test scenarios 2 and 3, is that in the third one, the injection of harmonic currents is limited due to the fact that a significant variation for fundamental voltage is present at the PCC. It can be observed that according to the proposed Smart Power Management system, the reserve current (rated converter current – fundamental current) is used in compensating the harmonic voltages, as the sum of the injected currents (fundamental, 5^{th} and 7^{th}) cannot overpass the maximum rated current of the converter (40A rated peak converter current). Therefore, the injection of harmonic currents is limited as the STATCOM operation mode is the main functionality of the system.

Finally, in the last test scenario, the system is purely performing in the STATCOM operation mode due to the fact that the fundamental voltage is decreased to the minimum allowed limit (0.95pu). In this case, Fig. 4-9b emphasize that the rated converter current is used in providing reactive power compensation. Therefore no current reserves are available for compensating harmonic voltages.

As a conclusion the Smart-STATCOM control strategy is self-controlled being able to provide compensation priority to the STATCOM functionality, mitigating harmonic voltages only when the rated current of the converter is not fully used in compensating the reactive power. In this way the most suitable combination of STATCOM and Active Filter functionalities is obtained in order to achieve maximum power quality at the PCC. Finally, the proposed novel control strategy which combines the implementation of STATCOM and Active Filter operation modes in a self controlled manner is successfully validated by the obtained laboratory results.

5. Conclusions and future work

5.1 Conclusions

Nowadays, an increasing awareness regarding power quality and stability problems has been experienced mainly due to the high penetration levels of wind energy into the power systems. It is worth to mention that some of the most important grid code compliance difficulties that can be found in WPPs are related to reactive power compensation and to keep the harmonics content within the allowed limits. Therefore, in order to improve the power quality of the WPPs, this project was focused on the control design implementation of a 3L-DNPC power conditioner based on a STATCOM which is able to perform as an Active Filter for 5^{th} and 7^{th} harmonics.

In the proposed control strategy, three operation modes were presented in order to achieve the desired PCC voltage quality improvement. Firstly, the STATCOM operation mode, which was the main functionality of the system, was analyzed. In this case, the main objective was to provide reactive power compensation and voltage control capabilities under dynamic and steady state conditions by injecting or absorbing fundamental reactive currents. Additionally, the performance of the Active Filter operation mode was studied in case 5^{th} and 7^{th} harmonic grid voltage distortion was present at the PCC. Then, harmonic voltage mitigation was achieved by injecting 5^{th} and 7^{th} harmonic reactive currents. Finally, the Smart-STATCOM operation mode introduced a novel control strategy, as depending on the grid voltage conditions the system was self-controlled by providing the most suitable combination of STATCOM and Active Filter functionalities. This operation mode was based on a Smart Power Management system, which was designed in order to provide compensation priority to the STATCOM functionality, mitigating harmonic voltages only when the rated current of the converter is not fully used in compensating the reactive power.

In order to achieve the desired system functionalities, several controllers were used: a PI controller which regulates the DC-link voltage and three resonant current controllers for fundamental, 5^{th} and 7^{th} harmonic frequencies. Special attention was paid to the current controllers design, as a very selective behaviour was pursued in order to avoid any interaction between the resonant controllers. Additionally, three droop controllers (for 50Hz, 250Hz and 350Hz frequencies) were used with the purpose of determining the reference currents to be injected for obtaining the desired PCC voltages. Finally, the synchronization method used in the proposed system was based on M-SOGI FLL algorithm. As a result, the fundamental, 5^{th} and 7^{th} grid frequencies were continuously estimated for online tuning of the resonant controllers. Additionally, this grid synchronization method was able to detect the grid voltages for each of the specified harmonic frequencies, which were used as a feedback for the droop controllers.

Afterwards, the overall control strategy was implemented in simulation in order to validate the performance of the system when performing in the previously mentioned operation modes.

Finally the proposed control system was tested in laboratory under STATCOM, Active Filter and Smart-STATCOM operation modes. It is worth to mention that successful results were achieved, since very similar responses were obtained compared to the simulation ones. As a general conclusion, it can be stated that the proposed novel control strategy, which simultaneously combines STATCOM and Active Filter functionalities (Smart-STATCOM operation mode), was validated in the laboratory setup. Therefore, the overall objectives of this project were accomplished, since the designed control strategy provides voltage control and harmonic voltage mitigation at the PCC. Thus, the power quality of the WPP can be improved by implementing the proposed control structure in a shunt-connected three level power converter.

5.2 Future Work

In this section the future tasks that can be carried out as an improvement of the presented project are detailed as follows:

- The proposed control structure could be tested under unbalances and grid faults, as one of the main STATCOM functionalities is to ride through any kind of grid voltage conditions.
- An advanced DC link voltage control strategy could be implemented in order to improve the efficiency of the 3L-DNPC converter. Therefore the minimum DC-link voltage necessary in order to inject the required currents to the grid would be provided.
- The proposed control system could be tested in case a non-linear load would be shun-connected to the PCC. Therefore a realistic way of producing PCC grid voltage distortion would be achieved.
- The STATCOM operation mode could be tested in a real field application by directly connecting the power conditioner to the grid.
- Due to the fact that the proposed control strategy has been designed for high power applications (by using a low switching frequency), the introduced functionalities could be implemented in a real wind turbine grid-side converter. [39, 40][39, 40]

References

[1] T. Ackerman, Ed., *Wind Power in Power Systems.* Royal Institute of Technology Stockholm, Sweden: John Wiley & Sons, Ltd, 2005.

[2] EWEA, "*Pure power. wind energy targets for 2020 and 2030*," European Wind Energy Association, 2011.

[3] M. Mohseni and S. M. Islam, "A review of enabling technologies for large wind power plants to comply with recent grid codes," in *Innovative Smart Grid Technologies Asia (ISGT), 2011 IEEE PES,* 2011, pp. 1-6.

[4] P. Maibach, J. Wernli, P. Jones and M. Obad, "STATCOM Technology for Wind Parks to Meet Grid Code Requirements," *ABB Library, Doc. no. 3BHS237435 ZAB E01,* 2007.

[5] R. Grunbaum, "FACTS for grid integration of wind power," in *Innovative Smart Grid Technologies Conference Europe (ISGT Europe), 2010 IEEE PES,* 2010, pp. 1-8.

[6] H. Bindner and P. Lundsager, "Integration of wind power in the power system," in *IECON 02 [Industrial Electronics Society, IEEE 2002 28th Annual Conference of the],* 2002, pp. 3309-3316 vol.4.

[7] R. Dugan, M. McGranaghan, S. Santoso and W. Beaty, *Electrical Power Systems Quality.* McGraw-Hill, 2004.

[8] N. T. Linh, "Power quality investigation of grid connected wind turbines," in *Industrial Electronics and Applications, 2009. ICIEA 2009. 4th IEEE Conference on,* 2009, pp. 2218-2222.

[9] EN 61400-21, "Wind turbines-part 21: Measurement and assessment of power quality characteristics of grid connected wind turbines," 2008.

[10] J. Martinez and P. C. Kjaer, "Fast voltage control in wind power plants," in *Power and Energy Society General Meeting, 2011 IEEE,* 2011, pp. 1-7.

[11] J. Martinez, P. C. Kjar, P. Rodriguez and R. Teodorescu, "Comparison of two voltage control strategies for a wind power plant," in *Power Systems Conference and Exposition (PSCE), 2011 IEEE/PES,* 2011, pp. 1-9.

[12] J. Martinez, P. C. Kjar, P. Rodriguez and R. Teodorescu, "VAr reserve concept applied to a wind power plant," in *Power Systems Conference and Exposition (PSCE), 2011 IEEE/PES,* 2011, pp. 1-8.

[13] S. L. Clark, P. Famouri and W. L. Cooley, "Elimination of supply harmonics," *Industry Applications Magazine, IEEE,* vol. 3, pp. 62-67, 1997.

[14] EN 50160, "Voltage characteristics of electricity supplied by public electicity networks," 2010.

[15] A. Moran, J. Dixon, J. Espinoza and R. Wallace, "Using Active Power Filters to Improve Power Quality," .

[16] J. Arrillaga and N. Watson, *Power System Harmonics.* Wiley, 2003.

[17] H. Akagi, "Modern active filters and traditional passive filters," Bulletin of the Polish Academy of Sciences, Tech. Rep. Vol. 54, No. 3, 2006.

[18] B. Wu, *High-Power Converters and AC Drives.* John Wiley & Sons, 2006.

[19] R. Teodorescu, M. Liserre and P. Rodriguez, *Grid Connected Converters for Photovoltaic and Wind Power Systems.* Wiley, 2011.

[20] P. Rodriguez, A. Luna, M. Ciobotaru, R. Teodorescu and F. Blaabjerg, "Advanced grid synchronization system for power converters under unbalanced and distorted operating conditions," in *IEEE Industrial Electronics, IECON 2006 - 32nd Annual Conference on,* 2006, pp. 5173-5178.

[21] A. Luna, J. Rocabert, G. Vazquez, P. Rodriguez, R. Teodorescu and F. Corcoles, "Grid synchronization for advanced power processing and FACTS in wind power systems," in *Industrial Electronics (ISIE), 2010 IEEE International Symposium on,* 2010, pp. 2915-2920.

[22] P. Rodriguez, A. Luna, I. Candela, R. Teodorescu and F. Blaabjerg, "Grid synchronization of power converters using multiple second order generalized integrators," in *Industrial Electronics, 2008. IECON 2008. 34th Annual Conference of IEEE,* 2008, pp. 755-760.

[23] F. Blaabjerg, R. Teodorescu, M. Liserre and A. V. Timbus, "Overview of Control and Grid Synchronization for Distributed Power Generation Systems," *Industrial Electronics, IEEE Transactions on,* vol. 53, pp. 1398-1409, 2006.

[24] R. Teodorescu, F. Blaabjerg, M. Liserre and P. C. Loh, "Proportional-resonant controllers and filters for grid-connected voltage-source converters," *Electric Power Applications, IEE Proceedings -,* vol. 153, pp. 750-762, 2006.

[25] H. Akagi, Y. Kanazawa and A. Nabae, "Instantaneous Reactive Power Compensators Comprising Switching Devices without Energy Storage Components," *Industry Applications, IEEE Transactions on,* vol. IA-20, pp. 625-630, 1984.

[26] H. Akagi, S. Ogasawara and Hyosung Kim, "The theory of instantaneous power in three-phase four-wire systems: A comprehensive approach," in *Industry Applications Conference, 1999. Thirty-Fourth IAS Annual Meeting. Conference Record of the 1999 IEEE,* 1999, pp. 431-439 vol.1.

[27] P. Rodriquez, R. Pindado and J. Pou, "Energy control of three-phase four-wire shunt active power filter," in *Industrial Electronics Society, 2003. IECON '03. the 29th Annual Conference of the IEEE,* 2003, pp. 1061-1066 Vol.2.

[28] P. Rodriguez, A. Luna, R. Teodorescu, F. Blaabjerg and M. Liserre, "Control of a three-phase four-wire shunt-active power filter based on DC-bus energy regulation," in *Optimization of Electrical and Electronic Equipment, 2008. OPTIM 2008. 11th International Conference on,* 2008, pp. 227-234.

[29] Hanxiang Cheng, Xianggen Yin and Shaohua Chen, "DC-link voltage control and performance analysis of StatCom," in *Universities Power Engineering Conference, 2004. UPEC 2004. 39th International,* 2004, pp. 348-352 Vol. 1.

[30] M. Aredes, J. Hafner and K. Heumann, "Three-phase four-wire shunt active filter control strategies," *Power Electronics, IEEE Transactions on,* vol. 12, pp. 311-318, 1997.

[31] J. Turunen, M. Salo and H. Tuusa, "The influence of the DC-link voltage control on the current harmonic filtering of the series hybrid active power filters," in *Industrial Electronics Society, 2005. IECON 2005. 31st Annual Conference of IEEE,* 2005, pp. 6 pp.

[32] A. Adamczyk, R. Teodorescu, R. N. Mukerjee and P. Rodriguez, "Overview of FACTS devices for wind power plants directly connected to the transmission network," in *Industrial Electronics (ISIE), 2010 IEEE International Symposium on,* 2010, pp. 3742-3748.

[33] H. Ren, D. Watts, Z. Mi, J. Lu, Zengqiang Mi and Jinling Lu, "A review of FACTS' practical consideration and economic evaluation," in *Power and Energy Engineering Conference, 2009. APPEEC 2009. Asia-Pacific,* 2009, pp. 1-5.

[34] N. Hingorani and L. Gyugyi, *Understnding FATCS: Concepts and Technology of Flexible AC Transmission Systems.* IEEE PRESS, 1999.

[35] X. Zhang, C. Rehtanz and B. Pal, *Flexible AC Transmission Systems: Modelling and Control.* Springer, 2006.

[36] H. Akagi, E. Watanabe and M. Aredes, *Instantaneous Power Theory and Applications to Power Conditioning.* John Wiley & Sons, 2007.

[37] EON Netz Grid Codes, "Requirements for offshore grid connections in the E.ON netz network," E.ON, 2008.

[38] V. Soares, P. Verdelho and G. D. Marques, "An instantaneous active and reactive current component method for active filters," *Power Electronics, IEEE Transactions on,* vol. 15, pp. 660-669, 2000.

Appendix A

αβ0 Reference Frame Transformations of Three Phase Signals

This section presents the equations that have been used in achieving the desired reference frame transformations. In this section the Clarke transformation is presented due to the fact that only natural (abc) and stationary (αβ0) coordinate systems are used in the main report. The main objective of these transformations is to generate the stationary components from the three phase ones and vice versa in order to simplify the analysis of a three-phase system. Therefore the Clarke transformation is applied to the three-phase currents in equations (A.1) and (A.2) in case a three-phase for-wire generic system is considered.

$$\begin{bmatrix} I_\alpha \\ I_\beta \\ I_0 \end{bmatrix} = \begin{bmatrix} T_{\alpha\beta 0} \end{bmatrix} \begin{bmatrix} I_a \\ I_b \\ I_c \end{bmatrix} = \frac{2}{3} \begin{bmatrix} 1 & -\frac{1}{2} & -\frac{1}{2} \\ 0 & \frac{\sqrt{3}}{2} & -\frac{\sqrt{3}}{2} \\ \frac{1}{2} & \frac{1}{2} & \frac{1}{2} \end{bmatrix} \begin{bmatrix} I_a \\ I_b \\ I_c \end{bmatrix} \tag{A.1}$$

$$\begin{bmatrix} I_a \\ I_b \\ I_c \end{bmatrix} = \begin{bmatrix} T_{\alpha\beta 0} \end{bmatrix}^{-1} \begin{bmatrix} I_\alpha \\ I_\beta \\ I_0 \end{bmatrix} = \begin{bmatrix} 1 & 0 & 1 \\ -\frac{1}{2} & \frac{\sqrt{3}}{2} & 1 \\ -\frac{1}{2} & -\frac{\sqrt{3}}{2} & 1 \end{bmatrix} \begin{bmatrix} I_\alpha \\ I_\beta \\ I_0 \end{bmatrix} \tag{A.2}$$

In the case a balanced three-phase or a three-phase three-wires system is considered, no zero-sequence currents can be obtained. Then $I_0 = I_a + I_b + I_c = 0$ and the previous equations can be reformulated in (A.3) and (A.4).

$$\begin{bmatrix} I_\alpha \\ I_\beta \end{bmatrix} = \begin{bmatrix} T_{\alpha\beta} \end{bmatrix} \begin{bmatrix} I_a \\ I_b \\ I_c \end{bmatrix} = \frac{2}{3} \begin{bmatrix} 1 & -\frac{1}{2} & -\frac{1}{2} \\ 0 & \frac{\sqrt{3}}{2} & -\frac{\sqrt{3}}{2} \end{bmatrix} \begin{bmatrix} I_a \\ I_b \\ I_c \end{bmatrix} \tag{A.3}$$

$$\begin{bmatrix} I_a \\ I_b \\ I_c \end{bmatrix} = \begin{bmatrix} T_{\alpha\beta} \end{bmatrix}^{-1} \begin{bmatrix} I_\alpha \\ I_\beta \end{bmatrix} = \begin{bmatrix} 1 & 0 \\ -\frac{1}{2} & \frac{\sqrt{3}}{2} \\ -\frac{1}{2} & -\frac{\sqrt{3}}{2} \end{bmatrix} \begin{bmatrix} I_\alpha \\ I_\beta \end{bmatrix} \tag{A.4}$$

Appendix B

C-Code Implementation of Current Controllers

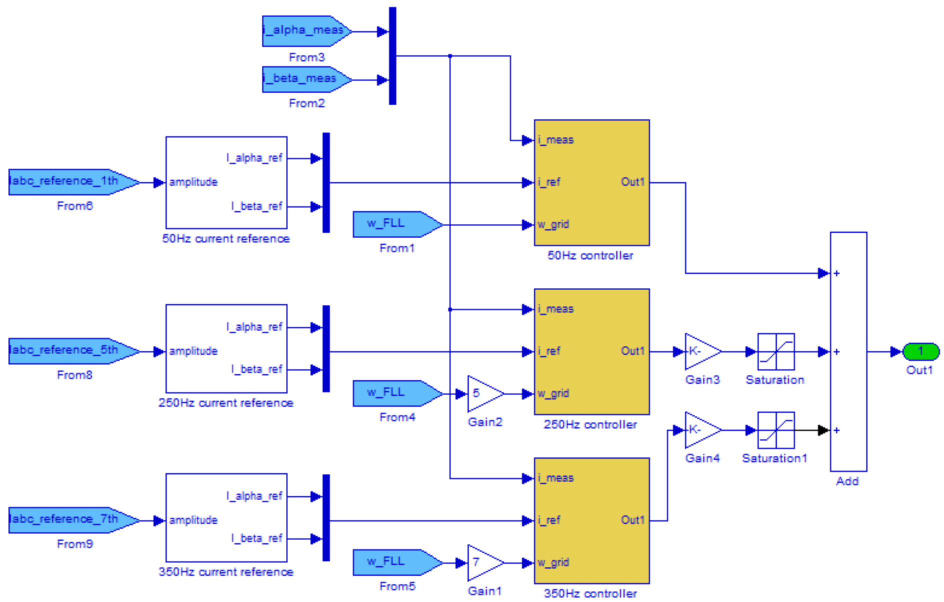

Fig. B-1 Current Control structure for 50Hz, 250Hz and 350Hz implemented in simulation

The initialization of the control variables and constant tuning parameters has been included in to a header file, which is executed before the following presented C-codes. Additionally, the introduced C-codes have been used in order to implement the current controllers in both simulation and laboratory.

```
//current control parameters
float error_alpha[3];
float error_beta[3];
float u_ref_alpha[3];
float u_ref_beta[3];
float voltage_alpha[3];
float voltage_beta[3];
const float Tsample = 1.6667e-004;
float omega;

float cosine_50;
float delta_1_50;
float delta_2_50;

const float K_50 = 1.59441128595;
const float K_alpha_1_50 = -3.04937601736;
const float K_alpha_2_50 = 1.4579489962;
const float alpha_1_50 = -1.91254041177;
const float alpha_2_50 = 0.914412115022;
```

```
const float a_50 = 1.59441128595;
const float b_50 = -3.04937601736;
const float c_50 = 1.4579489962;

float d_250;
const float a_250 = 2.30711864407;
const float b_250 = -4.25152542373;
const float c_250 = 2.04203389831;

float d_350;
const float a_350 = 3.20073519758;
const float b_350 = -5.72666;
const float c_350 = 2.73073388473;

float volt_alpha_total;
float volt_beta_total;
float theta_v_ref;
float u_ref_mag;

float u_limit;         //  700/sqrt(3)-->Vdc/sqrt(3)
float ONEoverU_LIMIT;  //  1/700-->1/Vdc
const float limit_magnitude = 0.57735025;   // 1/sqrt(3)
```

A.1 50Hz Current Controller Implementation

```
/* This sample sets the output equal to the input
         y0[0] = u0[0];
For complex signals use: y0[0].re = u0[0].re;
                         y0[0].im = u0[0].im;
                         y1[0].re = u1[0].re;
                         y1[0].im = u1[0].im;*/

if (Controller_start[0]) {

    error_alpha[2] = error_alpha[1];
    error_alpha[1] = error_alpha[0];
    error_alpha[0] = current_ref[0] - current_meas[0];

    //------------------------------*/
    u_ref_alpha[2] = u_ref_alpha[1];
    u_ref_alpha[1] = u_ref_alpha[0];

    //----------------------------*/
    error_beta[2] = error_beta[1];
    error_beta[1] = error_beta[0];
    error_beta[0] = current_ref[1] - current_meas[1];

    //----------------------------*/

    u_ref_beta[2] = u_ref_beta[1];
    u_ref_beta[1] = u_ref_beta[0];
```

```
    cosine_50 = 2*cos(omega_grid[0]*Tsample);
    delta_1_50 = - cosine_50 - alpha_1_50;
    delta_2_50 = 1 - alpha_2_50;


u_ref_alpha[0] = K_50*error_alpha[0] + K_alpha_1_50*error_alpha[1] +
K_alpha_2_50*error_alpha[2] - alpha_1_50*u_ref_alpha[1] -
alpha_2_50*u_ref_alpha[2] - delta_1_50*voltage_alpha[0] -
delta_2_50*voltage_alpha[1]; // ideal (no limit) "alpha" voltage reference

u_ref_beta[0]  = K_50*error_beta[0]  + K_alpha_1_50*error_beta[1]  +
K_alpha_2_50*error_beta[2]  - alpha_1_50*u_ref_beta[1]  -
alpha_2_50*u_ref_beta[2]  - delta_1_50*voltage_beta[0]  -
delta_2_50*voltage_beta[1]; // ideal (no limit) "beta" voltage reference

    //----------------------------------*/

    voltage_alpha[2] = voltage_alpha[1];
    voltage_alpha[1] = voltage_alpha[0];

    //--------------------------------*/

    voltage_beta[2] = voltage_beta[1];
    voltage_beta[1] = voltage_beta[0];
}
else {

    error_alpha[2] = 0;
    error_alpha[1] = 0;
    error_alpha[0] = 0;

    u_ref_alpha[2] = 0;
    u_ref_alpha[1] = 0;
    u_ref_alpha[0] = 0;

    error_beta[2] = 0;
    error_beta[1] = 0;
    error_beta[0] = 0;

    u_ref_beta[2] = 0;
    u_ref_beta[1] = 0;
    u_ref_beta[0] = 0;

    voltage_alpha[2] = 0;
    voltage_alpha[1] = 0;
    voltage_alpha[0] = 0;

    voltage_beta[2] = 0;
    voltage_beta[1] = 0;
    voltage_beta[0] = 0;
}

omega = omega_grid[0];
```

```
volt_alpha_total = u_ref_alpha[0];
volt_beta_total  = u_ref_beta[0];

theta_v_ref = atan2(u_ref_beta[0], u_ref_alpha[0]);// Ideal voltage reference
vector angle
u_ref_mag = sqrt(pow(u_ref_alpha[0],2)+ pow(u_ref_beta[0],2));//Ideal voltage
reference vector magnitude

u_limit = Vdc_converter[0]/sqrt(3);
ONEoverU_LIMIT = 1/Vdc_converter[0];

if (u_ref_mag < u_limit) {       // Voltage within the limits (u_limit =
Vdc/sqrt(3))
    voltage_alpha[0] = u_ref_alpha[0];
    voltage_beta[0]  = u_ref_beta[0] ;
    volt_scaled[0]   = volt_alpha_total * ONEoverU_LIMIT;       // Values are
scaled to fit within the inscribed circle of SVM (1/sqrt(3)),
    volt_scaled[1]   = volt_beta_total  * ONEoverU_LIMIT;
}
else {                           // Voltage is outside the Vdc/sqrt(3) limit
    voltage_alpha[0] = u_limit * cos(theta_v_ref);   // applied voltage is
limited maintaining the angle and reducing the magnitude
    voltage_beta[0]  = u_limit * sin(theta_v_ref);    // The actual signal
fedback to the controller is the limited one, minus the feedforward signal
    volt_scaled[0]   = limit_magnitude * cos(theta_v_ref);              //
Scaling is necesary for the modulation algorithm.
    volt_scaled[1]   = limit_magnitude * sin(theta_v_ref);
}
```

A.2 250Hz Current Controller Implementation

```
/* This sample sets the output equal to the input
         y0[0] = u0[0];
For complex signals use: y0[0].re = u0[0].re;
                         y0[0].im = u0[0].im;
                         y1[0].re = u1[0].re;
                         y1[0].im = u1[0].im;*/

if (controller_start[0]){

    error_alpha[2] = error_alpha[1];
    error_alpha[1] = error_alpha[0];
    error_alpha[0] = i_ref[0] - i_meas[0];

    v_alpha_ref[2] = v_alpha_ref[1];
    v_alpha_ref[1] = v_alpha_ref[0];

    error_beta[2] = error_beta[1];
    error_beta[1] = error_beta[0];
    error_beta[0] = i_ref[1] - i_meas[1];

    v_beta_ref[2] = v_beta_ref[1];
```

```
    v_beta_ref[1] = v_beta_ref[0];

    d_250 = -2*cos(w_grid[0]*Tsample);

    v_alpha_ref[0] = a_250*error_alpha[0] + b_250*error_alpha[1] +
c_250*error_alpha[2] - d_250*v_alpha_ref[1] - v_alpha_ref[2];
    v_ref[0] = v_alpha_ref[0];

    v_beta_ref[0] = a_250*error_beta[0] + b_250*error_beta[1] +
c_250*error_beta[2] - d_250*v_beta_ref[1] - v_beta_ref[2];
    v_ref[1] = v_beta_ref[0];
}
else {
    error_alpha[2] = 0;
    error_alpha[1] = 0;
    error_alpha[0] = 0;

    v_alpha_ref[2] = 0;
    v_alpha_ref[1] = 0;
    v_alpha_ref[0] = 0;

    error_beta[2] = 0;
    error_beta[1] = 0;
    error_beta[0] = 0;

    v_beta_ref[2] = 0;
    v_beta_ref[1] = 0;
    v_beta_ref[0] = 0;

    v_ref[0] = v_alpha_ref[0];
    v_ref[1] = v_beta_ref[0];
}
```

A.3 350Hz Current Controller Implementation

```
/* This sample sets the output equal to the input
         y0[0] = u0[0];
For complex signals use: y0[0].re = u0[0].re;
                         y0[0].im = u0[0].im;
                         y1[0].re = u1[0].re;
                         y1[0].im = u1[0].im;*/

if (controller_start[0]){

    error_alpha[2] = error_alpha[1];
    error_alpha[1] = error_alpha[0];
    error_alpha[0] = i_ref[0] - i_meas[0];

    v_alpha_ref[2] = v_alpha_ref[1];
    v_alpha_ref[1] = v_alpha_ref[0];

    error_beta[2] = error_beta[1];
    error_beta[1] = error_beta[0];
```

```
    error_beta[0] = i_ref[1] - i_meas[1];

    v_beta_ref[2] = v_beta_ref[1];
    v_beta_ref[1] = v_beta_ref[0];

    d_350 = -2*cos(w_grid[0]*Tsample);

    v_alpha_ref[0] = a_350*error_alpha[0] + b_350*error_alpha[1] +
c_350*error_alpha[2] - d_350*v_alpha_ref[1] - v_alpha_ref[2];
    v_ref[0] = v_alpha_ref[0];

    v_beta_ref[0] = a_350*error_beta[0] + b_350*error_beta[1] +
c_350*error_beta[2] - d_350*v_beta_ref[1] - v_beta_ref[2];
    v_ref[1] = v_beta_ref[0];
}
else {
    error_alpha[2] = 0;
    error_alpha[1] = 0;
    error_alpha[0] = 0;

    v_alpha_ref[2] = 0;
    v_alpha_ref[1] = 0;
    v_alpha_ref[0] = 0;

    error_beta[2] = 0;
    error_beta[1] = 0;
    error_beta[0] = 0;

    v_beta_ref[2] = 0;
    v_beta_ref[1] = 0;
    v_beta_ref[0] = 0;

    v_ref[0] = v_alpha_ref[0];
    v_ref[1] = v_beta_ref[0];
}
```

Appendix C

DC-Link Voltage Control C-Code Implementation

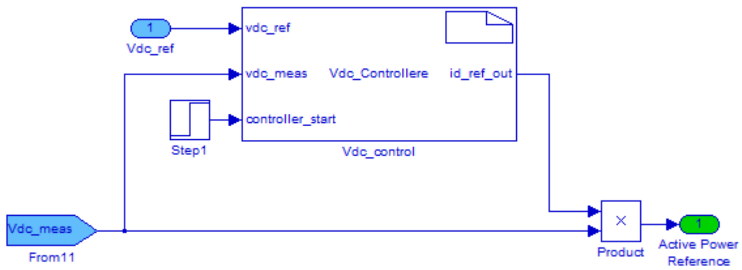

Fig. C-1DC-link voltage control structure implemented in simulation

The following introduced C-code corresponds to the one used in both simulation and laboratory implementation. It is worth to mention that the tuning parameters and control variables are initialized by using the following header file:

```
// Voltage control

float error_voltage[2];
float Id[2];
const float Tsample = 1.6667e-004;
const float a_pi = 0.2484;
const float b_pi = -0.2474;
```

Then the main C-code is given as:

```
/* This sample sets the output equal to the input
         y0[0] = u0[0];
For complex signals use: y0[0].re = u0[0].re;
                         y0[0].im = u0[0].im;
                         y1[0].re = u1[0].re;
                         y1[0].im = u1[0].im;*/

if (controller_start[0]){
    error_voltage[1] = error_voltage[0];
    error_voltage[0] = vdc_ref[0] - vdc_meas[0];

    id_ref[1] = id_ref[0];

    id_ref[0] = a_pi*error_voltage[0] + b_pi*error_voltage[1] +
id_limit[0]*(1 + delta_pi) - id_ref[1]*delta_pi;
}
else {
    error_voltage[1] = 0;
    error_voltage[0] = 0;

    id_ref[1] = 0;
```

```
    id_ref[0] = 0;

    id_limit[0] = 0;
}
if (id_ref[0] < id_max){
   if (id_ref[0] > -id_max){
    id_limit[0] = id_ref[0];
    id_ref_out[0] = id_limit[0];
   }

   else {
    id_limit[0] = -id_max;
    id_ref_out[0] = id_limit[0];
   }
}
else {
    id_limit[0] = id_max;
    id_ref_out[0] = id_limit[0];
}
```

Appendix D

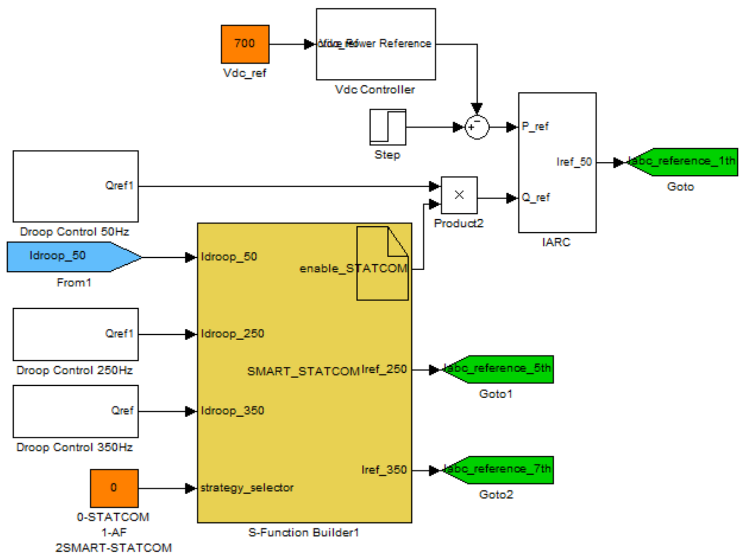

Fig. D-1 Smart Power Management strategy for implementing Smart-STATCOM functionality

In this appendix, the C-code implementation of the smart power management system is introduced in simulation. The following presented code corresponds to the S-function builder, which is emphasized in yellow in Fig. D-1. It receives the reference fundamental magnitude current to be injected in the system and the harmonic reference currents needed in order to satisfy the droop controller conditions for 5th and 7th harmonics. By performing its internal calculations it provides as an output one enable signal for the STATCOM functionality, as well as the final reference currents that will be injected by the current controllers. Finally it is worth to mention that the goto signals emphasized with green colour are provided as inputs for the different resonant current controllers.

```
if(strategy_selector[0] == 0){
        enable_STATCOM[0] = 1;
        enable_AF = 0;
    }

    if(strategy_selector[0] == 1){
        enable_STATCOM[0] = 0;
        enable_AF = 1;
    }

    if(strategy_selector[0] == 2){
        enable_STATCOM[0] = 1;
        enable_AF = 1;
    }

    I2_mag_ref_50 = sqrt(pow(Idroop_50[0],2) + (pow(Idroop_50[1],2)));
    i2_out = 40 - I2_mag_ref_50;
```

```
i2_limit_250 = i2_out*0.45454545;
i2_limit_350 = i2_out*0.54545454;

if(i2_limit_250 > 14){
    i2_limit_250 = 14;
}
if(i2_limit_350 > 12){
    i2_limit_350 = 12;
}
//250Hz output

I2_out_250 = Idroop_250[0]*enable_AF;

if(I2_out_250 < -i2_limit_250){
    I2_out_250 = -i2_limit_250*enable_AF;
}
if(I2_out_250 > i2_limit_250){
    I2_out_250 = i2_limit_250*enable_AF;
}

Iref_250[0] = I2_out_250;

//350Hz output

 I2_out_350 = Idroop_350[0]*enable_AF;

if(I2_out_350 < -i2_limit_350){
    I2_out_350 = -i2_limit_350*enable_AF;
}
if(I2_out_350 > i2_limit_350){
    I2_out_350 = i2_limit_350*enable_AF;
}

Iref_350[0] = I2_out_350;
```

Appendix E

Space Vector Modulation C-Code Implementation

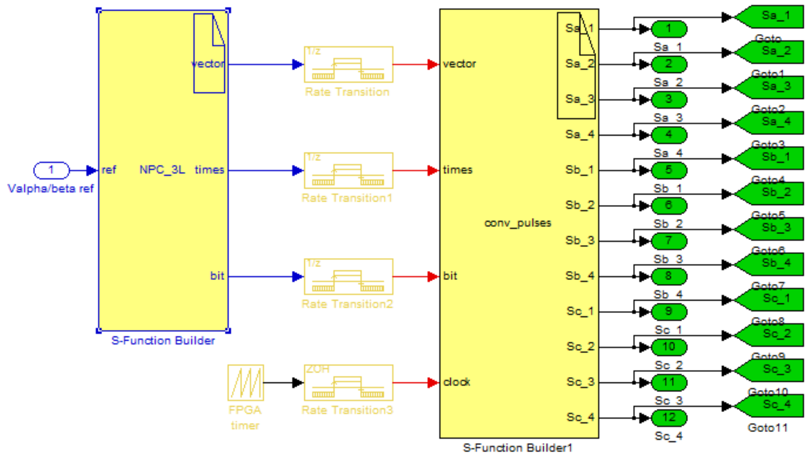

Fig. E-1 Space vector modulation control structure implemented in simulation

In this section, the SVM code implemented in both simulation and laboratory is introduced in order to provide more detailed information about the procedure that has been followed. In Fig. E-1 it can be observed that two main s-function builders have been used. The first one receives the alpha/beta reference voltage and it outputs the correspondent converter vectors and dwell time calculations. Finally, the second one is just creating the converter pulses which correspond to the previously calculated vectors and dwell times. It is worth to point out that the converter states corresponding to the desired voltage vectors and initialization variables are described by the following implemented header file:

```
static int CONV[27][12]
= {{ 0 , 0 , 1 , 1 ,   0 , 0 , 1 , 1 ,   0 , 0 , 1 , 1}, // 0  (NNN)
   { 0 , 1 , 1 , 0 ,   0 , 1 , 1 , 0 ,   0 , 1 , 1 , 0}, // 0  (000)
   { 1 , 1 , 0 , 0 ,   1 , 1 , 0 , 0 ,   1 , 1 , 0 , 0}, // 0  (PPP)
   { 0 , 1 , 1 , 0 ,   0 , 0 , 1 , 1 ,   0 , 0 , 1 , 1}, // 3  (0NN)
   { 1 , 1 , 0 , 0 ,   0 , 1 , 1 , 0 ,   0 , 1 , 1 , 0}, // 4  (P00)
   { 0 , 1 , 1 , 0 ,   0 , 1 , 1 , 0 ,   0 , 0 , 1 , 1}, // 5  (00N)
   { 1 , 1 , 0 , 0 ,   1 , 1 , 0 , 0 ,   0 , 1 , 1 , 0}, // 6  (PP0)
   { 0,  0 , 1 , 1 ,   0 , 1 , 1 , 0 ,   0 , 0 , 1 , 1}, // 7  (N0N)
   { 0 , 1 , 1 , 0 ,   1 , 1 , 0 , 0 ,   0 , 1 , 1 , 0}, // 8  (0P0)
   { 0 , 0 , 1 , 1 ,   0 , 1 , 1 , 0 ,   0 , 1 , 1 , 0}, // 9  (N00)
   { 0 , 1 , 1 , 0 ,   1 , 1 , 0 , 0 ,   1 , 1 , 0 , 0}, // 10 (0PP)
   { 0 , 0 , 1 , 1 ,   0 , 0 , 1 , 1 ,   0 , 1 , 1 , 0}, // 11 (NN0)
   { 0 , 1 , 1 , 0 ,   0 , 1 , 1 , 0 ,   1 , 1 , 0 , 0}, // 12 (00P)
   { 0 , 1 , 1 , 0 ,   0 , 0 , 1 , 1 ,   0 , 1 , 1 , 0}, // 13 (0N0)
   { 1 , 1 , 0 , 0 ,   0 , 1 , 1 , 0 ,   1 , 1 , 0 , 0}, // 14 (P0P)
   { 1 , 1 , 0 , 0 ,   0 , 1 , 1 , 0 ,   0 , 0 , 1 , 1}, // 15 (P0N)
   { 0 , 1 , 1 , 0 ,   1 , 1 , 0 , 0 ,   0 , 0 , 1 , 1}, // 16 (0PN)
   { 0 , 0 , 1 , 1 ,   1 , 1 , 0 , 0 ,   0 , 1 , 1 , 0}, // 17 (NP0)
   { 0 , 0 , 1 , 1 ,   0 , 1 , 1 , 0 ,   1 , 1 , 0 , 0}, // 18 (N0P)
```

```
   { 0 , 1 , 1 , 0 ,   0 , 0 , 1 , 1 ,   1 , 1 , 0 , 0}, // 19 (0NP)
   { 1 , 1 , 0 , 0 ,   0 , 0 , 1 , 1 ,   0 , 1 , 1 , 0}, // 20 (PN0)
   { 1 , 1 , 0 , 0 ,   0 , 0 , 1 , 1 ,   0 , 0 , 1 , 1}, // 21 (PNN)
   { 1 , 1 , 0 , 0 ,   1 , 1 , 0 , 0 ,   0 , 0 , 1 , 1}, // 22 (PPN)
   { 0 , 0 , 1 , 1 ,   1 , 1 , 0 , 0 ,   0 , 0 , 1 , 1}, // 23 (NPN)
   { 0 , 0 , 1 , 1 ,   1 , 1 , 0 , 0 ,   1 , 1 , 0 , 0}, // 24 (NPP)
   { 0 , 0 , 1 , 1 ,   0 , 0 , 1 , 1 ,   1 , 1 , 0 , 0}, // 25 (NNP)
   { 1 , 1 , 0 , 0 ,   0 , 0 , 1 , 1 ,   1 , 1 , 0 , 0}  // 26 (PNP)
  };

int v_0m, v_1, v_2, v_0p;
float T0m, T1, T2;

static int V[4][36] =
{ { 4 , 5 , 4 , 5 , 4 , 5 , 5 , 8 , 5 , 8 , 5 , 8 , 8 , 9 , 8 , 9 , 8 , 9 , 9
, 12 , 9 , 12 , 9 , 12 , 12 , 13 , 12 , 13 , 12 , 13 , 13 , 4 , 13 , 4 , 13 ,
4 },

  { 1 , 1 , 15 , 15 , 15 , 15 , 1 , 1 , 16 , 16 , 16 , 16 , 1 , 1 , 17 , 17 ,
17 , 17 , 1 , 1 , 18 , 18 , 18 , 18 , 1 , 1 , 19 , 19 , 19 , 19 , 1 , 1 , 20
, 20 , 20 , 20 },

  { 5 , 4 , 5 , 4 , 21 , 22 , 8 , 5 , 8 , 5 , 22 , 23 , 9 , 8 , 9 , 8 , 23 ,
24 , 12 , 9 , 12 , 9 , 24 , 25 , 13 , 12 , 13 , 12 , 25 , 26 , 4 , 13 , 4 ,
13 , 26 , 21 },

  { 3 , 6 , 3 , 6 , 3 , 6 , 6 , 7 , 6 , 7 , 6 , 7 , 7 , 10 , 7 , 10 , 7 , 10
, 10 , 11 , 10 , 11 , 10 , 11 , 11 , 14 , 11 , 14 , 11 , 14 , 14 , 3 , 14 , 3
, 14 , 3 }
};

float Vreal;
float Vimag;
float Tsample = 1.6667e-004;
int double_freq;
```

The used modulation algorithm is presented as follows:

```
/* This sample sets the output equal to the input
         y0[0] = u0[0];
For complex signals use: y0[0].re = u0[0].re;
                         y0[0].im = u0[0].im;
                         y1[0].re = u1[0].re;
                         y1[0].im = u1[0].im;*/

 Vreal = ref[0];
 Vimag = ref[1];
 angle = atan2(Vimag,Vreal);

if (angle < 0) {
    angle += TWOtimesPI;
}
dummy = angle + PIoverSIX;
if (dummy > TWOtimesPI) {
```

```
    sector_st = (dummy - TWOtimesPI) / PIoverTHREE;
}
else {
    sector_st = dummy / PIoverTHREE;
}
sector = angle / PIoverTHREE;
if (sector_st_prev == sector_st){    // normal operation, switching sequence
is postive-then negative
    if (double_freq == 0){
        double_freq = 1;
    }
    else{
        double_freq = 0;
    }
}
else {                               // change of sector, switching sequence
ensures at least one small vector (POO, OON, OPO, NOO, OOP, ONO)
    double_freq = double_freq;       // are applied at the beggining
}
sector_st_prev = sector_st;          // this variables is used to detect if
the vector at which the switching sequence
                                     // begins has changed. If it is the case,
then double_freq mast keep its value in
                                     // order to ensure proper commutation.

/*
 *    Determination of the starting state of the converter.
 *  The state depends on the sector the reference voltage is located.
 *  E.G. if the reference vector is located in the first sector, the starting
vector is
 *  (P00), meaning that leg A must be connected to the positive bar and legs
B and C to the neutral point.
 *  The zero selection depends on the STATE vector. The double sampling is
also considered by the value of "double_freq"
 */
switch (sector_st) {
    case 0:
        START[0]  = 1 ^ double_freq;
        START[1]  = 1;
        START[2]  = 0 ^ double_freq;
        START[3]  = 0;
//---------------------------------------
        START[4]  = 0;
        START[5]  = 1 ^ double_freq;
        START[6]  = 1;
        START[7]  = 0 ^ double_freq;
//---------------------------------------
        START[8]  = 0;
        START[9]  = 1 ^ double_freq;
        START[10] = 1;
        START[11] = 0 ^ double_freq;
        break;
    case 1:
        START[0]  = 0 ^ double_freq;
        START[1]  = 1;
        START[2]  = 1 ^ double_freq;
        START[3]  = 0;
```

```
//----------------------------------------
        START[4]  = 0 ^ double_freq;
        START[5]  = 1;
        START[6]  = 1 ^ double_freq;
        START[7]  = 0;
//----------------------------------------
        START[8]  = 0;
        START[9]  = 0 ^ double_freq;
        START[10] = 1;
        START[11] = 1 ^ double_freq;
        break;
    case 2:
        START[0]  = 0;
        START[1]  = 1 ^ double_freq;
        START[2]  = 1;
        START[3]  = 0 ^ double_freq;
//----------------------------------------
        START[4]  = 1 ^ double_freq;
        START[5]  = 1;
        START[6]  = 0 ^ double_freq;
        START[7]  = 0;
//----------------------------------------
        START[8]  = 0;
        START[9]  = 1 ^ double_freq;
        START[10] = 1;
        START[11] = 0 ^ double_freq;
        break;
    case 3:
        START[0]  = 0;
        START[1]  = 0 ^ double_freq;
        START[2]  = 1;
        START[3]  = 1 ^ double_freq;
//----------------------------------------
        START[4]  = 0 ^ double_freq;
        START[5]  = 1;
        START[6]  = 1 ^ double_freq;
        START[7]  = 0;
//----------------------------------------
        START[8]  = 0 ^ double_freq;
        START[9]  = 1;
        START[10] = 1 ^ double_freq ;
        START[11] = 0;
        break;
    case 4:
        START[0]  = 0;
        START[1]  = 1 ^ double_freq;
        START[2]  = 1;
        START[3]  = 0 ^ double_freq;
//----------------------------------------
        START[4]  = 0;
        START[5]  = 1 ^ double_freq;
        START[6]  = 1;
        START[7]  = 0 ^ double_freq;
//----------------------------------------
        START[8]  = 1 ^ double_freq;
        START[9]  = 1;
        START[10] = 0 ^ double_freq;
```

```
        START[11] = 0;
        break;
    case 5:
        START[0]  = 0 ^ double_freq;
        START[1]  = 1;
        START[2]  = 1 ^ double_freq;
        START[3]  = 0;
//-----------------------------------------
        START[4]  = 0;
        START[5]  = 0 ^ double_freq;
        START[6]  = 1;
        START[7]  = 1 ^ double_freq;
//-----------------------------------------
        START[8]  = 0 ^ double_freq;
        START[9]  = 1;
        START[10] = 1 ^ double_freq;
        START[11] = 0;
        break;
}
/*
 *   Depending on the sector the reference vector is located, the modulation
 * vector is rotated to the first sector
 */

switch (sector) {
    case 0:
        Va_mod = Vreal;
        Vb_mod = Vimag;
        break;
    case 1:
        Va_mod =  0.5*Vreal + sqrtTHREEoverTWO*Vimag;
        Vb_mod =  0.5*Vimag - sqrtTHREEoverTWO*Vreal;
        break;
    case 2:
        Va_mod = -0.5*Vreal + sqrtTHREEoverTWO*Vimag;
        Vb_mod = -0.5*Vimag - sqrtTHREEoverTWO*Vreal;
        break;
    case 3:
        Va_mod = -Vreal;
        Vb_mod = -Vimag;
        break;
    case 4:
        Va_mod = -0.5*Vreal - sqrtTHREEoverTWO*Vimag;
        Vb_mod = -0.5*Vimag + sqrtTHREEoverTWO*Vreal;
        break;
    case 5:
        Va_mod =  0.5*Vreal - sqrtTHREEoverTWO*Vimag;
        Vb_mod =  0.5*Vimag + sqrtTHREEoverTWO*Vreal;
        break;
}
/*
 *  Detection of the triangle the modulation vector is located
 */

if (Vb_mod > ONEoverTWOsqrtTHREE) {
    triangle = 5;
```

```
}
else {
    if (Vb_mod < sqrtTHREE*(Va_mod-ONEoverTHREE) ) {
        triangle = 4;
    }
    else {
        if (Vb_mod < -sqrtTHREE*(Va_mod-ONEoverTHREE)) {
            if (Vb_mod > ONEoversqrtTHREE*Va_mod) {
                triangle = 1;
            }
            else {
                triangle = 0;
            }
        }
        else {
            if (Vb_mod > ONEoversqrtTHREE*Va_mod) {
                triangle = 3;
            }
            else {
                triangle = 2;
            }
        }
    }
}
/*
 * Depending on the triangle, different vector base is selected.
 */
switch (triangle) {
    case 0:
        v_1 = -3*(Va_mod - ONEoverTHREE) - sqrtTHREE*Vb_mod;
        v_2 = TWOsqrtTHREE*Vb_mod;
        break;
    case 1:
        v_1 = -3*(Va_mod - ONEoverSIX) - sqrtTHREE*(Vb_mod -
ONEoverTWOsqrtTHREE);
        v_2 =  3*(Va_mod - ONEoverSIX) - sqrtTHREE*(Vb_mod -
ONEoverTWOsqrtTHREE);
        break;
    case 2:
        v_1 =  3*(Va_mod - ONEoverTHREE) + sqrtTHREE*Vb_mod;
        v_2 = -3*(Va_mod - ONEoverTHREE) + sqrtTHREE*Vb_mod;
        break;
    case 3:
        v_1 =  3*(Va_mod - ONEoverSIX) + sqrtTHREE*(Vb_mod -
ONEoverTWOsqrtTHREE);
        v_2 = -TWOsqrtTHREE*(Vb_mod - ONEoverTWOsqrtTHREE);
        break;
    case 4:
        v_1 = TWOsqrtTHREE*Vb_mod;
        v_2 = 3*(Va_mod - ONEoverTHREE) - sqrtTHREE*Vb_mod;
        break;
    case 5:
        v_1 = 3*(Va_mod - ONEoverSIX) - sqrtTHREE*(Vb_mod -
ONEoverTWOsqrtTHREE);
        v_2 = TWOsqrtTHREE*(Vb_mod - ONEoverTWOsqrtTHREE);
        break;
}
```

```
v_0 = 1 - v_1 - v_2;

t1 = Tsample*v_1;
t2 = Tsample*v_2;
t0 = Tsample - t1 - t2;

vec_index = triangle + 6*sector;

vec0 = V[0][vec_index];
vec1 = V[1][vec_index];
vec2 = V[2][vec_index];
vec3 = V[3][vec_index];

vector[0] = vec0;
vector[1] = vec1;
vector[2] = vec2;
vector[3] = vec3;

times[0]   = t0*0.5;
times[1]   = t1;
times[2]   = t2;

bit[0] = double_freq;

 /* This sample sets the output equal to the input
         y0[0] = u0[0];
For complex signals use: y0[0].re = u0[0].re;
                         y0[0].im = u0[0].im;
                         y1[0].re = u1[0].re;
                         y1[0].im = u1[0].im;*/

if(bit[0] == 0){
    v_0m = vector[0];
    v_1  = vector[1];
    v_2  = vector[2];
    v_0p = vector[3];

    T0m = times[0];
    T1  = times[1] + T0m;
    T2  = times[2] + T1;
}
else{
    v_0m = vector[3];
    v_1  = vector[2];
    v_2  = vector[1];
    v_0p = vector[0];

    T0m = times[0];
    T1  = times[2] + T0m;
    T2  = times[1] + T1;
}


if (clock[0] < T0m){
```

```
    Sa_1[0] = CONV[v_0m][0];
    Sa_2[0] = CONV[v_0m][1];
    Sa_3[0] = CONV[v_0m][2];
    Sa_4[0] = CONV[v_0m][3];

    Sb_1[0] = CONV[v_0m][4];
    Sb_2[0] = CONV[v_0m][5];
    Sb_3[0] = CONV[v_0m][6];
    Sb_4[0] = CONV[v_0m][7];

    Sc_1[0] = CONV[v_0m][8];
    Sc_2[0] = CONV[v_0m][9];
    Sc_3[0] = CONV[v_0m][10];
    Sc_4[0] = CONV[v_0m][11];
}
else{
    if ( (clock[0] >= T0m) && (clock[0] < T1) ){
        Sa_1[0] = CONV[v_1][0];
        Sa_2[0] = CONV[v_1][1];
        Sa_3[0] = CONV[v_1][2];
        Sa_4[0] = CONV[v_1][3];

        Sb_1[0] = CONV[v_1][4];
        Sb_2[0] = CONV[v_1][5];
        Sb_3[0] = CONV[v_1][6];
        Sb_4[0] = CONV[v_1][7];

        Sc_1[0] = CONV[v_1][8];
        Sc_2[0] = CONV[v_1][9];
        Sc_3[0] = CONV[v_1][10];
        Sc_4[0] = CONV[v_1][11];
    }
    else {
        if ( (clock[0] >= T1) && (clock[0] < T2) ){
            Sa_1[0] = CONV[v_2][0];
            Sa_2[0] = CONV[v_2][1];
            Sa_3[0] = CONV[v_2][2];
            Sa_4[0] = CONV[v_2][3];

            Sb_1[0] = CONV[v_2][4];
            Sb_2[0] = CONV[v_2][5];
            Sb_3[0] = CONV[v_2][6];
            Sb_4[0] = CONV[v_2][7];

            Sc_1[0] = CONV[v_2][8];
            Sc_2[0] = CONV[v_2][9];
            Sc_3[0] = CONV[v_2][10];
            Sc_4[0] = CONV[v_2][11];
        }
        else{
            Sa_1[0] = CONV[v_0p][0];
            Sa_2[0] = CONV[v_0p][1];
            Sa_3[0] = CONV[v_0p][2];
            Sa_4[0] = CONV[v_0p][3];
```

```
            Sb_1[0] = CONV[v_0p][4];
            Sb_2[0] = CONV[v_0p][5];
            Sb_3[0] = CONV[v_0p][6];
            Sb_4[0] = CONV[v_0p][7];

            Sc_1[0] = CONV[v_0p][8];
            Sc_2[0] = CONV[v_0p][9];
            Sc_3[0] = CONV[v_0p][10];
            Sc_4[0] = CONV[v_0p][11];
        }
    }
}
```